USE OF SURFACE COMPLEXATION MODELS IN SOIL CHEMICAL SYSTEMS

Sabine Goldberg

USDA–ARS,
U.S. Salinity Laboratory,
Riverside, California 92501

I. INTRODUCTION

A model is a simplified representation of reality considering only the characteristics of the system important to the problem at hand. An empirical model is a description of data without theoretical basis. A chemical model provides a description of a chemical system consistent with its chemical properties and should be simultaneously as simple and as chemically correct as possible. The ideal model is effective, comprehensive, realistic, and predictive (Barrow and Bowden, 1987). An effective model closely describes observations, a comprehensive model applies to a wide range of conditions without modification, a realistic model conforms to accepted theories of behavior, and a predictive model can be applied to different conditions.

Unlike empirical models, surface complexation models are chemical models that strive to satisfy the above characteristics and to give a general molecular description of adsorption phenomena using an equilibrium approach. The purpose of molecular theory is to derive thermodynamic properties such as activity coefficients and equilibrium constants from the principles of statistical mechanics (Sposito, 1981). The surface complexation models are designed to calculate values for the thermodynamic properties mathematically and constitute a family of models having similar characteristics. This model family includes the constant capacitance model (Stumm *et al.*, 1980), the triple-layer model (Davis *et al.*, 1978), the Stern variable surface charge–variable surface potential model (Bowden *et al.*, 1980), the generalized two-layer model (Dzombak and Morel, 1990), and the one-pK model (van Riemsdijk *et al.*, 1986). The major advancement of the surface complexation models is that they consider surface charge. Surface charge results from protonation and dissociation reactions as well as from surface complexation reactions of reactive surface hydroxyl

groups at mineral surfaces. The sign and magnitude of the mineral surface charge are dependent on the pH and the ionic strength of the electrolyte solution.

The purpose of this article is to comprehensively review five common surface complexation models of the mineral–solution interface and their use in describing soil chemical systems. Common model characteristics and adjustable parameters will be discussed. For each model, surface species, chemical reactions, equilibrium constant expressions, and surface activity coefficients will be defined. Applications of the model to ion adsorption on soil minerals and soils will be presented. Incorporation of surface complexation models into computer codes will be discussed.

II. DESCRIPTION OF MODELS

A. Common Characteristics of Surface Complexation Models

1. Balance of Surface Charge

The balance of surface charge on an oxide mineral in aqueous solution is (Sposito, 1984a)

$$\sigma_H + \sigma_{is} + \sigma_{os} + \sigma_d = 0 \tag{1}$$

where σ_H is the net proton charge, defined by $\sigma_H = F(\Gamma_H - \Gamma_{OH})$, where Γ is a surface excess concentration, σ_{is} is the inner-sphere complex charge resulting from the formation of inner-sphere complexes between adsorbing ions (other than H^+ and OH^-) and surface functional groups, σ_{os} is the outer-sphere complex charge resulting from the formation of outer-sphere complexes between adsorbing ions and surface functional groups or ions in inner-sphere complexes, σ_d is the dissociated charge, equal to minus the surface charge neutralized by electrolyte ions in solution that have not formed adsorbed complexes with surface functional groups.

All surface complexation models are based on a balance of surface charge expression. The surface functional group is defined as SOH, where S represents a metal ion of the oxide mineral surface bound to reactive hydroxyl group. The functional group can also be an aluminol or silanol group at the edge of a clay mineral particle. The balance of surface charge expression may be simplified depending upon the interfacial structure and the assumptions of the particular complexation model. The specific expressions will be provided in the detailed discussion of each model.

2. Electrostatic Potential Terms

All surface complexation models contain at least one coulombic correction factor to account for the effect of surface charge on surface complexation. These coulombic correction factors take the form of electrostatic potential terms, $e^{-F\Psi_i/RT}$ where Ψ_i is the surface potential (V) in the ith surface plane, F is the Faraday constant (C mol_c^{-1}), R is the molar gas constant (J mol^{-1} K^{-1}), and T is the absolute temperature (K) in the conditional equilibrium constant expressions. Surface complexation models of the oxide–solution interface can be considered as special cases of the van der Waals model in statistical mechanics (Sposito, 1983). In this model, charged surface complex species create a long-ranged mean electric force field from screened coulomb forces by mutual interaction. Short-ranged interactions are neglected. The mean field effect is responsible for the presence of electrostatic potential terms in the conditional equilibrium constant expressions. According to the van der Waals model, the activity coefficient differs from a value of one because the total potential energy changes when neutral surface hydroxyl groups are replaced by charged surface complexes (Sposito, 1983). Diffuse double-layer theory need not be invoked to lend chemical significance to the exponential terms (Sposito, 1983). Unfortunately, diffuse double-layer effects have been invoked almost universally in model applications to explain the presence of the exponential terms. The electrostatic potential terms should simply be considered as solid-phase activity coefficients correcting for the charges on the surface complexes.

3. Adjustable Parameters

The surface complexation models explicitly define equilibrium constant expressions for surface complexes. They contain mass balance equations for each type of surface site and charge balance equations for each surface plane of adsorption. Thus, all models contain the following adjustable parameters: K_i, the equilibrium constants; C_i, the capacitance density for the ith surface plane; and $[SOH]_T$, the total number of reactive surface hydroxyl groups. Values of the equilibrium constants are almost always obtained with the help of a computer program. Details for each model will be discussed below. Values for some of the capacitance density parameters can be obtained experimentally (Sposito, 1984a). However, the capacitance density values have almost universally been taken as adjustable. Details for experimental determinations of capacitance densities will be provided in the model descriptions.

The total number of reactive surface hydroxyl groups, $[SOH]_T$, is an important parameter in surface complexation models. The value of the surface site density has been determined either experimentally by tritium exchange (Davis and Leckie, 1978, 1980), potentiometric titration (Balistrieri and Murray, 1981; Hohl and Stumm, 1976; Kummert and Stumm, 1980), fluoride adsorption (Sigg, 1979), maximum adsorption (Goldberg and Sposito, 1984a; Goldberg, 1985, 1986a), calculated from crystal dimensions, or optimized to fit experimental adsorption data (Hayes *et al.*, 1988). For goethite these determinations range from 4 sites/nm^2 for potentiometric titration to 6–7 sites/nm^2 for fluoride adsorption to 17 sites/nm^2 for tritium exchange (Sigg, 1979). Crystallographic calculations of reactive surface hydroxyl groups on goethite provide a surface site density of 3 sites/nm^2 (Sposito, 1984a). Various measurements of surface site density are described in detail by James and Parks (1982). These authors also provide values of this parameter obtained with diverse methods for many oxide minerals.

Initial sensitivity analyses showed surface complexation models to be relatively insensitive to surface site density values for selenium adsorption on amorphous hydrous ferric oxide in the range of 3–12 sites/nm^2 (Hayes *et al.*, 1988) and for phosphate adsorption on a soil in the range of 1.25–2.5 sites/nm^2 (Goldberg and Sposito, 1984b). Recently, sensitivity analyses for acid–base titration data on goethite, aluminum oxide, and titanium oxide showed the models to be relatively insensitive to surface site density in the range of 2–20 sites/nm^2 (Hayes *et al.*, 1991). However, the actual values of the equilibrium constants decreased with increasing surface site density. More detailed investigations of both the constant capacitance model and the triple-layer model have indicated that for adsorption of phosphate, arsenate, selenite, selenate, silicate, molybdate, and borate the ability of the models to describe adsorption using both inner-sphere and outer-sphere surface complexes was sensitively dependent on the value of the surface site density (Goldberg, 1991). Further research is needed to determine the most appropriate experimental measurement of surface site density for surface complexation modeling.

The surface complexation models contain the assumption that ion adsorption occurs at only one or two types of surface sites. Clearly, soils are complex, multisite mixtures. However, experimental evidence suggests that even oxide mineral surfaces contain several sets of adsorption sites (Rochester and Topham, 1979a,b; Benjamin and Leckie, 1980, 1981). Thus, equilibrium constants determined for soils and even for pure mineral systems likely represent average composite values for all sets of reacting sites.

B. Constant Capacitance Model

The constant capacitance model of the oxide mineral–aqueous solution interface was developed by the research groups of Schindler and Stumm (Schindler and Gamsjäger, 1972; Hohl and Stumm, 1976; Schindler *et al.*, 1976; Stumm *et al.*, 1976, 1980). The model is based on the following assumptions: (1) all surface complexes are inner-sphere complexes, with anion adsorption occurring via a ligand exchange mechanism, (2) the constant ionic medium reference state determines the activity coefficients of the aqueous species in the conditional equilibrium constants and therefore no complexes are formed with ions in the background electrolyte, and (3) a linear relationship exists between surface charge and surface potential:

$$\sigma = (CSa/F)\Psi \tag{2}$$

where C is the capacitance density (F m^{-2}), S is the specific surface area (m^2 g^{-1}), a is the suspension density (g $liter^{-1}$), and σ has units of mol_c $liter^{-1}$. These assumptions greatly simplify the balance of surface charge expression:

$$\sigma = \sigma_H + \sigma_{is} \tag{3}$$

The surface charge on a particle, σ, equals the net proton charge plus the charge resulting from formation of inner-sphere surface complexes. There is no strict balance of surface charge in the constant capacitance model. Equation (3) is a model expression for the total particle charge. Figure 1 provides a diagram of the surface–solution interface in the constant capacitance model. The following equations are general surface complexation reactions (Hohl *et al.*, 1980):

$$\mathrm{SOH} + \mathrm{H^+} \rightleftarrows \mathrm{SOH_2^+} \tag{4}$$

$$\mathrm{SOH} \rightleftarrows \mathrm{SO^-} + \mathrm{H^+} \tag{5}$$

$$\mathrm{SOH} + \mathrm{M}^{m+} \rightleftarrows \mathrm{SOM}^{(m-1)} + \mathrm{H^+} \tag{6}$$

$$2\mathrm{SOH} + \mathrm{M}^{m+} \rightleftarrows (\mathrm{SO})_2\mathrm{M}^{(m-2)} + 2\mathrm{H^+} \tag{7}$$

$$\mathrm{SOH} + \mathrm{L}^{l-} \rightleftarrows \mathrm{SL}^{(l-1)-} + \mathrm{OH^-} \tag{8}$$

$$2\mathrm{SOH} + \mathrm{L}^{l-} \rightleftarrows \mathrm{S_2L}^{(l-2)-} + 2\mathrm{OH^-} \tag{9}$$

where SOH represents the surface functional group, M is a metal ion, $m+$ is the charge on the metal ion, L is a ligand, and $l-$ is the charge on the ligand. The intrinsic conditional equilibrium constants describing these

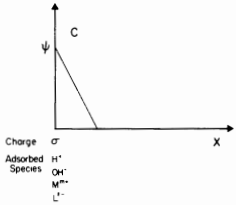

Figure 1. Placement of ions, potential, charge, and capacitance for the constant capacitance model. After Westall (1986), reproduced with permission from the American Chemical Society.

reactions are (Hohl *et al.*, 1980)

$$K_{+}(\text{int}) = \frac{[\text{SOH}_2^+]}{[\text{SOH}][\text{H}^+]} \exp[F\Psi/RT] \tag{10}$$

$$K_{-}(\text{int}) = \frac{[\text{SO}^-][\text{H}^+]}{[\text{SOH}]} \exp[-F\Psi/RT] \tag{11}$$

$$K_{\text{M}}^1(\text{int}) = \frac{[\text{SOM}^{(m-1)}][\text{H}^+]}{[\text{SOH}][\text{M}^{m+}]} \exp[(m-1)F\Psi/RT] \tag{12}$$

$$K_{\text{M}}^2(\text{int}) = \frac{[(\text{SO})_2\text{M}^{(m-2)}][\text{H}^+]^2}{[\text{SOH}]^2[\text{M}^{m+}]} \exp[(m-2)F\Psi/RT] \tag{13}$$

$$K_{\text{L}}^1(\text{int}) = \frac{[\text{SL}^{(l-1)-}][\text{OH}^-]}{[\text{SOH}][\text{L}^{l-}]} \exp[-(l-1)F\Psi/RT] \tag{14}$$

$$K_{\text{L}}^2(\text{int}) = \frac{[\text{S}_2\text{L}^{(l-2)-}][\text{OH}^-]^2}{[\text{SOH}]^2[\text{L}^{l-}]} \exp[-(l-2)F\Psi/RT] \tag{15}$$

where square brackets represent concentrations (mol liter^{-1}). The intrinsic conditional equilibrium constants are obtained by extrapolating the conditional equilibrium constants to zero net surface charge (Stumm *et al.*, 1980). A detailed explanation of the procedure is provided in Section III,A. Surface complexes exist in a chargeless environment in the standard state. To solve the equilibrium problem, two more equations are needed. The mass balance for the surface functional group is (Sigg and Stumm, 1981)

$$\begin{aligned}[\text{SOH}]_{\text{T}} = {} & [\text{SOH}] + [\text{SOH}_2^+] + [\text{SO}^-] + [\text{SOM}^{(m-1)}] \\ & + [(\text{SO})_2\text{M}^{(m-2)}] + [\text{SL}^{(l-1)-}] + [\text{S}_2\text{L}^{(l-2)-}]\end{aligned} \tag{16}$$

and the charge balance is (Sigg and Stumm, 1981)

$$\sigma = [SOH_2^+] - [SO^-] + (m-1)[SOM^{(m-1)}] + (m-2)[(SO)_2M^{(m-2)}] - (l-1)[SL^{(l-1)-}] - (l-2)[S_2L^{(l-2)-}] \quad (17)$$

This set of equations can be solved with a computer program using the mathematical approach outlined by Westall (1980).

C. Triple-Layer Model

The original triple-layer model was developed as an extension of the site-binding model (Yates *et al.*, 1974) by Davis and co-workers (1978; Davis and Leckie, 1978, 1980). In contrast to the constant capacitance model, the original triple-layer model assumes that all metals and ligands form outer-sphere surface complexes. Only the proton and the hydroxyl ion form inner-sphere surface complexes; all other surface complexes contain at least one water molecule between the ion and the surface functional group (Davis *et al.*, 1978). The infinite dilution reference state determines the activity coefficients of the aqueous species in the conditional equilibrium constants. The surface charge is thus composed of the net proton charge plus the charge resulting from the formation of outer-sphere complexes:

$$\sigma = \sigma_H + \sigma_{os} \quad (18)$$

The model derives its name from the three planes of charge used to represent the oxide surface. The potential-determining ions at the surface, protons and hydroxyl ions, are placed in the surface o-plane. The outer-sphere complexes are situated a little further from the surface in the β-plane. The diffuse layer starts at the d-plane and extends into the aqueous solution phase. Figure 2 provides a diagram of the surface–solution interface in the triple-layer model. Because the triple–layer model contains three surface planes, three charge–potential relations are needed (Davis *et al.*, 1978):

$$\Psi_o - \Psi_\beta = \sigma_o / C_1 \quad (19)$$

$$\Psi_\beta - \Psi_d = -\sigma_d / C_2 \quad (20)$$

$$\sigma_d = -(8RTc\,\varepsilon_0 D)^{1/2} \sinh(F\Psi_d / 2RT) \quad (21)$$

where σ has units of C m^{-2}, ε_0 is the permittivity of vacuum, D is the dielectric constant of water, and c is the concentration of a 1:1 background electrolyte. In the case of 1:2 and 2:1 background electrolytes, Eq. (21)

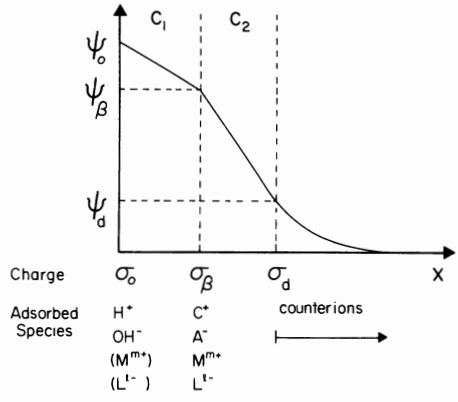

Figure 2. Placement of ions, potentials, charges, and capacitances for the triple-layer model. Parentheses represent ion placement allowed only in the modified triple-layer model. After Westall (1980), reproduced with permission from the American Chemical Society.

becomes much more complex (see, e.g., Sposito, 1984a). The reactions considered in the original triple-layer model include Eqs. (4), (5), and (6), although Eq. (6) is now written as

$$\mathrm{SOH} + \mathrm{M}^{m+} \rightleftarrows \mathrm{SO}^{-} - \mathrm{M}^{m+} + \mathrm{H}^{+} \tag{22}$$

representing the formation of an outer-sphere surface complex (Davis *et al.*, 1978). In the original triple-layer model the formation of the bidentate metal complex, Eq. (7), is replaced by the formation of a hydroxy-metal surface species:

$$\mathrm{SOH} + \mathrm{M}^{m+} + \mathrm{H_2O} \rightleftarrows \mathrm{SO}^{-} - \mathrm{MOH}^{(m-1)} + 2\mathrm{H}^{+} \tag{23}$$

Davis and Leckie (1978) found that this surface reaction was more consistent with their experimental data. In the original triple-layer model the ligand exchange reactions, Eqs. (8) and (9), are now written as outer-sphere surface complex formations (Davis and Leckie, 1980):

$$\mathrm{SOH} + \mathrm{H}^{+} + \mathrm{L}^{l} \rightleftarrows \mathrm{SOH_2^{+}} - \mathrm{L}^{l-} \tag{24}$$

$$\mathrm{SOH} + 2\mathrm{H}^{+} + \mathrm{L}^{l-} \rightleftarrows \mathrm{SOH_2^{+}} - \mathrm{LH}^{(l-1)-} \tag{25}$$

For anion adsorption reactions, Davis and Leckie (1980) found that they could obtain results more consistent with their experimental data by replacing the bidentate complex with a protonated surface species. Two

additional reactions are needed to describe the outer-sphere surface complexes formed by ions of the background electrolyte (Davis *et al.*, 1978):

$$\mathrm{SOH} + \mathrm{C}^+ \rightleftarrows \mathrm{SO}^- - \mathrm{C}^+ + \mathrm{H}^+ \tag{26}$$

$$\mathrm{SOH} + \mathrm{H}^+ + \mathrm{A}^- \rightleftarrows \mathrm{SOH}_2^+ - \mathrm{A}^- \tag{27}$$

where C^+ is the cation and A^- is the anion.

The intrinsic conditional equilibrium constants for the triple-layer model have a form similar to those for the constant capacitance model. The protonation and dissociation constants remain as written in Eqs. (10) and (11). The other intrinsic conditional equilibrium constants are (Davis *et al.*, 1978; Davis and Leckie, 1978, 1980)

$$K_{\mathrm{M}}^1(\mathrm{int}) = \frac{[\mathrm{SO}^- - \mathrm{M}^{m+}][\mathrm{H}^+]}{[\mathrm{SOH}][\mathrm{M}^{m+}]} \exp[F(m\Psi_\beta - \Psi_o)/RT] \tag{28}$$

$$K_{\mathrm{M}}^2(\mathrm{int}) = \frac{[\mathrm{SO}^- - \mathrm{MOH}^{(m-1)}][\mathrm{H}^+]^2}{[\mathrm{SOH}][\mathrm{M}^{m+}]} \exp[F((m-1)\Psi_\beta - \Psi_o)/RT] \tag{29}$$

$$K_{\mathrm{L}}^1(\mathrm{int}) = \frac{[\mathrm{SOH}_2^+ - \mathrm{L}^{l-}]}{[\mathrm{SOH}][\mathrm{H}^+][\mathrm{L}^{l-}]} \exp[F(\Psi_o - l\Psi_\beta)/RT] \tag{30}$$

$$K_{\mathrm{L}}^2(\mathrm{int}) = \frac{[\mathrm{SOH}_2^+ - \mathrm{LH}^{(l-1)-}]}{[\mathrm{SOH}][\mathrm{H}^+]^2[\mathrm{L}^{l-}]} \exp[F(\Psi_o - (l-1)\Psi_\beta)/RT] \tag{31}$$

$$K_{\mathrm{C}^+}(\mathrm{int}) = \frac{[\mathrm{SO}^- - \mathrm{C}^+][\mathrm{H}^+]}{[\mathrm{SOH}][\mathrm{C}^+]} \exp[F(\Psi_\beta - \Psi_o)/RT] \tag{32}$$

$$K_{\mathrm{A}^-}(\mathrm{int}) = \frac{[\mathrm{SOH}_2^+ - \mathrm{A}^-]}{[\mathrm{SOH}][\mathrm{H}^+][\mathrm{A}^-]} \exp[F(\Psi_o - \Psi_\beta)/RT] \tag{33}$$

As in the constant capacitance model, the intrinsic conditional equilibrium constants are obtained by extrapolation (Davis *et al.*, 1978). Surface complexes exist in a chargeless environment in the standard state. A detailed explanation is provided in Section III,B. The mass balance equation for the surface functional group is

$$\begin{aligned}[\mathrm{SOH}]_{\mathrm{T}} = {} & [\mathrm{SOH}] + [\mathrm{SOH}_2^+] + [\mathrm{SO}^-] + [\mathrm{SO}^- - \mathrm{M}^{m+}] \\ & + [\mathrm{SO}^- - \mathrm{MOH}^{(m-1)}] + [\mathrm{SOH}_2^+ - \mathrm{L}^{l-}] \\ & + [\mathrm{SOH}_2^+ - \mathrm{LH}^{(l-1)-}] + [\mathrm{SO}^- - \mathrm{C}^+] + [\mathrm{SOH}_2^+ - \mathrm{A}^-]\end{aligned} \tag{34}$$

Last, three charge balance equations are needed:

$$\sigma_o + \sigma_\beta + \sigma_d = 0 \tag{35}$$

$$\sigma_o = \frac{F}{Sa}\{[SOH_2^+] + [SOH_2^+ - L^{l-}] + [SOH_2^+ - LH^{(l-1)-}] + [SOH_2^+ - A^-] - [SO^-] - [SO^- - M^{m+}] - [SO^- - MOH^{(m-1)}] - [SO^- - C^+]\} \quad (36)$$

$$\sigma_\beta = \frac{F}{Sa}\{m[SO^- - M^{m+}] + (m-1)[SO^- - MOH^{(m-1)}] + [SO^- - C^+] - l[SOH_2^+ - L^{l-}] - (l-1)[SOH_2^+ - LH^{(l-1)-}] - [SOH_2^+ - A^-]\} \quad (37)$$

This set of equations can be solved with a computer program using a mathematical approach similar to that for the constant capacitance model (Westall, 1980).

Extensions of the original triple-layer model to describe ion adsorption as inner-sphere surface complexes in the *o*-plane have been carried out (Blesa *et al.*, 1984a; Hayes and Leckie, 1986, 1987; Hayes *et al.*, 1988). Blesa *et al.* (1984a) were the first to extend the triple-layer model to describe inner-sphere surface complexation via ligand exchange in modeling boron adsorption on the iron oxide, magnetite, and on zirconium dioxide. Later work by Hayes and co-workers described lead (Hayes and Leckie, 1986, 1987), cadmium (Hayes and Leckie, 1987), and selenite adsorption (Hayes *et al.*, 1988) on iron oxides using inner-sphere surface complexes.

In the modification of the triple-layer model developed by Hayes and Leckie (1986, 1987), the standard state for both solution and surface species is chosen as zero surface charge and without ionic interactions. The reference state for all species is infinite dilution and zero surface charge. The result of these changes is that the exponential terms become ratios of solution and surface activity coefficients and that the intrinsic conditional equilibrium constants are equivalent to the thermodynamic equilibrium constants (Hayes and Leckie, 1987).

In the modified triple-layer model the surface charge is composed of the net proton charge plus the charge resulting from the formation of inner-sphere and outer-sphere surface complexes:

$$\sigma = \sigma_H + \sigma_{is} + \sigma_{os} \quad (38)$$

Figure 2 indicates the placement of metal and ligand ions into the *o*-plane in the modified triple-layer model.

In the modified triple-layer model, inner-sphere surface complexation by metal ions is described by Eq. (6), as in the constant capacitance model. Only this metal surface complexation reaction is considered. Inner-sphere surface complexation by anions via ligand exchange is described by

Eq. (8), as in the constant capacitance model. The intrinsic conditional equilibrium constants for these reactions are Eqs. (12) and (14), where Ψ is replaced by Ψ_o. In addition to these reactions an additional surface complexation reaction between the cation of the background electrolyte and the adsorbed anion is considered:

$$\mathrm{SOH} + \mathrm{L}^{l-} + \mathrm{H}^{+} + \mathrm{C}^{+} \rightleftarrows \mathrm{SL}^{(l-1)-} - \mathrm{C}^{+} + \mathrm{H_2O} \tag{39}$$

The intrinsic conditional equilibrium constant expression for this reaction is

$$K_{\mathrm{LC}^-}(\mathrm{int}) = \frac{[\mathrm{SL}^{(l-1)-} - \mathrm{C}^{+}]}{[\mathrm{SOH}][\mathrm{L}^{l-}][\mathrm{H}^{+}][\mathrm{C}^{+}]} \exp[F(\Psi_\beta - (l-1)\Psi_o)/RT] \tag{40}$$

In the modified triple-layer model the mass balance is

$$\begin{aligned}[\mathrm{SOH}]_\mathrm{T} = {} & [\mathrm{SOH}] + [\mathrm{SOH_2^+}] + [\mathrm{SO^-}] + [\mathrm{SOM}^{(m-1)}] + [\mathrm{SO^-} - \mathrm{M}^{m+}] \\ & + [\mathrm{SO^-} - \mathrm{MOH}^{(m-1)}] + [\mathrm{SL}^{(l-1)-}] + [\mathrm{SL}^{(l-1)-} - \mathrm{C}^{+}] \\ & + [\mathrm{SOH_2^+} - \mathrm{L}^{l-}] + [\mathrm{SOH_2^+} - \mathrm{LH}^{(l-1)-}] + [\mathrm{SO^-} - \mathrm{C}^{+}] \\ & + [\mathrm{SOH_2^+} - \mathrm{A}^{-}] \end{aligned} \tag{41}$$

In the modified triple-layer model the charge balance in the o-plane is

$$\begin{aligned}\sigma_o = \frac{F}{Sa}\{ & [\mathrm{SOH_2^+}] + [\mathrm{SOH_2^+} - \mathrm{L}^{l-}] + [\mathrm{SOH_2^+} - \mathrm{LH}^{(l-1)-}] \\ & + (m-1)[\mathrm{SOM}^{(m-1)}] + [\mathrm{SOH_2^+} - \mathrm{A}^{-}] - [\mathrm{SO^-}] \\ & - [\mathrm{SO^-} - \mathrm{M}^{m+}] - [\mathrm{SO^-} - \mathrm{MOH}^{(m-1)}] - (l-1)[\mathrm{SL}^{(l-1)-}] \\ & - (l-1)[\mathrm{SL}^{(l-1)-} - \mathrm{C}^{+}] - [\mathrm{SO^-} - \mathrm{C}^{+}]\} \end{aligned} \tag{42}$$

and the charge balance in the β-plane is

$$\begin{aligned}\sigma_\beta = \frac{F}{Sa}\{ & m[\mathrm{SO^-} - \mathrm{M}^{m+}] + (m-1)[\mathrm{SO^-} - \mathrm{MOH}^{(m-1)}] \\ & + [\mathrm{SL}^{(l-1)-} - \mathrm{C}^{+}] + [\mathrm{SO^-} - \mathrm{C}^{+}] - l[\mathrm{SOH_2^+} - \mathrm{L}^{l-}] \\ & - (l-1)[\mathrm{SOH_2^+} - \mathrm{LH}^{(l-1)-}] - [\mathrm{SOH_2^+} - \mathrm{A}^{-}]\} \end{aligned} \tag{43}$$

D. Stern Variable Surface Charge–Variable Surface Potential Model

The Stern variable surface charge–variable surface potential (VSC–VSP) model was developed by Bowden, Barrow, and their co-workers (Bowden *et al.*, 1977, 1980; Barrow *et al.*, 1980a, 1981; Barrow, 1987). This

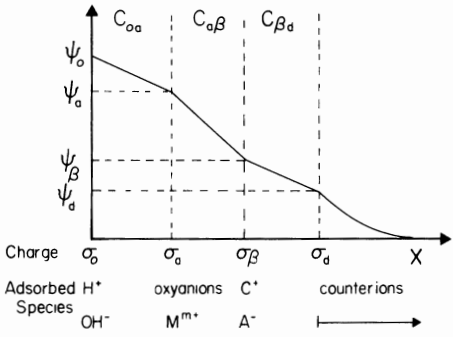

Figure 3. Placement of ions, potentials, charges, and capacitances for the Stern VSC–VSP model. After Bowden *et al.* (1980).

model is actually a mixture of the constant capacitance model and the original triple-layer model and might also be called the four-layer model. The Stern VSC–VSP model assumes that protons, hydroxyl ions, and "strongly adsorbed" oxyanions and metals form inner-sphere surface complexes. The balance of surface charge expression in this model is the same as in the modified triple-layer model, Eq. (38). The protons and hydroxyl ions reside in the *o*-plane close to the surface. The "strongly adsorbed" ions are placed in an *a*-plane a short distance away from the surface *o*-plane. The major cations and anions are assumed to form outer-sphere surface complexes and are placed in the β-plane a short distance away from the *a*-plane (Barrow *et al.*, 1980a). The fourth plane, the *d*-plane, indicates the start of the diffuse double layer. Figure 3 provides a diagram of the surface–solution interface in the Stern VSC–VSP model. The surface functional group is defined as OH—S—OH_2. This convention allows only one protonation or dissociation to occur for every two surface hydroxyl groups (Barrow *et al.*, 1980a). The Stern VSC–VSP model emphasizes parameter optimization and defines no surface reactions, provides no equilibrium constant expressions for these reactions, and defines no specific surface species. The model equations are given in Barrow *et al.* (1980a) and Bowden *et al.* (1980). Because the Stern VSC–VSP model contains four surface planes, four charge–potential equations and four charge balance equations are needed:

$$\Psi_o - \Psi_a = \sigma_o / C_{oa} \tag{44}$$

$$\Psi_a - \Psi_\beta = (\sigma_o + \sigma_a) / C_{a\beta} \tag{45}$$

$$\Psi_\beta - \Psi_d = -\sigma_d / C_{\beta d} \tag{46}$$

where σ has units of $mol_c\ m^{-2}$ and C has units of $mol_c\ V^{-1}\ m^{-2}$. The diffuse layer charge, σ_d, is calculated as in the triple-layer model, Eq. (21). However, the result from Eq. (21) is in $C\ m^{-2}$ and must be divided by the Faraday constant to obtain $mol_c\ m^{-2}$. The remaining charge balance equations are

$$\sigma_o + \sigma_a + \sigma_\beta + \sigma_d = 0 \tag{47}$$

$$\sigma_o = \frac{N_S\{K_H[H^+]\exp(-F\Psi_o/RT) - K_{OH}[OH^-]\exp(F\Psi_o/RT)\}}{1 + K_H[H^+]\exp(-F\Psi_o/RT) + K_{OH}[OH^-]\exp(F\Psi_o/RT)} \tag{48}$$

$$\sigma_a = \frac{N_T \sum_i Z_i K_i a_i \exp(-Z_i F\Psi_a/RT)}{1 + \sum_i K_i a_i \exp(-Z_i F\Psi_a/RT)} \tag{49}$$

$$\sigma_\beta = \frac{N_S\{[K_{cat}[C^+]\exp(-F\Psi_\beta/RT) - K_{an}[A^-]\exp(F\Psi_\beta/RT)]\}}{1 + K_{cat}[C^+]\exp(-F\Psi_\beta/RT) + K_{an}[A^-]\exp(F\Psi_\beta/RT)} \tag{50}$$

where N_S is the maximum surface charge density ($mol_c\ m^{-2}$), N_T is the maximum adsorption of specifically adsorbed ions ($mol_c\ m^{-2}$), K_i is the binding constant, a_i is the activity, and Z_i is the charge of the ith specifically adsorbed ion.

In the Stern VSC–VSP approach, no mass balance is carried out. Despite the fact that their values are available experimentally, the total number of surface sites and the maximum adsorption are adjustable parameters. In solving the set of above equations, values of N_S, N_T, the binding constants K_i, and the capacitances C_i, are chosen to optimize model fit to the data. The charge densities σ_i and the electrostatic potentials Ψ_i subsequently are calculated via a computer program (Barrow, 1979).

Sposito (1984b) does not consider the Stern VSC–VSP model to be a chemical model because it lacks chemical reactions and equilibrium constant expressions. The model is not self-consistent chemically because it does not reduce to the triple layer model when "strongly adsorbed" ions are absent from the a-plane (Sposito, 1984b).

E. Generalized Two-Layer Model

The generalized two-layer model was developed by Dzombak and Morel (1990) as an expansion of the diffuse layer model proposed by Stumm and co-workers (1970; Huang and Stumm, 1973). Like the constant capacitance model, the generalized two-layer model assumes that all surface complexes are inner-sphere complexes. The surface charge expression is

the same as in the constant capacitance model, Eq. (2). The generalized two-layer model is like the triple layer model and the Stern VSC–VSP model in that it considers a diffuse layer. The model is named after the two planes of charge used to represent the surface. All surface complexes are placed into the surface plane. The diffuse layer commences at the *d*-plane and extends into the solution phase. Figure 4 provides a diagram of the surface–solution interface in the generalized two-layer model. As in the triple-layer model, the surface charge, σ, has units of C m^{-2}. The relationship between the surface charge and the surface potential is defined by electric double-layer theory, Eq. (21). No capacitance parameters are required in the generalized two-layer model. The model employs the infinite dilution reference state for the solution and a reference state of zero charge and potential for the surface (Dzombak and Morel, 1990).

The surface reactions considered in the generalized two-layer model include Eqs. (4) and (5). Metal ion adsorption is considered to occur on two types of sites: a small set of high-affinity "strong" sites and a large set of low-affinity "weak" sites. Adsorption on both sets of sites takes the form of Eq. (6):

$$S^sOH + M^{m+} \rightleftarrows S^sOM^{(m-1)} + H^+ \tag{51}$$

$$S^wOH + M^{m-} \rightleftarrows S^wOM^{(m-1)} + H^+ \tag{52}$$

where s represents the high-affinity and w represents the low-affinity sites. In the generalized two-layer model no bidentate surface species [Eq. (7)

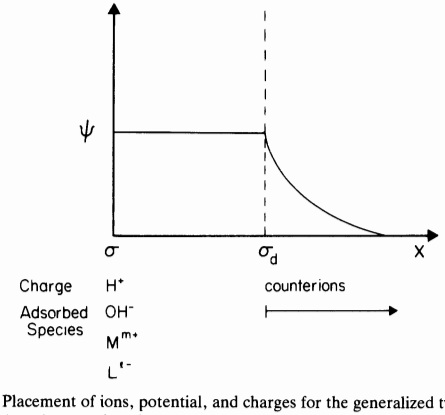

Figure 4. Placement of ions, potential, and charges for the generalized two-layer model. After Dzombak and Morel (1990), reproduced with permission from John Wiley and Sons.

for metals or Eq. (9) for ligands] are defined. The ligand exchange reactions are

$$\mathrm{SOH} + \mathrm{L}^{l-} + \mathrm{H}^{+} \rightleftarrows \mathrm{SL}^{(l-1)-} + \mathrm{H_2O} \tag{53}$$

$$\mathrm{SOH} + \mathrm{L}^{l-} + 2\mathrm{H}^{+} \rightleftarrows \mathrm{SHL}^{(l-2)-} + \mathrm{H_2O} \tag{54}$$

For ligand exchange, it is not necessary to specify two sets of binding sites. The intrinsic conditional equilibrium constants for the generalized two-layer model are similar to those for the constant capacitance model. Equations (10) and (11) describe protonation and dissociation. Metal surface complexation is described by two constants like Eq. (12), for the reaction of both strong sites, $\mathrm{S^sOH}$, and weak sites, $\mathrm{S^wOH}$. The intrinsic conditional equilibrium constants for ligand exchange are

$$K_{\mathrm{L}}^{1}(\mathrm{int}) = \frac{[\mathrm{SL}^{(l-1)-}]}{[\mathrm{SOH}][\mathrm{L}^{l-}][\mathrm{H}^{+}]} \exp[-(l-1)F\Psi/RT] \tag{55}$$

$$K_{\mathrm{L}}^{2}(\mathrm{int}) = \frac{[\mathrm{SHL}^{(l-2)-}]}{[\mathrm{SOH}][\mathrm{L}^{l-}][\mathrm{H}^{+}]^{2}} \exp[-(l-2)F\Psi/RT] \tag{56}$$

Application of the generalized two-layer model to systems containing both metal and ligand species is difficult because the pool of binding sites for protonation–dissociation and ligand adsorption is split into two sets of binding sites of different affinity for metal adsorption. For this reason, mass balance and charge balance equations will be provided separately for metal and ligand adsorption. For metal surface complexation these equations are

$$[\mathrm{S^sOH}]_{\mathrm{T}} = [\mathrm{S^sOH}] + [\mathrm{S^sOH_2^+}] + [\mathrm{S^sO^-}] + [\mathrm{S^sOM}^{(m-1)}] \tag{57}$$

$$[\mathrm{S^wOH}]_{\mathrm{T}} = [\mathrm{S^wOH}] + [\mathrm{S^wOH_2^+}] + [\mathrm{S^wO^-}] + [\mathrm{S^wOM}^{(m-1)}] \tag{58}$$

$$\sigma = \frac{F}{Sa}\{[\mathrm{S^sOH_2^+}] + [\mathrm{S^wOH_2^+}] + (m-1)[\mathrm{S^sOM}^{(m-1)}] + (m-1)[\mathrm{S^wOM}^{(m-1)}] - [\mathrm{S^sO^-}] - [\mathrm{S^wO^-}]\} \tag{59}$$

For ligand surface complexation the equations are

$$[\mathrm{SOH}]_{\mathrm{T}} = [\mathrm{SOH}] + [\mathrm{SOH_2^+}] + [\mathrm{SO^-}] + [\mathrm{SL}^{(l-1)-}] + [\mathrm{SHL}^{(l-2)-}] \tag{60}$$

$$\sigma = \frac{F}{Sa}\{[\mathrm{SOH_2^+}] - [\mathrm{SO^-}] - (l-1)[\mathrm{SL}^{(l-1)-}] - (l-2)[\mathrm{SHL}^{(l-2)-}]\} \tag{61}$$

These equations can be solved with a computer program or approximated using hand calculations as described by Dzombak and Morel (1990).

F. One-p*K* Model

The one-p*K* model was first proposed by Bolt and van Riemsdijk (1982) and was developed by van Riemsdijk and co-workers (1986, 1987; Hiemstra *et al.*, 1987; van Riemsdijk and van der Zee, 1991). In the one-p*K* model the surface functional group is defined as a singly coordinated oxygen atom that carries either one or two protons, leading to surface sites SOH and SOH_2, respectively. The constant capacitance model, the triple-layer model, and the generalized two-layer model could all be written based on the one-p*K* concept for singly coordinated oxygen atoms. The Stern model of the surface–solution interface has been chosen for the one-p*K* model (van Riemsdijk *et al.*, 1987). This model assumes that protons and hydroxyl ions form inner-sphere surface complexes and reside in the *o*-plane close to the surface. Cations and anions form outer-sphere surface complexes at the Stern plane, or *d*-plane. The Stern plane indicates the start of the diffuse double layer. The surface charge on a particle is equal to the net proton charge:

$$\sigma = \sigma_H \tag{62}$$

Figure 5 provides a diagram of the surface–solution interface in the one-p*K* Stern model. Because the one-p*K* Stern model contains two planes, two

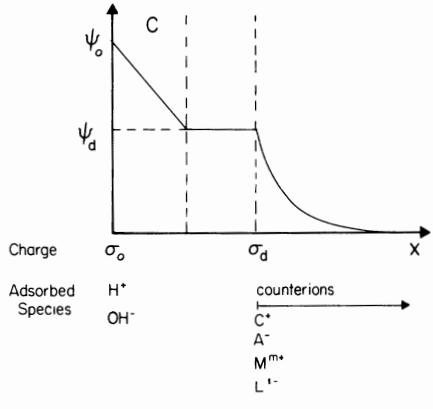

Figure 5. Placement of ions, potentials, charges, and capacitance for the one-p*K* Stern model. After Westall (1986), reproduced with permission from the American Chemical Society.

charge–potential relations are used (Hiemstra *et al.*, 1987):

$$\sigma_o = C(\Psi_o - \Psi_d) \tag{63}$$

where the units of σ are C m^{-2}. The relation between charge and potential in the Stern or *d*-plane is provided by diffuse double-layer theory, Eq. (21).

The surface complexation reactions defined in the one-p*K* model are (van Riemsdijk *et al.*, 1987; Hiemstra *et al.*, 1987; van Riemsdijk and van der Zee, 1991)

$$\mathrm{SOH^{1/2-} + H^+ \rightleftarrows SOH_2^{1/2+}} \tag{64}$$

$$\mathrm{SOH^{1/2-} + M^{m+} \rightleftarrows SOH^{1/2-} - M^{m+}} \tag{65}$$

$$\mathrm{SOH^{1/2-} + M^{m+} + H_2O \rightleftarrows SOH^{1/2-} - MOH^{(m-1)} + H^+} \tag{66}$$

$$\mathrm{SOH_2^{1/2+} + L^{l-} \rightleftarrows SOH_2^{1/2+} - L^{l-}} \tag{67}$$

$$\mathrm{SOH^{1/2-} + C^+ \rightleftarrows SOH^{1/2-} - C^+} \tag{68}$$

$$\mathrm{SOH_2^{1/2+} + A^- \rightleftarrows SOH_2^{1/2+} - A^-} \tag{69}$$

The intrinsic equilibrium constants for the one-p*K* model are as follows (van Riemsdijk *et al.*, 1987; Hiemstra *et al.*, 1987; van Riemsdijk and van der Zee, 1991):

$$K_{\mathrm{H}} = \frac{[\mathrm{SOH_2^{1/2+}}]}{[\mathrm{SOH^{1/2-}}][\mathrm{H^+}]} \exp[F\Psi_o/RT] \tag{70}$$

$$K_{\mathrm{M}}^1 = \frac{[\mathrm{SOH^{1/2-} - M^{m+}}]}{[\mathrm{SOH^{1/2-}}][\mathrm{M^{m+}}]} \exp[mF\Psi_d/RT] \tag{71}$$

$$K_{\mathrm{M}}^2 = \frac{[\mathrm{SOH^{1/2-} - MOH^{(m-1)}}][\mathrm{H^+}]}{[\mathrm{SOH^{1/2-}}][\mathrm{M^{m+}}]} \exp[(m-1)F\Psi_d/RT] \tag{72}$$

$$K_{\mathrm{L}} = \frac{[\mathrm{SOH_2^{1/2+} - L^{l-}}]}{[\mathrm{SOH_2^{1/2+}}][\mathrm{L^{l-}}]} \exp[-lF\Psi_d/RT] \tag{73}$$

$$K_{\mathrm{C^+}} = \frac{[\mathrm{SOH^{1/2-} - C^+}]}{[\mathrm{SOH^{1/2-}}][\mathrm{C^+}]} \exp[F\Psi_{\mathrm{d}}/RT] \tag{74}$$

$$K_{\mathrm{A^-}} = \frac{[\mathrm{SOH_2^{1/2+} - A^-}]}{[\mathrm{SOH_2^{1/2+}}][\mathrm{A^-}]} \exp[-F\Psi_d/RT] \tag{75}$$

The mass balance of singly coordinated oxygen atoms N_{S} is

$$N_{\mathrm{S}} = [\mathrm{SOH^{1/2-}}] + [\mathrm{SOH_2^{1/2+}}] \tag{76}$$

The surface charge balance equation is

$$\sigma_o = 1/2[SOH_2^{1/2+} - SOH^{1/2-}] \quad (77)$$

The set of equations can be solved using a computer algorithm based in part on the method of Westall (1980).

III. APPLICATION OF MODELS TO PROTONATION–DISSOCIATION REACTIONS ON OXIDES, CLAY MINERALS, AND SOILS

A. Constant Capacitance Model

The constant capacitance model has been used to describe the amphoteric acid–base behavior of inorganic surface hydroxyl groups on oxide minerals. The adsorption of protons and hydroxyl ions has been investigated on the following minerals: amorphous silica (Schindler and Kamber, 1968; Osaki *et al.*, 1990b), anatase (TiO_2) (Schindler and Gamsjäger, 1972), aluminum oxide (γ-Al_2O_3) (Hohl and Stumm, 1976; Kummert and Stumm, 1980), bayerite [γ-$Al(OH)_3$] (Pulfer *et al.*, 1984), boehmite (γ-AlOOH) (Bleam *et al.*, 1991), goethite (α-FeOOH) (Sigg, 1979; Lövgren *et al.*, 1990), magnetite (Fe_3O_4) (Regazzoni *et al.*, 1983), and amorphous iron oxide (Farley *et al.*, 1985).

In general, values of the intrinsic protonation and dissociation constants described by Eqs. (10) and (11) can be obtained from alkimetric or acidimetric titration curves carried out in the absence of specifically adsorbing metal or ligand ions (Stumm *et al.*, 1980). In this analysis, the assumption is made that σ, the net surface charge, is equal to $[SOH_2^+]$ below the zero point of charge, ZPC, and is equal to $-[SO^-]$ above the ZPC. The ZPC is defined as the pH value at which surface charge is zero. In the constant capacitance model the ZPC is also defined as

$$ZPC = 1/2[\log K_+(\text{int}) - \log K_-(\text{int})] \quad (78)$$

A plot of the logarithm of the conditional equilibrium constant, ${}^cK_\pm$, versus surface charge, σ, will yield the logarithm of the intrinsic equilibrium constant, $K_\pm(\text{int})$, upon linear extrapolation to zero surface charge. The conditional equilibrium constants for protonation–dissociation are defined as

$${}^cK_+ = [SOH_2^+]/([SOH][H^+]) \quad (79)$$

$${}^cK_- = [SO^-][H^+]/[SOH] \quad (80)$$

By combining Eq. (10) with Eq. (79), and Eq. (11) with Eq. (80), one can relate the intrinsic protonation and dissociation constants and the conditional protonation and dissociation constants:

$$K_{\pm}(\text{int}) = {}^{c}K_{\pm} \exp(\pm F\Psi/RT) \tag{81}$$

where the positive sign represents the protonation constant and the negative sign represents the dissociation constant. Upon substituting for surface potential, Ψ, from Eq. (2), taking the logarithms of both sides, and solving for $\log {}^{c}K_{\pm}$, the following equation is obtained:

$$\log {}^{c}K_{\pm} = \log K_{\pm}(\text{int}) \pm \sigma F^2/[CSaRT(\ln 10] \tag{82}$$

By plotting the titration data as $\log {}^{c}K_{\pm}$ versus σ, an estimate of $\log K_{\pm}(\text{int})$ is obtained from the y intercept, where $\sigma = 0$. The capacitance parameter can be obtained from the slope of such a plot.

Values of $\log K_{\pm}(\text{int})$ have been obtained in the above fashion for anatase (Schindler and Gamsjäger, 1972), aluminum oxide (Hohl and Stumm, 1976; Kummert and Stumm, 1980), goethite (Sigg, 1979), magnetite (Regazzoni *et al.*, 1983), and amorphous iron oxide (Farley *et al.*, 1985). Figure 6 provides an example of the linear extrapolation technique for the titanium oxide, anatase (Schindler and Gamsjäger, 1972). Table I presents values of $\log K_{\pm}(\text{int})$ obtained by various authors using the linear extrapolation technique. The assumptions of the linear extrapolation tech-

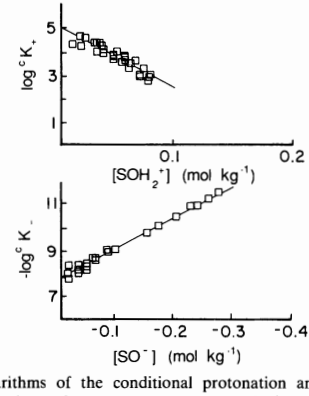

Figure 6. The logarithms of the conditional protonation and dissociation constants as a function of surface charge for anatase, TiO_2, $\log K_{+}(\text{int}) = 4.98$, $\log K_{-}(\text{int}) = -7.80$, $C_{+} = 1.10$ F m^{-2}, $C_{-} = 2.22$ F m^{-2}. From Schindler and Gamsjäger (1972).

Table I

Values of Intrinsic Protonation and Dissociation Constants Obtained with the Constant Capacitance Model Using Linear Extrapolation[a]

Solid	Ionic medium	$\log K_+(\text{int})$	$\log K_-(\text{int})$	Reference
Aluminum oxides				
γ-Al_2O_3	0.1 *M* $NaClO_4$	7.2	−9.5	Hohl and Stumm (1976)
γ-Al_2O_3	0.1 *M* $NaClO_4$	7.4	−10.0	Kummert and Stumm (1980)
γ-$Al(OH)_3$	1 *M* KNO_3	5.24	−8.08	Pulfer *et al.* (1984)
γ-AlOOH	0.001 *M* KNO_3	5.6	−8.6	Bleam *et al.* (1991)
Iron oxides				
$Fe(OH)_3$(am)	0.1 *M* $NaNO_3$	6.6	−9.1	Farley *et al.* (1985)
α-FeOOH	0.1 *M* $NaClO_4$	6.4	−9.25	Sigg (1979)
α-FeOOH	0.1 *M* $NaClO_4$	5.9	−8.65	Sigg (1979)
Fe_3O_4	0.1 *M* KNO_3	5.19	−8.44	Regazzoni *et al.* (1983)
Fe_3O_4	0.01 *M* KNO_3	4.66	−8.81	Regazzoni *et al.* (1983)
Fe_3O_4	0.001 *M* KNO_3	4.40	−8.97	Regazzoni *et al.* (1983)
Silicon oxides				
SiO_2(am)	0.1 *M* $NaClO_4$	—	−6.8	Schindler and Kamber (1968)
SiO_2(am)	1.0 *M* LiCl	—	−6.57	Sigg (1973)
SiO_2(am)	1.0 *M* $NaClO_4$	—	−6.71	Sigg (1973)
SiO_2(am)	1.0 *M* CsCl	—	−5.71	Sigg (1973)
SiO_2(am)	1.0 *M* $NaClO_4$	—	−5.7	Fürst (1976)
SiO_2(am)	1.0 *M* $NaClO_4$	—	−6.56	Gisler (1980)
Quartz	0.1 *M* $NaClO_4$	—	−8.4	Osaki *et al.* (1990b)
Titanium oxides				
Anatase	3.0 *M* $NaClO_4$	4.98	−7.80	Schindler and Gamsjäger (1972)
Rutile	1.0 *M* $NaClO_4$	4.46	−7.75	Fürst (1976)
Rutile	1.0 *M* $NaClO_4$	4.13	−7.39	Gisler (1980)
Clay minerals				
Kaolinite	0.01 *M* NaCl	2.4	−6.5	Motta and Miranda (1989)
Montmorillonite	0.01 *M* NaCl	2.0	−5.6	Motta and Miranda (1989)
Illite	0.01 *M* NaCl	7.5	−11.7	Motta and Miranda (1989)

[a] Adapted from Schindler and Stumm (1987) and expanded.

nique lead to large differences between the value of $\log K_+(\text{int})$ and the absolute value of $\log K_-(\text{int})$ (Westall, 1986).

A weakness of the constant capacitance model is that the value of the capacitance, C_+, obtained from linear extrapolations below the ZPC is usually not the same as the value, C_-, obtained above the ZPC. Table II provides values of $C_\pm$ obtained from linear extrapolations of titration data for the iron oxide goethite and the aluminum oxide boehmite. It is clear that for two batches of goethite and for three experiments on the same batch of boehmite, the capacitance exhibits great variability even when variations in $\log K_\pm(\text{int})$ are small. Because of this variability, single values

Table II

Values of Capacitance Obtained with the Constant Capacitance Model Using Linear Extrapolation

Solid	$\log K_+$(int)	C_+ (F m^{-2})[a]	$\log K_-$(int)	C_- (F m^{-2})[b]
Geothite[c]				
α-FeOOH(I)	5.9	1.5	−8.65	3.5
α-FeOOH(II)	6.4	2.7	−9.25	4.4
Boehmite γ-AlOOH[d]				
Experiment 1	5.8	1.3	−8.5	0.7
Experiment 2	5.5	2.8	−8.7	0.9
Experiment 3	5.5	2.9	−8.8	2.0

[a] C_+ is obtained from the slope of extrapolation for $\log K_+$(int).
[b] C_- is obtained from the slope of extrapolation for $\log K_-$(int).
[c] Calculated from Sigg (1979) data for two batches of goethite.
[d] Calculated from Bleam *et al.* (1991) data for three experiments of one batch of boehmite.

of C, considered optimum [e.g., for goethite $C = 1.8$ F m^{-2} (Sigg, 1979) and for aluminum oxide $C = 1.06$ F m^{-2} (Westall and Hohl, 1980)], have often been used in applications of the constant capacitance model. The ability of the constant capacitance model to describe potentiometric titration data on an oxide mineral using the protonation–dissociation constants obtained from the extrapolation method is indicated in Fig. 7. It is clear that the model represents the titration data very well (Schindler and Gamsjäger, 1972).

Values for the protonation–dissociation constants can also be obtained by optimization of potentiometric titration data using a computer program such as FITEQL (Westall, 1982). FITEQL uses a simultaneous, nonlinear, least-squares method to fit equilibrium constants to experimental data. FITEQL also contains surface complexation models, including the constant capacitance model, to describe surface complexation. Application of the FITEQL program to the titration data of Bleam *et al.* (1991) produced values of $\log K_+$(int) = 6.02 and $\log K_-$(int) = −8.45. It can be seen that the difference between the absolute value of $\log K_-$(int) and the value of $\log K_+$(int), $\Delta \log K_\pm$(int), is less for the nonlinear FITEQL optimization than for the linear extrapolation technique (values provided in Table I).

The constant capacitance model has been modified and extended to describe potentiometric titration data on the clay mineral kaolinite (Schindler *et al.*, 1987). In addition to the amphoteric surface hydroxyl group, SOH, Schindler *et al.* (1987) postulated a second surface functional group, XH, which is weakly acidic and can undergo ion exchange with cations from the background electrolyte. An additional assumption is made that cations

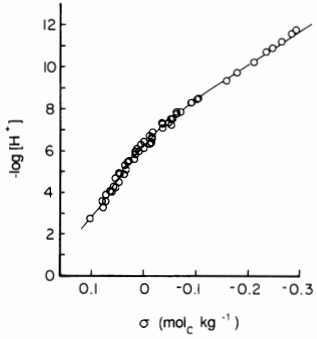

Figure 7. Fit of the constant capacitance model to potentiometric titration data on anatase, TiO_2. Model result is obtained using $\log K_{\pm}(\text{int})$ from linear extrapolation (Fig. 6) and is represented by a solid line. From Schindler and Gamsjäger (1972).

from the background electrolyte can bind with SOH, forming weak outer-sphere surface complexes. Thus, in addition to Eqs. (4) and (5), the following reactions are defined:

$$\text{SOH} + \text{C}^+ \rightleftarrows \text{SO}^- - \text{C}^+ + \text{H}^+ \tag{83}$$

$$\text{XH} + \text{C}^+ \rightleftarrows \text{XC} + \text{H}^+ \tag{84}$$

In addition to Eqs. (10) and (11), the equilibrium constants for this application are

$$K_{\text{C}^+} = \frac{[\text{SO}^- - \text{C}^+][\text{H}^+]}{[\text{SOH}][\text{C}^+]} \tag{85}$$

$$K_{\text{XC}^+} = \frac{[\text{XC}][\text{H}^+]}{[\text{XH}][\text{C}^+]} \tag{86}$$

The fit of the constant capacitance model to titration data on hydrogen kaolinite is indicated in Fig. 8. Values of $K_{\pm}(\text{int})$, K_{C^+}, and K_{XC^+} were optimized using the computer program FITEQL (Westall, 1982). Schindler *et al.* (1987) considered the model fit acceptable but suggested that systematic errors might be due to extension of the Davies equation to ionic strength up to 1 *M* and to the use of the same capacitance value for all ionic strengths.

An alternative method for the description of potentiometric titration data on clay minerals was used by Motta and Miranda (1989). These authors used the same modeling approach on these heterogeneous systems as

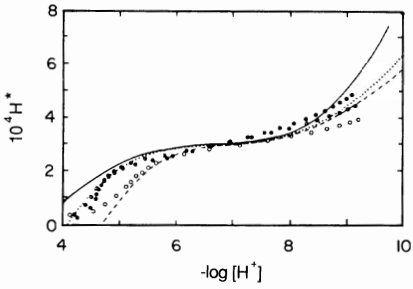

Figure 8. Fit of the constant capacitance model to potentiometric titration data on hydrogen kaolinite. H^* represents the number of hydrogen ions originating from the kaolinite–water interface; $\log K_+(\text{int}) = 4.37$, $\log K_-(\text{int}) = -9.18$, $\log K_{Na^+} = -9.84$, $\log K_{XNa^+} = -2.9$, $C = 2.2$ F m^{-2}. Model results are represented by a dashed line ($I = 0.01$ M $NaClO_4$), dotted line ($I = 0.1$ M $NaClO_4$), and solid line ($I = 1.0$ M $NaClO_4$). From Schindler *et al.* (1987).

had been used for oxide minerals. Values for protonation–dissociation constants were obtained by extrapolating to zero surface charge as described above. Values of $\log K_\pm(\text{int})$ for the clay minerals kaolinite, montmorillonite, and illite are given in Table I.

B. Triple-Layer Model

The triple-layer model has been used to describe the amphoteric behavior of inorganic surface hydroxyl groups in inert background electrolytes. The adsorption of protons and hydroxyl ions and inert background electrolytes has been investigated on the following surfaces: goethite (α-FeOOH) (Davis *et al.*, 1978; Balistrieri and Murray, 1979, 1981; Hsi and Langmuir, 1985; Hayes, 1987), amorphous iron oxide (Davis and Leckie, 1978; Hsi and Langmuir, 1985), magnetite (Fe_3O_4) and zirconium dioxide (Regazzoni *et al.*, 1983), titanium oxide (Davis *et al.*, 1978; Sprycha, 1984), manganese oxide (δ-MnO_2) (Balistrieri and Murray, 1982a; Catts and Langmuir, 1986), colloidal silica (Milonjić, 1987), α-Al_2O_3 (Smit and Holten, 1980), γ-Al_2O_3 (Sprycha, 1989a,b), boehmite (γ-AlOOH) (Wood *et al.*, 1990), and soils (Charlet and Sposito, 1987).

Values of the intrinsic protonation and dissociation constants provided in Eqs. (10) and (11) and the intrinsic surface complexation constants for the background electrolyte provided in Eqs. (32) and (33) can be obtained from potentiometric titration curves carried out in the absence of specific

metal or ligand adsorption. The assumption is made that σ_o, the surface charge density in the surface o-plane, is equal to (F/Sa) $([SOH_2^+] + [SOH_2^+ - A^-])$ below the ZPC and is equal to $(-F/Sa)([SO^-] + [SO^- - C^+])$ above the ZPC. Intrinsic equilibrium constant values are obtained by linear extrapolation (Davis *et al.*, 1978) or by the double-extrapolation method (James *et al.*, 1978). The additional assumptions are made that at low ionic strength σ_o is equal to $(F/Sa)[SOH_2^+]$ below the ZPC and is equal to $(-F/Sa)[SO^-]$ above the ZPC and that at high ionic strength, σ_o is equal to $(F/Sa)[SOH_2^+ - A^-]$ below the ZPC and is equal to $(-F/Sa)[SO^- - C^+]$ above the ZPC. A plot of the logarithm of the conditional equilibrium constant ${}^cK_\pm$, ${}^cK_{C^-}$, or ${}^cK_{A^-}$ versus surface charge will yield the logarithm of the intrinsic equilibrium constant $K_\pm(\text{int})$, $K_{C^-}(\text{int})$, or $K_{A^-}(\text{int})$ upon extrapolation.

The conditional equilibrium constants for protonation–dissociation are defined in Eqs. (79) and (80) and are related to the intrinsic protonation–dissociation constants by Eq. (81). The conditional surface complexation constants for the background electrolyte are

$$ {}^cK_{C^-} = \frac{[SO^- - C^+][H^+]}{[SOH][C^+]} \tag{87} $$

$$ {}^cK_{A^-} = \frac{[SOH_2^+ - A^-]}{[SOH][H^+][A^-]} \tag{88} $$

By combining Eq. (32) with Eq. (87), and Eq. (33) with Eq. (88), one can relate the intrinsic surface complexation constants and the conditional surface complexation constants:

$$ K_{C^-}(\text{int}) = {}^cK_{C^-} \exp[F(\Psi_\beta - \Psi_o)/RT] \tag{89} $$

$$ K_{A^-}(\text{int}) = {}^cK_{A^-} \exp[F(\Psi_o - \Psi_\beta)/RT] \tag{90} $$

upon taking the logarithms of both sides of Eqs. (81), (89) and (90) and solving for $\log {}^cK_i$ the following equations are obtained:

$$ \log {}^cK_\pm = \log K_\pm(\text{int}) \pm \frac{F\Psi_o}{RT \ln(10)} \tag{91} $$

$$ \log {}^cK_{C^-} = \log K_{C^-}(\text{int}) + \frac{F(\Psi_o - \Psi_\beta)}{RT \ln(10)} \tag{92} $$

$$ \log {}^cK_{A^-} = \log K_{A^-}(\text{int}) + \frac{F(\Psi_\beta - \Psi_o)}{RT \ln(10)} \tag{93} $$

Fractional surface charges are defined for a positive surface below the ZPC as

$$ \alpha_+ = \sigma_o / N_S \tag{94} $$

and for a negative surface above the ZPC as

$$\alpha_- = -\sigma_o/N_S \tag{95}$$

where $N_S = (F/Sa)[SOH]_T$ is the surface mass balance in units of C m^{-2} (Davis *et al.*, 1978). By plotting the titration data of $\log {}^cK_i$ versus α_+ or α_-, an estimate of $\log K_i(\text{int})$ is obtained from the y intercept, where α_+ or $\alpha_- = 0$ when $\sigma_o = \Psi_o = 0$. The capacitance parameter, C_1, can be extracted from the slopes of such plots using Eqs. (92) and (93) (Smit and Holten, 1980; Sposito, 1984a; Blesa *et al.*, 1984b). Values of $\log K_i(\text{int})$ for protonation–dissociation and background electrolyte surface complexation have been obtained by linear extrapolation for goethite (Davis *et al.*, 1978; Hayes, 1987), amorphous iron oxide (Davis and Leckie, 1978), magnetite and zirconium dioxide (Regazzoni *et al.*, 1983), titanium oxide (Davis *et al.*, 1978), and soils (Charlet and Sposito, 1987). Figure 9 provides an example of the linear extrapolation technique for amorphous iron oxide (Davis and Leckie, 1978).

Using the definitions Eqs. (94) and (95) and the previous assumptions, expressions for α_+ and α_- can be calculated and are provided in Table III. Equations (91), (92), and (93) can now be written in terms of α_+ and α_- (Davis *et al.*, 1978):

$$\log K_+(\text{int}) = \text{pH} + \log\left(\frac{\alpha_+}{1-\alpha_+}\right) + \frac{F\Psi_o}{RT\ln(10)} \tag{96}$$

$$\log K_-(\text{int}) = -\text{pH} + \log\left(\frac{\alpha_-}{1-\alpha_-}\right) - \frac{F\Psi_o}{RT\ln(10)} \tag{97}$$

$$\log K_{C^+}(\text{int}) = -\text{pH} + \log\left(\frac{\alpha_-}{1-\alpha_-}\right) - \log[C^+] + \frac{F(\Psi_\beta - \Psi_o)}{RT\ln(10)} \tag{98}$$

$$\log K_{A^-}(\text{int}) = \text{pH} + \log\left(\frac{\alpha_+}{1-\alpha_+}\right) - \log[A^-] + \frac{F(\Psi_o - \Psi_\beta)}{RT\ln(10)} \tag{99}$$

In the double-extrapolation technique developed by James *et al.* (1978), two extrapolations are carried out. The intrinsic protonation–dissociation constants are obtained from extrapolation of Eqs. (96) and (97) to α_+ or $\alpha_- = 0$ and zero electrolyte concentration: $\sigma_o = 0$, $C = 0$, $\Psi_o = \Psi_\beta$. The intrinsic surface complexation constants are obtained from extrapolation of Eqs. (98) and (99) to α_+ or $\alpha_- = 0$ and infinite electrolyte concentration: $\sigma_o = 0$, $C = 1\ M$, $\Psi_o = \Psi_\beta$. Again, as in the linear extrapolation procedure, the capacitance parameter, C_1, can be obtained from the slopes of the plots of Eqs. (98) and (99). Values of $\log K_i(\text{int})$ for protonation–dissociation and background electrolyte surface complexation have been obtained by double extrapolation for goethite (Balistrieri and Murray, 1979, 1981;

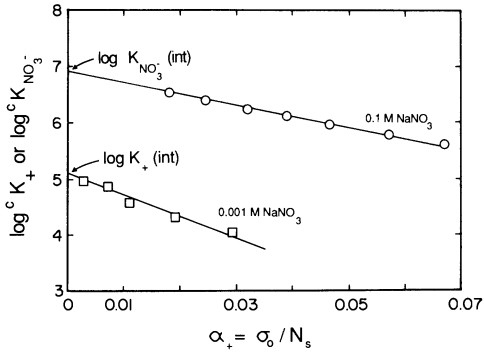

Figure 9. The logarithms of the conditional protonation constant and the anion surface complexation constant for the background electrolyte as a function of fractional surface charge for amorphous iron oxide; $\log K_+(\text{int}) = 5.1$, $\log K_{NO_3^-}(\text{int}) = 6.9$. From Davis and Leckie (1978), based on experimental data of Yates (1975).

Hsi and Langmuir, 1985), amorphous iron oxide (Hsi and Langmuir, 1985), boehmite (Wood *et al.*, 1990), manganese oxide (Balistrieri and Murray, 1982a; Catts and Langmuir, 1986), titanium oxide (James and Parks, 1982), and colloidal silica (Milonjić, 1987). Figure 10 provides an example of the double-extrapolation procedure for manganese oxide (Balistrieri and Murray, 1982a).

Table III

Approximations for Estimating Intrinsic Protonation–Dissociation and Surface Complexation Constants by Extrapolation

Ionic strength	pH < ZPC	pH > ZPC
Low	$\sigma_o = (F/Sa)[SOH_2^+]$	$\sigma_0 = (-F/Sa)[SO^-]$
	$[SOH] = [SOH]_T - [SOH_2^+]$	$[SOH] = [SOH]_T - [SO^-]$
	$\alpha_+ = [SOH_2^+]/[SOH]_T$	$\alpha_- = [SO^-]/[SOH]_T$
	$[SOH_2^+]/[SOH] = \alpha_+/(1 - \alpha_+)$	$[SO^-]/[SOH] = \alpha_-/(1 - \alpha_-)$
High	$\sigma_o = (F/Sa)[SOH_2^+ - A^-]$	$\sigma_o = (-F/Sa)[SO^- - C^+]$
	$[SOH] = [SOH]_T - [SOH_2^+ - A^-]$	$[SOH] = [SOH_T] - [SO^- - C^+]$
	$\alpha_+ = [SOH_2^+ - A^-]/[SOH]_T$	$\alpha_- = [SO^- - C^+]/[SOH]_T$
	$[SOH_2^+ - A^-]/[SOH] = \alpha_+/(1 - \alpha_+)$	$[SO^- - C^+]/[SOH] = \alpha_-/(1 - \alpha_-)$

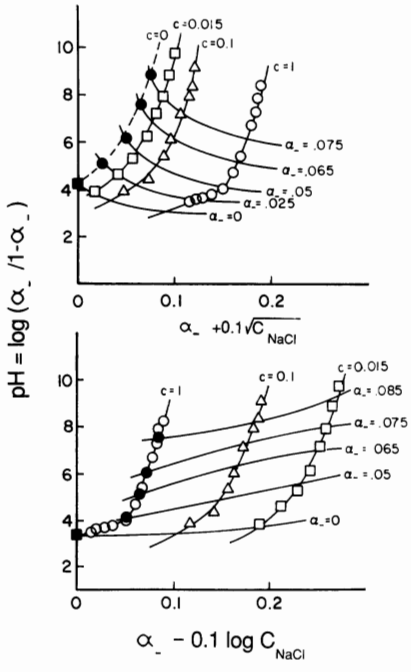

Figure 10. Determination of the intrinsic dissociation constant (top) and cation surface complexation constant for the background electrolyte (bottom) for manganese oxide. The fractional surface charge α_- is multiplied by an arbitrary constant solely to separate data of different concentrations; $\log K_-(\text{int}) = -4.2$, $\log K_{Na^+}(\text{int}) = -3.3$. From Balistrieri and Murray (1982a).

An alternative method of determining intrinsic protonation–dissociation constants and surface complexation constants for the background electrolyte has been developed (Sprycha, 1983; 1989a,b; Sprycha and Szczypa, 1984). In this method the assumption is made that the zeta potential, ζ, is equal to the diffuse layer potential, Ψ_d, at low ionic strength. The protonation–dissociation constants are determined from zeta potential data using a double straight-line extrapolation method (Sprycha and Szczypa, 1984). The assumption is made that σ_d, the diffuse layer charge, is equal to $(F/Sa)[SOH_2^+]$ below the ZPC and is equal to $(-F/Sa)[SO^-]$ above the

ZPC. The intrinsic conditional protonation–dissociation constants are calculated from the following equations obtained by taking the logarithm of both sides of Eqs. (79) and (80) (Sprycha and Szczypa, 1984):

$$\log {}^{c}K_{+} = \mathrm{pH} + \log[\mathrm{SOH}_2^+] - \log[\mathrm{SOH}] \quad (100)$$

$$\log {}^{c}K_{-} = -\mathrm{pH} + \log[\mathrm{SO}^-] - \log[\mathrm{SOH}] \quad (101)$$

The straight lines are extrapolated to the pH of the ZPC and then to zero electrolyte concentration to obtain the intrinsic protonation–dissociation constants.

The surface complexation constants for the background electrolyte are calculated from extrapolation of direct measurements of adsorption densities to zero surface charge (Sprycha, 1983, 1984, 1989a,b). In the Sprycha method the following equations, obtained by taking the logarithm of both sides of Eqs. (87) and (88), are used (Sprycha, 1989b):

$$\log {}^{c}K_{\mathrm{C}^+} = -\mathrm{pH} - \log[\mathrm{SOH}] - \log[\mathrm{C}^+] + \log[\mathrm{SO}^- - \mathrm{C}^+] \quad (102)$$

$$\log {}^{c}K_{\mathrm{A}^-} = \mathrm{pH} - \log[\mathrm{SOH}] - \log[\mathrm{A}^-] + \log[\mathrm{SOH}_2^+ - \mathrm{A}^-] \quad (103)$$

The intrinsic surface complexation constants are obtained by extrapolating conditional surface complexation constants as a function of pH to the ZPC. The capacitance parameter, C_1, can be obtained from the slope of charge versus potential curves [Eq. (19)] calculated using potential differences determined with Eqs. (92) and (93). The capacitance parameter, C_2, can be obtained after determining the potential distribution within the electric double layer using electrokinetic data and Eq. (20). Values of $\log K_{\pm}$(int), $\log K_{\mathrm{C}^+}$(int), $\log K_{\mathrm{A}^-}$(int), C_1, and C_2 have been obtained with the Sprycha method for anatase, TiO_2 (Sprycha, 1984), and aluminum oxide (γ-Al_2O_3) (Sprycha, 1989a,b). Figure 11 indicates the extrapolation techniques of the Sprycha method for aluminum oxide (Sprycha, 1989a,b).

Table IV presents values of $\log K_{\pm}$, $\log K_{\mathrm{C}^+}$(int), and $\log K_{\mathrm{A}^-}$(int) obtained by various researchers using all three extrapolation methods. As can be seen from Table IV for goethite and rutile, the intrinsic equilibrium constants for double extrapolation are almost identical to those obtained with the linear extrapolation technique. The intrinsic equilibrium constants obtained using the Sprycha method are also very similar to those obtained using the double-extrapolation method, although the latter constants are considered to be less accurate because of the asymptotic nature of the extrapolation (Sprycha, 1984, 1989a).

A weakness of the triple-layer model is that, as in the constant capacitance model, the value of the capacitance, C_{1+}, obtained from extrapolation below the ZPC is not equivalent to the capacitance value, C_{1-}, obtained from extrapolation above the ZPC (Smit and Holten, 1980; Blesa

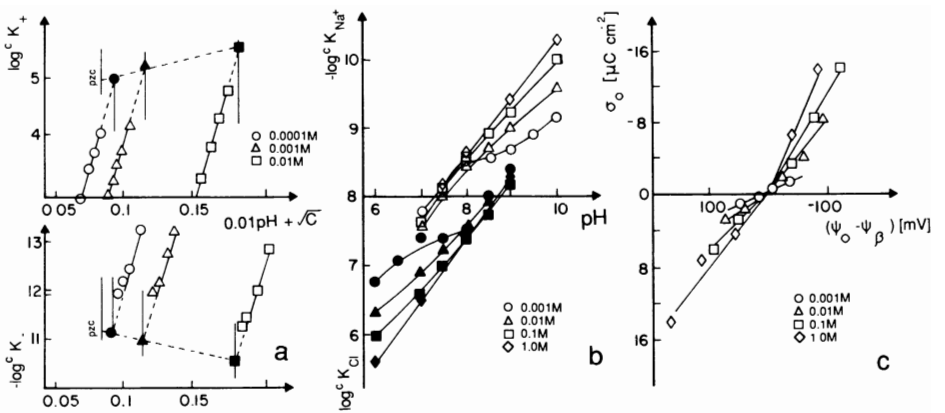

Figure 11. Determination of (a) the intrinsic protonation and dissociation constants (from Sprycha, 1989a), (b) the background electrolyte surface complexation constants, and (c) the capacitance, C_1 (from Sprycha, 1989b); $\log K_+(\text{int}) = 5.0$, $\log K_-(\text{int}) = -11.25$, $\log K_{Na}\text{-}(\text{int}) = -8.6$, $\log K_{Cl}\text{-}(\text{int}) = 7.5$.

Table IV

Values of Intrinsic Protonation–Dissociation and Background Electrolyte Surface Complexation Constants Obtained with the Triple-Layer Model by Extrapolation

Solid	Ionic medium	$\log K_+$(int)	$\log K_-$(int)	$\log K_{c^+}$(int)	$\log K_{A^-}$(int)	Reference
			Linear extrapolation			
α-Al_2O_3	NaBr	—	—	−4.0	5.0	Smit and Holten (1980)
γ-Al_2O_3	NaCl	4.9	−11.3	—	—	Sprycha (1989a)
α-FeOOH[a]	KNO_3	4.2	−10.8	−8.9	6.1	Davis *et al.* (1978)
α-FeOOH	$NaNO_3$	5.8	−11.1	−8.8	7.7	Hayes (1987)
Fe_3O_4	KNO_3	4.4	−9.0	−7.2	6.2	Regazzoni *et al.* (1983)
$Fe(OH)_3$(am)	$NaNO_3$	5.1	−10.7	−9.0	6.9	Davis and Leckie (1978)
TiO_2, rutile[a]	KNO_3	2.6	−9.0	−7.1	4.5	Davis *et al.* (1978)
TiO_2, rutile[a]	$LiNO_3$	2.6	−9.0	−7.1	4.5	Davis *et al.* (1978)
ZrO_2	KNO_3	4.2	−8.6	−7.6	5.2	Regazzoni *et al.* (1983)
Oxisol soil	NaCl	2.33	−6.34	−2.06	−1.80	Charlet and Sposito (1987)
Oxisol soil	KNO_3	2.07	−5.97	−2.0	2.4	Charlet and Sposito (1987)
Ultisol soil[b]	NaCl	1.8	−5.9	—	—	Charlet and Sposito (1987)
			Double extrapolation			
γ-AlOOH	KNO_3	5.4	−11.7	−6.3	10.9	Wood *et al.* (1990)
α-FeOOH	NaCl	4.9	−10.4	−9.6	5.5	Balistrieri and Murray (1979)
α-FeOOH	KCl	4.9	−10.4	−9.6	5.5	Balistrieri and Murray (1979)
α-FeOOH	$NaNO_3$	4.5	−12.0	−10.1	7.0	Hsi and Langmuir (1985)

(*continues*)

Table IV (*Continued*)

Solid	Ionic medium	$\log K_+$(int)	$\log K_-$(int)	$\log K_{C^-}$(int)	$\log K_{A^-}$(int)	Reference
			Double extrapolation			
α-FeOOH[a]	KNO_3	4.2	−10.5	−9.0	6.2	James and Parks (1982)
α-Fe_2O_3[c]	KCl	6.7	−10.3	−9.5	7.5	James and Parks (1982)
$Fe(OH)_3$(am)	$NaNO_3$	4.8	−11.1	−9.3	7.0	Hsi and Langmuir (1985)
TiO_2, anatase[d]	NaCl	3.2	−8.7	−7.1	4.6	James and Parks (1982)
TiO_2, rutile[d]	$NaClO_4$	2.7	−9.1	−7.2	4.5	James and Parks (1982)
TiO_2, rutile[d]	$NaNO_3$	2.8	−9.1	−7.2	4.5	James and Parks (1982)
TiO_2, rutile[a]	KNO_3	2.6	−9.0	−7.1	4.5	James and Parks (1982)
TiO_2, rutile[a]	$LiNO_3$	2.7	−9.1	−7.2	4.0	James and Parks (1982)
δ-MnO_2	NaCl	—	−4.2	−3.3	—	Balistrieri and Murray (1982a)
δ-MnO_2	$NaNO_3$	—	−6.2	−3.5	—	Catts and Langmuir (1986)
SiO_2(am)	LiCl	—	−8.2	−6.5	—	Milonjić (1987)
SiO_2(am)	NaCl	—	−8.2	−6.9	—	Milonjić (1987)
SiO_2(am)	KCl	—	−8.2	−7.0	—	Milonjić (1987)
SiO_2(am)	CsCl	—	−8.2	−7.0	—	Milonjić (1987)
			Sprycha electrokinetic extrapolation			
γ-Al_2O_3	NaBr	—	—	−8.7	8.9	Sprycha (1983)
γ-Al_2O_3	NaCl	5.0	−11.25	−8.6	7.5	Sprycha (1989a,b)
TiO_2, anatase	NaCl	3.1	−8.9	−5.8	6.2	Sprycha (1984)

[a] Based on experimental data of Yates (1975).
[b] Based on experimental data of Gallez *et al.* (1976).
[c] Based on experimental data of Breeuwsma and Lyklema (1971).
[d] Based on experimental data of Bérubé and deBruyn (1968a,b).

et al., 1984b). Smit and Holten (1980) obtained $C_{1+} = 1.5$ F m^{-2} and $C_{1-} = 3.5$ F m^{-2} for aluminum oxide in NaBr solution. Table V provides values of C_1 annd C_2 obtained from the Sprycha electrokinetic extrapolation technique for three different ionic strengths and four solution pH values. It is clear that the capacitances are not completely constant, as assumed in the triple-layer model, but vary with changing pH and ionic strength (Sprycha, 1984, 1989b). Capacitance values also vary as a function of solution temperature (Blesa *et al.*, 1984b). With the exception of the above three studies, the capacitances have universally been taken as adjustable parameters in applications of the triple-layer model (Sposito, 1984a). The capacitance C_2 is fixed at 0.2 F m^{-2} and the capacitance C_1 is adjusted to optimize the fit of the triple-layer model to the experimental data.

The ability of the triple-layer model to describe potentiometric titration data on an iron oxide mineral is indicated in Fig. 12. The model describes the titration data relatively well especially at high ionic strength. As for the constant capacitance model, use of the extrapolation procedures leads to large differences between $\log K_+(\text{int})$ and the absolute value of $\log K_-(\text{int})$ (Koopal *et al.*, 1987). Application of the FITEQL program to the titration data of Yates (1975) on titanium oxide produced values of $\log K_+(\text{int}) = 5.15$ and $\log K_-(\text{int}) = -6.61$, giving a much smaller value of $\Delta \log K_\pm(\text{int})$ (Westall and Hohl, 1980). However, it was pointed out by Koopal *et al.* (1987) that the numerical procedure can provide good fits with either a large or a small value of $\Delta \log K_\pm(\text{int})$, depending on which is chosen as the starting value in the FITEQL optimization. Values of the intrinsic equilibrium constants for surface complexation of background electrolytes can also be obtained using the computer program FITEQL containing the triple-layer model (Westall, 1982).

Table V

Values of Capacitance Obtained with the Triple-Layer Model Using Sprycha Electrokinetic Extrapolation Above the ZPC[a]

Capacitance (F m^{-2})	pH 7	pH 8	pH 9	pH 10
	0.001 *M* NaCl			
C_1	1.20	1.02	1.05	1.08
C_2	0.14	0.20	0.20	0.19
	0.01 *M* NaCl			
C_1	1.25	1.12	1.17	1.27
	0.1 *M* NaCl			
C_1	1.35	1.35	1.47	1.58

[a] Adapted from Sprycha (1984).

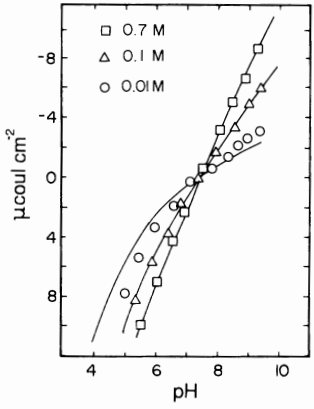

Figure 12. Fit of the triple-layer model to potentiometric titration data on goethite for three ionic strengths of NaCl and KCl. Model results are represented by solid lines; $\log K_{+}(\text{int}) = 5.57$, $\log K_{-}(\text{int}) = -9.52$, and $\log K_{Na^+}(\text{int}) = -8.40$ were obtained by double extrapolation; $\log K_{Cl^-}(\text{int}) = 7.00$ was adjusted to fit the data with $C_1 = 1.4$ F m^{-2}. From Balistrieri and Murray (1981), reproduced with permission from the American Journal of Science.

The kinetics of adsorption/desorption on oxide surfaces can be investigated using relaxation techniques. Sasaki *et al.* (1983) used the electric field pulse technique to investigate adsorption/desorption kinetics of chloride and perchlorate anions on goethite. Surface complexation modeling results are necessary to analyze the kinetic data. Sasaki *et al.* (1983) were able to describe both their adsorption and their kinetic data using the triple-layer model. The magnitude of the $K_{Cl^-}(\text{int})$ value obtained was in good agreement with that previously found by Davis *et al.* (1978).

The first application of the triple-layer model of heterogeneous natural samples was carried out on a Brazilian Oxisol, a variable-charge soil, by Charlet (1986; Charlet and Sposito, 1987). The authors simultaneously measured proton titration and background electrolyte adsorption. The intrinsic equilibrium constants obtained for protonation–dissociation on the Oxisol were similar to those for strongly acidic oxide minerals, whereas the intrinsic equilibrium constants obtained for surface complexation of the background electrolytes were similar to values found for oxide minerals. These results indicate that the Oxisol behaved similarly to strongly acidic oxides (Charlet and Sposito, 1987).

C. Stern VSC–VSP Model

The Stern VSC–VSP model has been used to describe the surface charge densities of various minerals in inert background electrolytes. The charging behavior has been investigated for iron oxides, goethite (Barrow *et al.*, 1980a; Madrid *et al.*, 1983; Bloesch *et al.*, 1987), lepidocrocite (Madrid *et al.*, 1983; Madrid and Diaz-Barrientos, 1988), and hematite (Madrid *et al.*, 1983), manganese oxides, cryptomelane and birnessite (McKenzie, 1981), clay minerals (Madrid and Diaz-Barrientos, 1988; Madrid *et al.*, 1989), and soils (Bowden *et al.*, 1977). Unlike in the constant capacitance model and the triple-layer model, where values of surface site density, equilibrium constants, and capacitances can be obtained from experiment, in the Stern VSC–VSP model these parameters are optimized to fit the charging data. Table VI presents values of N_S, $\log K_H$, $\log K_{OH}$, $\log K_{cat}$, $\log K_{an}$, $C_{o\beta}$, and $C_{\beta d}$ obtained by computer optimization for various minerals. The ability of the Stern VSC–VSP model to describe potentiometric titration data on an iron oxide mineral is indicated in Fig. 13. The model described the titration data well.

Application of the Stern VSC–VSP model to potentiometric titration data on the clay minerals illite and pyrophyllite was carried out (Madrid *et al.*, 1989). The fit appeared good; however, evaluation of the fit of the model is difficult because the raw experimental titration data were not presented. Application of the Stern VSC–VSP model to charging data for a heterogeneous system has been studied for soil clays from a Spanish Eutrochrept soil (Madrid *et al.*, 1983). The model fit was less satisfactory for the soil clays than for reference iron oxide minerals. However, again, the fit of the model is difficult to evaluate since no raw titration data were presented.

A simplified Stern VSC–VSP model containing no β-plane and allowing no surface complexation for the background electrolyte was originally developed by Bowden *et al.* (1977). These authors fit titration data on an Acrohumox soil with this model (see Fig. 14). Madrid and Diaz-Barrientos (1988) fit titration data on the clay mineral montmorillonite using the simplified Stern VSC–VSP model.

The Stern VSC–VSP model was applied to mixtures of iron oxides and clay minerals (Madrid and Diaz-Barrientos 1988; Madrid *et al.*, 1989). For this application, the Stern VSC–VSP model was used for iron oxides and illite and the simplified Stern VSC–VSP model was used for montmorillonite. A common diffuse layer is considered. Additional parameters are σ_p, the permanent charge on the clay surface, and R, the proportion of clay surface in the mixture. Each surface has its own surface charge densities, N_S, binding constants, K_i, and capacitances, C_i. The fit of the Stern

Table VI

Values of Maximum Surface Charge Density, Binding Constants, and Capacitances Obtained with the Stern VSC–VSP Model by Computer Optimization of Charging Data

Solid	Ionic medium	N_S (μmol m^{-2})	$C_{o\beta}$ (F m^{-2})	$C_{\beta d}$ (F m^{-2})	log K_H	log K_{OH}	log K_{cat}	log K_{an}	Reference
Iron oxides									
Goethite	NaCl	5.58	3.10	12.4	7.59	5.76	−0.14	−0.96	Barrow *et al.* (1980a)[a]
Goethite	NaCl	10.00	0.914	0.965	7.94	3.98	−0.086	−0.18	Bloesch *et al.* (1987)
Goethite	NaCl	45	—[b]	—[b]	7.2	4.2	−1.2	−0.92	Madrid *et al.* (1983)
Lepidocrocite	NaCl	10	—[b]	—[b]	7.5	7.3	−1.5	−0.52	Madrid *et al.* (1983)
Hematite	NaCl	12	—[b]	—[b]	7.9	8.4	−1.4	−0.52	Madrid *et al.* (1983)
Manganese oxides									
Cryptomelane 41	$NaNO_3$	7.6	2.0	1.3	1	12	−0.3	−0.3	McKenzie (1981)
Cryptomelane 42	$NaNO_3$	10.5	2.5	0.97	2	12	−0.3	−0.3	McKenzie (1981)
Birnessite 40	$NaNO_3$	28	7.7	4.3	1	12	−0.3	−0.3	McKenzie (1981)
Birnessite 44	$NaNO_3$	22	5.2	1.4	4	12	−0.3	−0.3	McKenzie (1981)
Soil clays									
Eutrochrept 3	NaCl	17	—[b]	—[b]	7.60	8.00	−0.40	−0.52	Madrid *et al.* (1983)
Eutrochrept 4	NaCl	20	—[b]	—[b]	6.04	7.26	−1.4	−0.097	Madrid *et al.* (1983)
Eutrochrept 5	NaCl	43	—[b]	—[b]	6.11	7.64	−2.0	−0.52	Madrid *et al.* (1983)
Clay minerals									
Illite	NaCl	9.3	—[b]	—[b]	3.4	5.8	2.7	−2.0	Madrid *et al.* (1989)
Pyrophyllite	NaCl	11	—[b]	—[b]	−0.081	7.7	−1.5	4.3	Madrid *et al.* (1989)

[a] Based on experimental data of Hingston (1970).

[b] Parameters required in model application whose values were not provided by the authors.

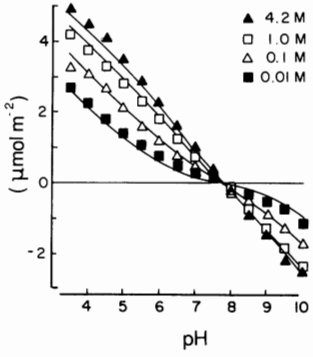

Figure 13. Fit of the Stern VSC–VSP model to potentiometric titration data on goethite for four ionic strengths of NaCl. Model results are represented by solid lines. Model parameter values are provided in Table VI. After Barrow *et al.* (1980a), based on experimental data of Hingston (1970).

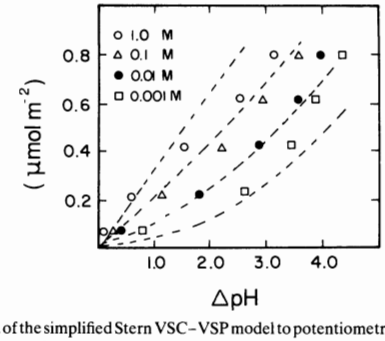

Figure 14. Fit of the simplified Stern VSC–VSP model to potentiometric titration data on an Acrohumox soil for four ionic strengths of NaCl. Model results are represented by dashed lines. From Bowden *et al.* (1977), based on experimental data of van Raij and Peech (1972).

VSC–VSP model to mixtures could only be evaluated for lepidocrocite–montmorillonite; no model fits to data were presented for other mixtures. No raw titration data were presented for lepidocrocite–montmorillonite, but the model fit, as best could be evaluated, was good. Additional research is needed to evaluate the applicability of the Stern VSC–VSP model for describing charging behavior of oxide–clay mixtures.

D. Generalized Two-Layer Model

So far, application of the generalized two-layer model has been restricted to reactions occurring on the surface of hydrous ferric oxide (Dzombak and Morel, 1990). Dzombak and Morel much preferred computer optimization of equilibrium constants over graphical extrapolation techniques. They considered nonlinear least-squares optimization with the computer program FITEQL (Westall, 1982), containing the generalized two-layer model, to be less tedious and more precise than graphical methods. Additional advantages of computer optimization are that the parameters are considered bias free and that quality-of-fit criteria and parameter standard deviations are available.

In obtaining best estimates for intrinsic conditional protonation–dissociation constants, Dzombak and Morel (1990) applied FITEQL to individual titration data sets at each ionic strength. The individual optimum values of $\log K_{\pm}(\text{int})$ were weighted to obtain the best estimate using the following equation:

$$\overline{\log K(\text{int})} = \sum \frac{(1/\sigma_{\log K(\text{int})})_i}{\sum(1/\sigma_{\log K(\text{int})})_i} [\log K(\text{int})]_i \qquad (104)$$

where $(\sigma_{\log K(\text{int})})_i$ is the standard deviation calculated by FITEQL for $\log K(\text{int})$ of the ith data set. Table VII presents values of individual $\log K_{\pm}(\text{int})$ and best estimates of $\log K_{\pm}(\text{int})$ obtained by FITEQL computer optimization for hydrous ferric oxide. Values of $\overline{\log K_{\pm}(\text{int})}$ obtained by Dzombak and Morel (1990) compare well with average values for a literature compilation of experimental $\log K_{\pm}(\text{int})$ values provided in Goldberg and Sposito (1984a) for iron oxide minerals. These authors found $\overline{\log K_{+}(\text{int})} = 7.31 \pm 1.11$ and $\overline{\log K_{-}(\text{int})} = -8.80 \pm 0.80$. The large standard deviations result because data for diverse iron oxides were averaged. The ability of the generalized two-layer model to describe potentiometric titration data on hydrous ferric oxide is indicated in Fig. 15. The model describes the data well using both individual data set values and best estimates of $\log K_{\pm}(\text{int})$.

Table VII

Values of Intrinsic Protonation and Dissociation Constants Obtained with the Generalized Two-Layer Model Using FITEQL Computer Optimization for Hydrous Ferric Oxide[a]

Ionic medium	$\log K_+(\text{int}) \pm \sigma$	$\log K_-(\text{int}) \pm \sigma$	Experimental data source
0.1 *M* $NaNO_3$	7.03 ± 0.035	−8.74 ± 0.065	Davis (1977)
0.01 *M* $NaNO_3$	7.57 ± 0.038	−8.74 ± 0.15[b]	Davis (1977)
0.001 *M* $NaNO_3$	8.20 ± 0.045	−8.74 ± 0.15[b]	Davis (1977)
0.1 *M* $NaClO_4$	7.69 ± 0.048	−9.25 ± 0.118	Swallow (1978)
0.25 *M* $NaClO_4$	7.17 ± 0.032	−9.51 ± 0.095	Swallow (1978)
0.5 *M* $NaClO_4$	6.63 ± 0.033	−9.10 ± 0.065	Swallow (1978)
0.01 *M* KNO_3	7.10 ± 0.026	−8.89 ± 0.045	Yates (1975)
0.1 *M* $NaNO_3$	7.08 ± 0.028	−9.01 ± 0.034	Hsi and Langmuir (1985)
0.01 *M* $NaNO_3$	7.58 ± 0.110	−8.40 ± 0.126	Hsi and Langmuir (1985)
0.001 *M* $NaNO_3$	7.54 ± 0.040	−8.40 ± 0.15[b]	Hsi and Langmuir (1985)
$\overline{\log K_\pm(\text{int})}$	7.29 ± 0.10[c]	−8.93 ± 0.07[c]	

[a] From Dzombak and Morel (1990)

[b] $\log K_-(\text{int})$ and $\sigma_{\log K_-(\text{int})}$ fixed at these values. Convergence was not possible unless one value of $\log K_\pm(\text{int})$ was fixed.

[c] 95% confidence intervals.

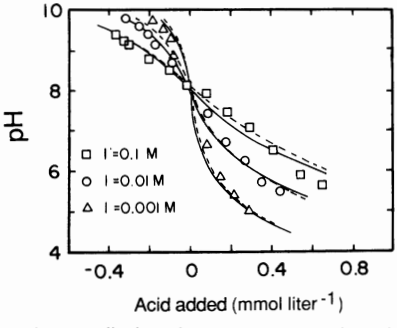

Figure 15. Fit of the generalized two-layer model to potentiometric titration data on hydrous ferric oxide for three ionic strengths of $NaNO_3$. Model results are represented by solid lines for individual $\log K_\pm(\text{int})$ and by dashed lines for $\overline{\log K_\pm(\text{int})}$. Model parameter values are provided in Table VII. After Dzombak and Morel (1990), based on experimental data of Hsi and Langmuir (1985), reproduced with permission from John Wiley and Sons.

E. One-p*K* Model

The one-p*K* model has been used to describe potentiometric titration data for various minerals in inert background electrolyte solution. The one-p*K* model was applied to titration data on titanium oxide (van Riemsdijk *et al.*, 1986), hematite (α-Fe_2O_3), amorphous iron oxide (van Riemsdijk *et al.*, 1987), $Al(OH)_3$ gibbsite, and γ-Al_2O_3 (Hiemstra *et al.*, 1987). In the most simplified application of the one-p*K* model, no surface complexation reactions are considered for the background electrolyte. In this approach, the capacitance of the Stern layer is the only adjustable parameter. The association constant K_H is obtained from the ZPC:

$$\log K_H = pH_0 = ZPC \tag{105}$$

where pH_0 is the proton concentration at the ZPC (van Riemsdijk *et al.*, 1986). Titration data on titanium oxide (van Riemsdijk *et al.*, 1986) and gibbsite (Hiemstra *et al.*, 1987) were modeled successfully in this fashion. The ability of the simplified one-p*K* model to describe potentiometric titration data on titanium oxide is indicated in Fig. 16.

An improvement in the model fit can be obtained by inclusion of surface complexation constants for the background electrolyte. Values of

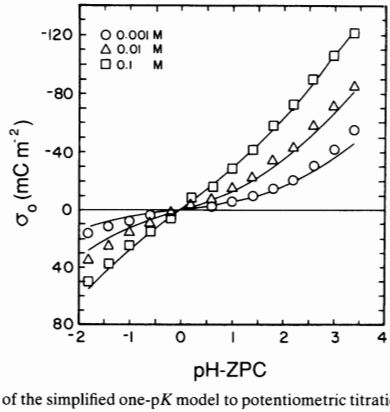

Figure 16. Fit of the simplified one-p*K* model to potentiometric titration data on titanium oxide for three ionic strengths of KNO_3. Model results are represented by solid lines; $\log K_H = 5.80$ and $C = 1.33$ F m^{-2}. From van Riemsdijk *et al.* (1986), based on experimental data of Yates (1975).

equilibrium constants and capacitance were obtained with a computer algorithm and are presented in Table VIII. Hiemstra *et al.* (1987) were able to describe potentiometric titration data well on gibbsite with two different approaches. The model fit using no surface complexation constants for the background electrolyte was good but produced a low value of capacitance. A larger value of capacitance was obtained using surface complexation constants for the background electrolyte and the assumption that only the edge surface area of gibbsite is reactive. The quality of the model fit was virtually identical and excellent in both cases. Figure 17 indicates the ability of the one-pK model to describe potentiometric titration data on gibbsite.

The one-pK model was expanded to include surface heterogeneity (van Riemsdijk *et al.*, 1986). It was found that the shape of the potentiometric

Table VIII

Values of Equilibrium Constants and Capacitance Obtained with the One-pK Model by Computer Optimization of Potentiometric Titration Data

Solid	Ionic medium	log K_H	log K_{C^+}	log K_{A^-}	C (F m^{-2})	Reference
TiO_2	KNO_3	5.8	—	—	1.33	van Riemsdijk *et al.* (1986)
TiO_2	KNO_3	5.8	−1.02	−1.28	0.83	van Riemsdijk *et al.* (1986)
α-Fe_2O_3	KNO_3	8.4	—	—	1.72	van Riemsdijk *et al.* (1987)
Fe_2O_3(am)	KNO_3	7.9	−0.75	−0.89	1.54	van Riemsdijk *et al.* (1987)
α-$Al(OH)_3$	NaCl	10	—	—	0.26	Hiemstra *et al.* (1987)
α-$Al(OH)_3$	NaCl	10	−0.1	−0.1	1.40[a]	Hiemstra *et al.* (1987)
γ-Al_2O_3[b]	NaCl	8.5	−0.1[c]	−0.1[c]	1.2	Hiemstra *et al.* (1987)
γ-Al_2O_3[d]	$NaClO_4$	8.3	−0.1[c]	−0.1[c]	1.1	Hiemstra *et al.* (1987)
γ-Al_2O_3[e]	$NaClO_4$	8.3	−0.1[c]	−0.1[c]	1.0	Hiemstra *et al.* (1987)
γ-Al_2O_3[f]	$NaClO_4$	8.7	−0.1[c]	−0.1[c]	1.2	Hiemstra *et al.* (1987)

[a] Considering only the singly coordinated groups at the particle edges to be reactive.
[b] Based on experimental data of Huang and Stumm (1973).
[c] log K_{C^+} and log K_{A^-} fixed at the gibbsite values.
[d] Based on experimental data of Westall and Hohl (1980).
[e] Based on experimental data of Hohl and Stumm (1976).
[f] Based on experimental data of Kummert and Stumm (1980).

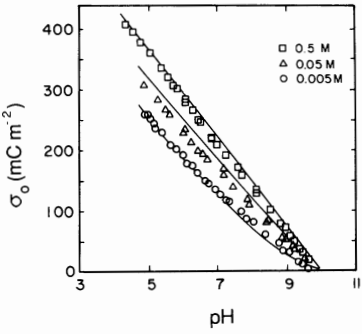

Figure 17. Fit of the one-pK model to potentiometric titration data on gibbsite for three ionic strengths of NaCl, assuming that only the edge surface area is reactive. Model results are represented by solid lines; $\log K_H = 10$, $\log K_{Na^+} = \log K_{Cl^-} = -0.1$, and $C = 1.40$ F m^{-2}. After Hiemstra *et al.* (1987).

titration curves was insensitive toward the degree of heterogeneity, allowing a homogeneous model to be used to represent a heterogeneous oxide system (van Riemsdijk *et al.*, 1986). The one-pK model is a special case of a more generalized model called the multisite complexation model, MUSIC, developed by Hiemstra *et al.* (1989a,b). This model considers equilibrium constants for the various types of surface groups on the various crystal planes of oxide minerals and was used to describe the charging behavior of gibbsite, goethite, hematite, rutile, and silica (Hiemstra *et al.*, 1989b). The MUSIC model has not yet been applied to describe ion adsorption. Because of its increased complexity such an application may entail an unreasonably large number of adjustable parameters.

IV. APPLICATION OF MODELS TO METAL ION ADSORPTION REACTIONS ON OXIDES, CLAY MINERALS, AND SOILS

A. Constant Capacitance Model

Characterization of metal ion adsorption behavior as a function of solution pH results in curves termed adsorption edges. The constant capacitance model has been used to describe metal ion adsorption edges on silica

(Schindler *et al.*, 1976; Osaki *et al.*, 1990a,b), aluminum oxide (Hohl and Stumm, 1976), iron oxide (Sigg, 1979; Lövgren *et al.*, 1990), titanium oxide (Fürst, 1976; Gisler, 1980), and the clay mineral kaolinite (Schindler *et al.*, 1987 Osaki *et al.*, 1990b). The conditional equilibrium constants for metal adsorption in the constant capacitance model are

$$ {}^{c}K^{1}_{M} = \frac{[SOM^{(m-1)}][H^{+}]}{[SOH][M^{m+}]} \tag{106} $$

$$ {}^{c}K^{2}_{M} = \frac{[(SO)_2M^{(m-2)}][H^{+}]^2}{[SOH]^2[M^{m+}]} \tag{107} $$

In order to graphically evaluate the surface complexation constants, the simplifying assumption is made that $\Psi = 0$. This assumption produces the result that the conditional intrinsic equilibrium constants are equal to the conditional equilibrium constants: $K^{i}_{M}(\text{int}) = {}^{c}K^{i}_{M}$. For the special case of a divalent metal ion, M^{2+}, this expression holds true universally even without any simplifying assumption because a neutral surface complex is formed. Excellent fits to metal adsorption data were obtained with the constant capacitance model despite the simplification. Figure 18 presents the ability of the constant capacitance model to describe metal adsorption on silica. The lack of dependence of the equilibrium constants on surface charge indicates a self-consistency problem in such applications of the constant capacitance model (Sposito, 1984a).

This limitation can be overcome by computer optimization of the intrinsic surface complexation constants. This approach negates the requirement for simplifying assumptions and has been used by Lövgren *et al.* (1990).

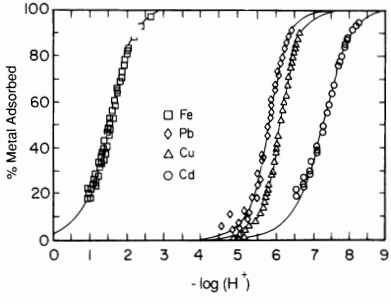

Figure 18. Fit of the constant capacitance model to metal adsorption on silica. Model results are represented by solid lines. Model parameters are provided in Table IX. From Schindler *et al.* (1976).

These authors described aluminum complexation on the iron oxide, goethite, using the surface complexes $SOAlOH^+$ and $SOAl(OH)_2$, where $\log K_{AlOH^+}(\text{int}) = -1.49$ and $\log K_{Al(OH)_2}(\text{int}) = -9.10$. Table IX provides values for metal surface complexation constants obtained with the constant capacitance model for various materials.

Table IX

Values of Metal Surface Complexation Constants Obtained with the Constant Capacitance Model Using Graphical Methods[a]

Solid	Metal	Ionic medium	$\log {}^cK^1_M$	$\log {}^cK^{2,b}_M$	Reference
γ-Al_2O_3	Ca^{2+}	0.1 *M* $NaNO_3$	−6.1	—	Huang and Stumm (1973)
γ-Al_2O_3	Mg^{2+}	0.1 *M* $NaNO_3$	−5.4	—	Huang and Stumm (1973)
γ-Al_2O_3	Ba^{2+}	0.1 *M* $NaNO_3$	−6.6	—	Huang and Stumm (1973)
γ-Al_2O_3	Pb^{2+}	0.1 *M* $NaClO_4$	−2.2	−8.1	Hohl and Stumm (1976)
α-FeOOH	Mg^{2+}	0.1 *M* $NaClO_4$	−6.2	−14.7	Sigg (1979)
Fe_3O_4	Co^{2+}	$I = 0$	−2.44	−6.71	Tamura *et al.* (1983)
SiO_2(am)	Mg^{2+}	1 *M* $NaClO_4$	−7.7	−17.15	Gisler (1980)
SiO_2(am)	Fe^{3+}	3 *M* $NaClO_4$	−1.77	−4.22	Schindler *et al.* (1976)
SiO_2(am)	Fe^{3+}	0.1 *M* $NaClO_4$	−0.81	—	Osaki *et al.* (1990b)
SiO_2(am)	Cu^{2+}	1 *M* $NaClO_4$	−5.52	−11.19	Schindler *et al.* (1976)
SiO_2(am)	Cd^{2+}	1 *M* $NaClO_4$	−6.09	−14.20	Schindler *et al.* (1976)
SiO_2(am)	Pb^{2+}	1 *M* $NaClO_4$	−5.09	−10.68	Schindler *et al.* (1976)
SiO_2(am)	Co^{2-}	0.1 *M* $NaClO_4$	−5.83	−11.4	Osaki *et al.* (1990b)
SiO_2(am)	Zn^{2-}	0.1 *M* $NaClO_4$	−3.8	−9.2	Osaki *et al.* (1990b)
Quartz	Fe^{3+}	0.1 *M* $NaClO_4$	−0.97	—	Osaki *et al.* (1990b)
Quartz	Co^{2-}	0.1 *M* $NaClO_4$	−5.0	—	Osaki *et al.* (1990b)
Quartz	Zn^{2-}	0.1 *M* $NaClO_4$	−4.4	—	Osaki *et al.* (1990b)
TiO_2, rutile	Mg^{2+}	1 *M* $NaClO_4$	−5.90	−13.13	Gisler (1980)
TiO_2, rutile	Co^{2-}	1 *M* $NaClO_4$	−4.30	−10.16	Gisler (1980)
TiO_2, rutile	Cu^{2+}	1 *M* $NaClO_4$	−1.43	−5.04	Fürst (1976)
TiO_2, rutile	Cd^{2+}	1 *M* $NaClO_4$	−3.32	−9.00	Fürst (1976)
TiO_2, rutile	Pb^{2+}	1 *M* $NaClO_4$	0.44	−1.95	Fürst (1976)
δ-MnO_2	Ca^{2+}	0.1 *M* $NaNO_3$	−5.5	—	Stumm *et al.* (1970)
Kaolin	Fe^{3+}	0.1 *M* $NaClO_4$	−0.683	—	Osaki *et al.* (1990b)
Kaolin	Co^{2+}	0.1 *M* $NaClO_4$	−2.8	—	Osaki *et al.* (1990b)
Kaolin	Zn^{2+}	0.1 *M* $NaClO_4$	−2.1	—	Osaki *et al.* (1990b)
Particulates[c]	Fe^{3+}	0.1 *M* $NaClO_4$	−0.78 ± 0.6	—	Osaki *et al.* (1990b)
Particulates[c]	Co^{2+}	0.1 *M* $NaClO_4$	−3.5 ± 0.5	—	Osaki *et al.* (1990b)
Particulates[c]	Zn^{2+}	0.1 *M* $NaClO_4$	−2.9 ± 0.2	−7.9	Osaki *et al.* (1990b)
Sediments[c]	Fe^{3+}	0.1 *M* $NaClO_4$	−0.74 ± 0.8	—	Osaki *et al.* (1990b)
Sediments[c]	Co^{2+}	0.1 *M* $NaClO_4$	−2.9 ± 0.7	—	Osaki *et al.* (1990b)
Sediments[c]	Zn^{2+}	0.1 *M* $NaClO_4$	−2.5 ± 0.4	—	Osaki *et al.* (1990b)

[a] Adapted from Schindler and Stumm (1987) and expanded.
[b] For divalent metal ions $\log K^2_M(\text{int}) = \log {}^cK^2_M$.
[c] Averages for three particulars or three sediments obtained from natural waters of Japan.

Application of the constant capacitance model to metal adsorption edges on the clay mineral kaolinite and particulate and sediment samples from natural waters was carried out by Osaki *et al.* (1990b). These authors used the same modeling approach on these heterogeneous systems as had been used for oxide minerals. The equilibrium constants for adsorption of Co^{2+} and Zn^{2+} exhibited good reproducibility, however, the standard deviation of $\log {}^{c}K^{1}_{Fe}$ was great (see Table IX).

An alternative model for the description of metal adsorption on kaolinite is the extended constant capacitance model introduced in Section III,A (Schindler *et al.*, 1987). In this application, reactions given by Eqs. (4), (5), (6), (7), (83), and (84) are defined. In addition, an ion exchange reaction of the surface functional group, XH, between the cation of the background electrolyte and the metal ion, M^{2+}, is defined:

$$2XC + M^{2+} \rightleftarrows X_2M + 2C^{+} \tag{108}$$

The equilibrium constants for this application are given in Eqs. (10), (11), (12), (13), (85), (86), and (109):

$$K_{XM} = [X_2M][C^{+}]^2/([XC]^2[M^{2+}]) \tag{109}$$

The fit of the constant capacitance model to adsorption of lead on hydrogen kaolinite is indicated in Fig. 19. Despite the fact that values of the equilibrium constants were obtained using the computer program FITEQL, the assumption was made that $\Psi = 0$. As for potentiometric titration data (see Section III,A), Schindler *et al.* (1987) considered the model fit acceptable.

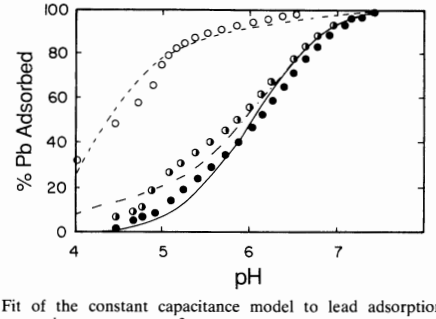

Figure 19. Fit of the constant capacitance model to lead adsorption on kaolinite; $\log K_{XPb} = 2.98$, $\log {}^{c}K^{1}_{Pb} = -2.45$, $\log {}^{c}K^{2}_{Pb} = -8.11$. Model results are represented by a dashed line ($I = 0.01$ *M* $NaClO_4$), dotted line ($I = 0.1$ *M* $NaClO_4$), and solid line ($I = 1.0$ *M* $NaClO_4$). From Schindler *et al.* (1987).

"Adsorptive additivity" is a concept developed by Honeyman (1984) that multicomponent mixtures of oxides can be represented as a collection of pure solids. Upon testing this hypothesis for binary oxide mixtures, Honeyman (1984) found significant deviations. The constant capacitance model was used to test models of particle interaction of binary mixtures of amorphous silica–iron (Anderson and Benjamin, 1990a) and iron–aluminum (Anderson and Benjamin, 1990b). "Adsorptive additivity" was not observed for these systems. In binary Si–Fe oxide suspensions, silica was considered to partially dissolve, and soluble silicate to adsorb onto iron oxide (Anderson and Benjamin, 1990a). Silver, zinc, and cadmium adsorption were virtually unaffected. In binary Fe–Al suspensions, the reactive iron surface was considered blocked or replaced by reactive aluminum surface (Anderson and Benjamin, 1990b). Cadmium and silver adsorption were decreased and zinc adsorption was increased in the binary system. This divergent behavior was qualitatively described by the assumed mechanism.

The surface precipitation model extends the surface complexation modeling approach by considering precipitation of ions on the solid. This model was developed by Farley *et al.* (1985) and incorporated into the constant capacitance model. Loss of ions from solution is described by surface complexation at low concentration and by surface precipitation as a solid solution at high concentration. The solid solution composition varies continuously between the original solid and the pure precipitate of the sorbing ion. The surface precipitation model can be incorporated into any surface complexation model, such as the generalized two-layer model (see Section IV,D). Reactions of the surface precipitation model for divalent metal sorption onto a trivalent oxide are (Farley *et al.*, 1985) as follows:

Adsorption of M^{2+} onto $S(OH)_3(s)$:

$$\equiv SOH + M^{2+} + 2H_2O \rightleftarrows S(OH)_{3(s)} + {=}MOH_2^+ + H^+ \qquad (110)$$

Precipitation of M^{2+}:

$${=}MOH_2^+ + M^{2+} + 2H_2O \rightleftarrows M(OH)_{2(s)} + {=}MOH_2^+ + 2H^+ \qquad (111)$$

Precipitation of S^{3+}:

$$\equiv SOH + S^{3+} + 3H_2O \rightleftarrows S(OH)_{3(s)} + \equiv SOH + 3H^+ \qquad (112)$$

The equilibrium constants for the reactions as written are: K_{adsM} for Eq. (110), $1/K_{\text{spM}}$ for Eq. (111), and $1/K_{\text{spS}}$ for Eq. (112). The ability of the surface precipitation model to describe lead adsorption on amorphous iron hydroxide is indicated in Fig. 20. It can be seen that the model describes the data well although very few data points are available. The surface precipitation model has also been applied to cadmium, cobalt,

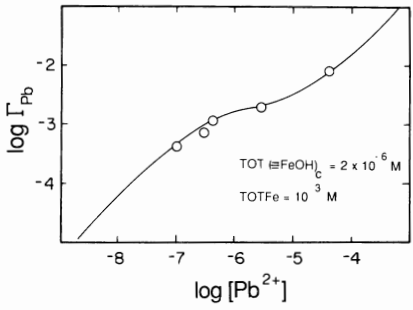

Figure 20. Fit of the constant capacitance model containing the surface precipitation model to a lead sorption isotherm on amorphous iron hydroxide at pH 4.5. Model results are represented by a solid line. Γ_{Pb} = ([≡PbOH] + [$Pb(OH_{2(s)})$])/TOTFe; log K_{adsPb} = 5.0, log K_{spPb} = 6.9, log K_{spFe} = 2.6. From Farley *et al.* (1985), based on experimental data of Benjamin (1978).

manganese, and zinc adsorption on calcite (Comans and Middelburg, 1987) and to manganese adsorption on siderite (Wersin *et al.*, 1989).

B. Triple-Layer Model

The triple-layer model has been used to describe alkaline earth and metal ion adsorption edges on aluminum oxide, titanium oxide, amorphous iron oxide (Davis and Leckie, 1978; Benjamin and Bloom, 1981; Zachara *et al.*, 1987; Cowan *et al.*, 1991), goethite (α-FeOOH) (Balistrieri and Murray, 1981, 1982b; Hayes, 1987), manganese oxide (Balistrieri and Murray, 1982a; Catts and Langmuir, 1986), and soil (Charlet, 1986; Charlet and Sposito, 1989). Intrinsic conditional equilibrium constants for the triple-layer model have been obtained by using the computer programs MINEQL (Westall *et al.*, 1976) and MICROQL (Westall, 1979), or by computer optimization using the FITEQL program (Westall, 1982). In general, in the application of the triple-layer model to metal adsorption, the reactions Eqs. (22) and (23), with their equilibrium constants Eqs. (28) and (29), are considered. Figure 21 presents the ability of the triple-layer model to describe silver adsorption on amorphous iron oxide. The ability of the model to fit the adsorption data is good.

Table X provides values for intrinsic metal surface complexation constants obtained with the triple-layer model for various materials. Adsorption of the alkaline earth cations calcium and magnesium on manganese

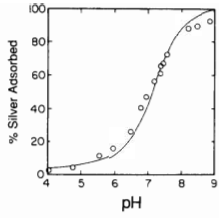

Figure 21. Fit of the triple-layer model to silver adsorption on amorphous iron oxide. Model results are represented by a solid line; $\log K^1_{Ag}(\text{int}) = -4.9$, $\log K^2_{Ag}(\text{int}) = -12.1$. From Davis and Leckie (1978).

Table X

Values of Intrinsic Metal Surface Complexation Constants Obtained with the Triple-Layer Model by Computer Optimization

Solid	Metal	Ionic medium	$\log K^1_M(\text{int})$	$\log K^2_M(\text{int})$	Reference
			Original triple-layer model		
γ-Al_2O_3[a]	Pb^{2+}	$NaClO_4$	−5.0	−10.3	Davis and Leckie (1978)
$Fe(OH)_3$(am)	Ag^-	$NaNO_3$	−4.9	−12.1	Davis and Leckie (1978)
$Fe(OH)_3$(am)	Cu^{2+}	$NaNO_3$	−4.1	−9.0	Davis and Leckie (1978)
$Fe(OH)_3$(am)	Cd^{2+}	$NaNO_3$	−4.8	−11.25	Benjamin and Bloom (1981)
$Fe(OH)_3$(am)	Co^{2+}	$NaNO_3$	−4.8	−11.60	Benjamin and Bloom (1981)
$Fe(OH)_3$(am)	Zn^{2+}	$NaNO_3$	−4.8	−10.50	Benjamin and Bloom (1981)
$Fe(OH)_3$(am)	Ca^{2+}	$NaNO_3$	−6.3	—	Zachara *et al.* (1987)
α-FeOOH	Ca^{2+}	NaCl	−5.00	−14.50	Balistrieri and Murray (1981)
α-FeOOH	Mg^{2+}	NaCl	−5.45	−14.25	Balistrieri and Murray (1981)
α-FeOOH	Cu^{2+}	NaCl	−3.0	−7.0	Balistrieri and Murray (1982b)
α-FeOOH	Pb^{2+}	NaCl	−1.8	−5.0	Balistrieri and Murray (1982b)
α-FeOOH	Zn^{2+}	NaCl	—	−9.15	Balistrieri and Murray (1982b)
α-FeOOH	Cd^{2+}	NaCl	−1.3	−9.35	Balistrieri and Murray (1982b)
TiO_2[b]	Cd^{2+}	KNO_3	−1.8	−8.7	Davis and Leckie (1978)
δ-MnO_2	Ca^{2+}	NaCl	—	−4.0[c]	Balistrieri and Murray (1982a)
δ-MnO_2	Mg^{2+}	NaCl	—	−3.3[c]	Balistrieri and Murray (1982a)
δ-MnO_2	Cu^{2+}	$NaNO_3$	−0.1	−7.5	Catts and Langmuir (1986)
δ-MnO_2	Pb^{2+}	$NaNO_3$	1.8	−6.5	Catts and Langmuir (1986)
δ-MnO_2	Zn^{2+}	$NaNO_3$	−1.5	−8.8	Catts and Langmuir (1986)
			Modified triple-layer model		
Oxisol soil	Ca^{2+}	$Ca(ClO_4)_2$	−1.26[d]	—	Charlet (1986)
Oxisol soil	Mg^{2+}	$Mg(ClO_4)_2$	−1.76[d]	—	Charlet (1986)
α-FeOOH	Pb^{2+}	$NaNO_3$	2.30[d]	—	Hayes (1987)
α-FeOOH	Cd^{2+}	$NaNO_3$	−1.05[d]	—	Hayes (1987)
α-FeOOH	Ba^{2+}	$NaNO_3$[e]	−5.10	−14.20	Hayes (1987)

[a] Based on experimental data of Hohl and Stumm (1976).
[b] Based on experimental data of Stiglich (1976).
[c] Bidentate surface complexes as described by Eqs. (113) and (114).
[d] Inner-sphere surface complexes as described by Eqs. (6) and (12) where $\Psi = \Psi_o$.
[e] Intrinsic surface complexation constants for Na^+ and NO_3^- adsorption were also adjusted.

oxide was proposed to occur via bidentate complex formation and not via hydrolysis complex formation (Balistrieri and Murray, 1982a). This reaction is written as

$$S(OH)_2 + M^{2-} \rightleftarrows S(O)_2M + 2H^+ \quad (113)$$

Because a neutral surface complex is formed, the intrinsic conditional equilibrium constant for this reaction is equal to the conditional equilibrium constant and is given by

$$K^2_M(\text{int}) = {}^cK^2_M = [S(O)_2M][H^+]^2/([S(OH)_2][M^{2+}]) \quad (114)$$

Values of these constants are provided in Table X.

Adsorption reactions of actinide elements were investigated for uranium adsorption on goethite and amorphous iron oxide (Hsi and Langmuir, 1985), plutonium adsorption on goethite (Sanchez *et al.*, 1985), thorium adsorption on goethite (LaFlamme and Murray, 1987; Hunter *et al.*, 1988) and manganese oxide (Hunter *et al.*, 1988), and neptunium adsorption on amorphous iron oxide (Girvin *et al.*, 1991). In most of these applications of the triple-layer model a large number of surface complexation constants were fit to the adsorption data. Plutonium adsorption on goethite was described using four surface complexes: SO^-—$PuOH^{3+}$, SO^-—$Pu(OH)_2^{2+}$, SO^-—$Pu(OH)_3^+$, and SO^-—$Pu(OH)_4$ (Sanchez *et al.*, 1985). Thorium adsorption was described using five complexes, SO^-—Th^{4+}, SO^-—$ThOH^{3+}$, SO^-—$Th(OH)_2^{2+}$, SO^-—$Th(OH)_3^+$, and SO^-—$Th(OH)_4$, for goethite (LaFlamme and Murray, 1987; Hunter *et al.*, 1988) and three surface complexes, SO^-—$Th(OH)_2^{2+}$, SO^-—$Th(OH)_3^+$, and SO^-—$Th(OH)_4$ for manganese oxide (Hunter *et al.*, 1988).

Uranium adsorption on iron oxides as the uranyl species was accurately described using two surface complexes: SO^-—UO_2OH^+ and SO^-—$(UO_2)_3(OH)_5^+$ (Hsi and Langmuir, 1985). Fit of the triple-layer model to plutonium adsorption on amorphous iron oxide as the plutonyl species was excellent using one surface complex: SOH—$NpO_2(OH)$ (Girvin *et al.*, 1991). Hsi and Langmuir (1985) observed that excellent fits to their data could also be obtained by adding additional uranyl surface complexes or by varying the combination of surface constants. This observation was also made by Catts and Langmuir (1986), who added surface complexes for SO^-—$M(OH)_2$ and SO^-—MNO_3^+ (in addition to SO^-—M^{2+} and SO^-—MOH^+) to describe copper and zinc adsorption on manganese oxide. As has been observed previously in surface complexation modeling, good fits can be obtained for various combinations of surface complexes. For this reason it is necessary to limit the surface complexation reactions to a small number of the simplest and most chemically reasonable surface complexes. As the number of adjustable parameters is increased, the quality of the model fit improves. This does not

necessarily indicate any increased chemical insight and may compromise the representation of chemical reality.

The modified triple-layer model was applied by Hayes and Leckie (1987) to describe ionic strength effects on cadmium and lead adsorption on goethite. These authors found that only by using an inner-sphere surface complex could the small ionic strength dependence of the adsorption reactions of these cations be accurately described. These authors assert that the modified triple-layer model can be used to distinguish between inner-sphere and outer-sphere surface complexes.

Hayes (1987) used the pressure-jump relaxation technique to investigate lead adsorption/desorption kinetics on goethite The author was able to describe both his adsorption and his kinetic data using the modified triple-layer model. Based on the kinetic results, an inner-sphere surface complex between a lead ion and an adsorbed nitrate ion, $SOHPb^{2+}—NO_3^-$, was postulated in addition to the inner-sphere surface complex, $SOPb^+$, obtained from equilibrium results. The magnitude of the $\log K^1_{Pb}(int)$ value obtained from kinetics was identical to that obtained from equilibrium data. This result is expected because surface complexation model parameter values from equilibrium experiments are necessary to analyze the kinetic data. Therefore the kinetic approach is not independent.

The first application of the triple-layer model to alkaline earth metal adsorption on heterogeneous systems was the study of Charlet (1986; Charlet and Sposito, 1989) on a Brazilian Oxisol soil. These authors found good fits of the triple-layer model to calcium and magnesium adsorption on the Oxisol using inner-sphere surface complexes. However, Charlet and Sposito (1989) suggested that these cations may also form outer-sphere surface complexes.

C. Stern VSC–VSP Model

The Stern VSC–VSP model has been used to describe adsorption of the metals copper, lead, and zinc on the iron oxide (goethite) surface (Barrow *et al.*, 1981). Application of the model to other metal ions or other oxide surfaces is not available. In the Stern VSC–VSP model values of surface site density, maximum adsorption, equilibrium constants, and capacitances were optimized to fit charge and adsorption data. Table XI presents values of N_S, N_T, $\log K_i$, and C_i obtained by computer optimization for metal adsorption on goethite. For copper and zinc the adsorption of the species MOH^+ and MCl^+ is postulated; for lead the adsorption of Pb^{2+} and $PbCl^+$ is postulated based on goodness-of-fit criteria (Barrow *et al.*, 1981). The ability of the Stern VSC–VSP model to describe zinc adsorption on goethite is indicated in Fig. 22. The model describes the data very well.

Table XI

Values of Maximum Surface Charge Density, Maximum Adsorption Density, Binding Constants, and Capacitances Obtained with the Stern VSC–VSP Model by Computer Optimization for Metal Adsorption on Goethite[a]

Parameter	Copper[b]	Lead[b]	Zinc[c]
Maximum surface charge density (μmol m^{-2})	10.0	10.0	10.4
Maximum metal adsorption density (μmol m^{-2})	6.0	6.0	7.28
Capacitances			
$C_{o\alpha}$ (F m^{-2})	6.30	5.54	4.8
$C_{o\beta}$ (F m^{-2})	1.82	1.82	0.99
$C_{\beta d}$ (F m^{-2})	0.97	0.97	0.97
Binding constants			
log K_H	8.0	8.0	8.02
log K_{OH}	6.69	6.69	6.03
log K_{Na}	−0.7	−0.7	−0.96
log K_{Cl}	−0.36	−0.36	−0.92
log K_{MOH^+}	8.61	—	6.45
log $K_{M^{2+}}$	—	7.89	—
log K_{MCl^+}	6.60	5.60	6.01

[a]From Barrow *et al.* (1981).
[b]Based on experimental data of Forbes *et al.* (1976).
[c]Based on experimental data of Bolland *et al.* (1977).

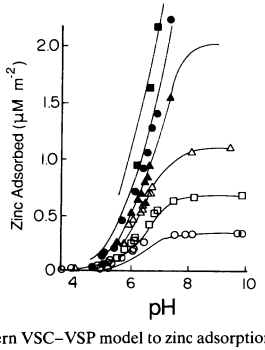

Figure 22. Fit of the Stern VSC–VSP model to zinc adsorption on goethite. Model results are represented by solid lines. Model parameter values are provided in Table XI. From Barrow *et al.* (1981), based on experimental data of Bolland *et al.* (1977).

The Stern VSC–VSP model was extended to describe ion adsorption by soil materials (Barrow, 1983) and then further extended to describe the rate of adsorption (Barrow, 1986a). This model was applied to a range of anions but generally was limited to one soil sample (details will be provided in Section V,C). The extended Stern VSC–VSP model has been called a mechanistic model and has been applied to describe zinc adsorption on several soils (Barrow, 1986c). The mechanistic Stern VSC–VSP model contains the following assumptions: (1) individual sites react with adsorbing ions as with sites on variable-charge oxides, (2) a range of sites exists whose summed adsorption behavior can be modeled by a distribution of parameters of the variable-charge model, and (3) the initial adsorption reaction induces a diffusion gradient into the particle interior and begins a solid-state diffusion process. The equations for the mechanistic Stern VSC–VSP model describe the following conditions (Barrow, 1986a):

(A) Heterogeneity of the surface:

$$P_j = 1/(\sigma/\sqrt{\Delta 2\pi}) \exp[-0.5(\Psi_{a0j} - \bar{\Psi}_{a0}/\sigma)^2] \tag{115}$$

where P_j is the probability that a particle has initial potential Ψ_{a0j}, $\bar{\Psi}_{a0}$ is the average of Ψ_{a0j}, and σ is the standard deviation of Ψ_{a0j}.

(B) Adsorption on each component of the surface:

(1) at equilibrium:

$$\theta_j = \frac{K_i \alpha \gamma c \exp(-Z_i F \Psi_{aj}/RT)}{1 + K_i \alpha \gamma c \exp(-Z_i F \Psi_{aj}/RT)} \tag{116}$$

where θ_j is the proportion of the jth component occupied by the ith ion, K_i and Z_i are the binding constant and valence for the ith adsorbing ion, Ψ_{aj} is the potential of the jth component, α is the fraction of adsorbate present as the ith ion, γ is the activity coefficient, and c is the total concentration of adsorbate.

(2) rate of adsorption:

$$\theta_{jt} = \frac{K_1^* c(1 - \theta_j) - k_2^* \theta_j}{k_1^* c + k_2^*} \{1 - \exp[-t(k_1^* c + k_2^*)]\} \tag{117}$$

where θ_{jt} is the increment in θ_j over time interval t, and

$$k_1^* = k_1 \alpha \gamma \exp(\vec{\alpha} F \Psi_{aj}/RT) \tag{118}$$

$$k_2^* = k_2 \alpha \gamma \exp(-\vec{\alpha} F \Psi_{aj}/RT) \tag{119}$$

where k_1 and k_2 are rate coefficients and $\vec{\alpha}$ and $\vec{\alpha}$ are transfer coefficients.

(C) Diffusive penetration:

$$M_j = 2/\sqrt{\pi}\left\{C_{0j}\sqrt{(\bar{D}ft)} + \sum^{k}(C_{kj} - C_{kj-1})\sqrt{[\bar{D}f_k(t - t_k)]}\right\} \tag{120}$$

where M_j is the amount of material transferred to the interior of the jth component on an area basis, C_{0j} is the surface concentration of the adsorbed ion at time t, C_{kj} is the value of C_{0j} at time t_k, $\tilde{D}$ is the coefficient related to the diffusion coefficient via the thickness of the adsorbed layer, and f is the thermodynamic factor.

(D) Feedback effects on potential:

(1) for a single period of measurement:

$$\Psi_{aj} = \Psi_{a0j} - m_1\theta_j \tag{121}$$

where Ψ_{aj} is the potential of the jth component after reaction and m_1 is a parameter.

(2) for measurement through time:

$$\Psi_{aj} = \Psi_{a0j} - m_1\theta_j - m_2M_j/N_{mj} \tag{122}$$

where N_{mj} is the maximum adsorption on component j and m_2 is a parameter.

(E) Effects of temperature :

$$\tilde{D} = A\exp(-E/RT) \tag{123}$$

where E is an activation energy and A is a parameter.

These equations were incorporated into a computer program. The continuous distribution of Eq. (115) was divided into 30 discrete elements. The 30 sets of equations were solved by an iterative procedure using a computer program and the criterion of goodness of fit to ion sorption (Barrow, 1983). Because of the very large number of adjustable parameters, the use of the mechanistic Stern VSC–VSP model should be regarded as a curve-fitting procedure, although of course fit to the data is usually excellent.

The mechanistic Stern VSC–VSP model has been used to describe the effects of time and temperature on zinc sorption on an Australian soil (Barrow, 1986b), the effect of pH on zinc sorption on several soils (Barrow, 1986c), and the point of zero salt effect for zinc sorption on an Australian soil (Barrow and Ellis, 1986b). The model was able to describe the data well in all cases using the assumption that the species $ZnOH^+$ adsorbs on the surface. Serious difficulties in the use of the model result because calcium carbonate was added to raise the pH and calcium nitrate solutions were used as the background electrolyte. Unless calcium can be shown to act solely as an inert background electrolyte, the chemical significance of the parameters obtained in these modeling procedures is expected to be compromised by specific adsorption of calcium.

The mechanistic Stern VSC–VSP model has also been used to describe zinc, nickel, and cadmium adsorption by a goethite slightly contaminated

with silicon (Barrow *et al.*, 1989). As was the case for soil, excellent fits to the adsorption data were obtained. Although in these experiments pH was adjusted with additions of sodium hydroxide, the background electrolyte was still calcium nitrate.

D. Generalized Two-Layer Model

Application of the generalized two-layer model to metal adsorption has been restricted to the hydrous ferric oxide surface (Dzombak and Morel, 1990). As discussed in Section II,D, adsorption of metal ions is postulated to occur on two types of sites of high or low affinity. Intrinsic conditional equilibrium constants for the generalized two-layer model for metal adsorption were obtained with the computer program FITEQL (Westall, 1982). Individual values of $\log K_M^i(\text{int})$ and best estimates of $\overline{\log K_M^i(\text{int})}$ were obtained as described for protonation–dissociation constants in Section III,D. Metal adsorption is defined by reaction Eqs. (51) and (52) for silver, cobalt, nickel, cadmium, zinc, copper, lead, and mercury. For adsorption of alkaline earth cations, the reaction on the strong sites, Eq. (51), is replaced by:

$$S^sOH + M^{2+} \rightleftarrows S^sOHM^{2+} \tag{124}$$

For strontium adsorption an additional reaction on the weak sites is defined:

$$S^wOH + Sr^{2+} + H_2O \rightleftarrows S^wOSrOH + 2H^+ \tag{125}$$

Adsorption of trivalent chromium metal occurs only on the strong sites by one reaction:

$$S^sOH + Cr^3 + H_2O \rightleftarrows S^sOCrOH^+ + 2H^+ \tag{126}$$

Table XII presents values of best estimates of $\overline{\log K_M^i(\text{int})}$ obtained by FITEQL computer optimization. The ability of the generalized two-layer model to describe copper adsorption on hydrous ferric oxide is indicated in Fig. 23. The model describes the data very well using both individual data set values and the best estimates of $\overline{\log K_M^i(\text{int})}$.

The surface precipitation model for metal ions (see Section IV,A) has been incorporated into the generalized two-layer model (Dzombak and Morel, 1990). Adsorption of metal ions is assumed to occur on both the strong and the weak sites via the reactions

$$\equiv S^sOH + M^{2+} + H_2O \rightleftarrows S^s(OH)_{3(s)} + \equiv MOH_2^+ + H^+ \tag{127}$$

$$\equiv S^wOH + M^{2+} + H_2O \rightleftarrows S^w(OH)_{3(s)} + \equiv MOH_2^+ + H^+ \tag{128}$$

Table XII

Values of Intrinsic Metal Surface Complexation and Surface Precipitation Constants Obtained with the Generalized Two-Layer Model Using FITEQL Computer Optimization for Hydrous Ferric Oxide[a]

Metal	$\overline{\log K^1_M(\text{int})}$[b]	$\overline{\log K^2_M(\text{int})}$[c]	$\overline{\log K^3_M(\text{int})}$[d]	Number of data sets[e]
		Surface complexation[f]		
Ca^{2+}	4.97 ± 0.10	−5.85 ± 0.19	—	9
Sr^{2+}	5.01 ± 0.03	−6.58 ± 0.23	−17.60 ± 3.06	12
Ba^{2+}	5.46 ± 0.12	—	—	6
Ag^{+}	−1.72 ± 0.20	—	—	6
Co^{2+}	−0.46 ± 0.12	−3.01 ± 0.14	—	13
Ni^{2+}	0.37 ± 0.58	—	—	2
Cd^{2+}	0.47 ± 0.03	−2.90	—	24
Zn^{2+}	0.99 ± 0.02	−1.99 ± 0.06	—	21
Cu^{2+}	2.89 ± 0.07	—	—	10
Pb^{2+}	4.65 ± 0.14	—	—	4
Hg^{2+}	7.76 ± 0.02	6.45 ± 0.12	—	12
Cr^{3+}	2.06 ± 0.15	—	—	4
		Surface precipitation[g]		
	$\overline{\log K^S_S(\text{int})}$	$\overline{\log K^W_s(\text{int})}$	$\log K_{spM}$	
Zn^{2+}	3.49	0.51	11.7	1
Hg^{2+}	10.26	8.95	3.88	11

[a] From Dzombak and Morel (1990).

[b] $\log K^1_M(\text{int})$ is defined for reaction Eq. (124) for alkaline earth metals, for reaction Eq. (126) for chromium, and for reaction Eq. (51) for all other metals.

[c] $\log K^2_M(\text{int})$ is defined for reaction Eq. (52).

[d] $\log K^3_M(\text{int})$ is defined for reaction Eq. (125).

[e] Experimental data sources provided in Chapter 6 of Dzombak and Morel (1990).

[f] 95% confidence intervals.

[g] $\log K_{spFe} = 2.5$, $\log K^S_S(\text{int}) = \log K^1_M(\text{int}) + \log K_{spFe}$, $\log K^W_S(\text{int}) = \log K^2_M(\text{int}) + \log K_{spFe}$.

The intrinsic equilibrium constants for the reactions as written are $K^s_s(\text{int})$ for Eq. (127) and $K^w_s(\text{int})$ for Eq. (128). The reactions for precipitation of M^{2+} and Fe^{3+} are as written in Eqs. (111) and (112). The surface precipitation model generally describes the metal sorption data well.

E. One-p*K* Model

Application of the one-pK model to metal adsorption has so far been restricted to cadmium adsorption on the iron oxides, hematite and amorphous iron oxide (van Riemsdijk *et al.*, 1987). Adsorption of cadmium was

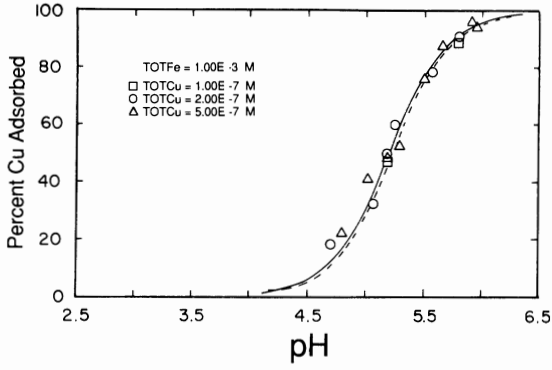

Figure 23. Fit of the generalized two-layer model to copper adsorption on hydrous ferric oxide. Model results are represented by a solid line for individual $\log K^1_{Cu}(\text{int})$ and a dashed line for $\log K^1_{Cu}(\text{int})$; $\log K^1_{Cu}(\text{int}) = 2.91$, $\log K^2_{Cu}(\text{int})$ was not necessary; $\log K^1_{Cu}(\text{int})$ is provided in Table XII. From Dzombak and Morel (1990), based on experimental data of Benjamin (1978) and Leckie *et al.* (1980), reproduced with permission from John Wiley and Sons.

modeled as occurring in the Stern plane. Good model fits to data were obtained by considering only the formation of the hydrolysis surface complex as given in Eq. (66). The adsorption density of the metal surface complex formed by reaction Eq. (65) was negligible (van Riemsdijk *et al.*, 1987). The equilibrium constant expression for the hydrolysis surface complex is provided by Eq. (72). To describe the adsorption of cadmium on iron oxides, values for $\log K_H$, $\log K_{C^+}$, $\log K_{A^-}$, and C were obtained from potentiometric titration data and have already been provided in Table VIII. To describe cadmium adsorption on hematite, no surface complexation constants for the background electrolyte are considered. The ability of the simplified one-pK model to describe cadmium adsorption on hematite is indicated in Fig. 24. The model describes the data quite well. To describe cadmium adsorption on amorphous iron oxide, values of $\log K_{C^+}$ and $\log K_{A^-}$ were included. The fit was similar in quality to that obtained on hematite (van Riemsdijk *et al.*, 1987). The value of the equilibrium constant, $\log K^2_{Cd} = -6.97$, for amorphous iron oxide is very similar to that for hematite, $\log K^2_{Cd} = -6.41$.

The one-pK model was expanded to include surface heterogeneity (van Riemsdijk *et al.*, 1987). As for surface charging behavior, the sensitivity of metal adsorption toward the degree of heterogeneity was low. The fit of the model could not be improved significantly by including surface heterogeneity, thus allowing a homogeneous model to be used.

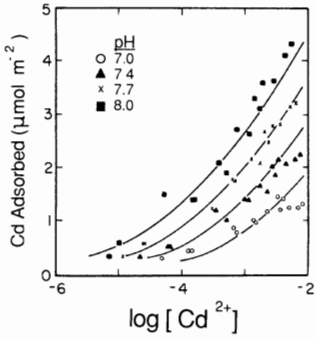

Figure 24. Fit of the simplified one-pK model to cadmium adsorption on amorphous iron oxide. Model results are represented by solid lines; log $K^2_{Cd} = -6.41$. From van Riemsdijk *et al.* (1987).

V. APPLICATION OF MODELS TO INORGANIC ANION ADSORPTION REACTIONS ON OXIDES, CLAY MINERALS, AND SOILS

A. Constant Capacitance Model

Characterization of anion adsorption behavior as a function of solution pH results in curves termed adsorption envelopes. The constant capacitance model has been used to describe inorganic anion adsorption envelopes on iron oxides (Sigg and Stumm, 1981; Goldberg and Sposito, 1984a; Goldberg, 1985, 1986a,b; Goldberg and Glaubig, 1985), aluminum oxides (Hohl *et al.*, 1980; Goldberg and Sposito, 1984a; Goldberg and Glaubig, 1985, 1988a; Goldberg, 1986a,b; Bleam *et al.*, 1991), clay minerals (Goldberg, 1986b; Goldberg and Glaubig, 1986b, 1988b,c; Motta and Miranda, 1989), and soils (Goldberg and Sposito, 1984b; Goldberg, 1986b; Goldberg and Glaubig, 1986a, 1988b,c; Sposito *et al.*, 1988). In the application of the constant capacitance model to inorganic anion adsorption, the surface complexation reactions are usually written in terms of undissociated acids (Sigg and Stumm, 1981). The reactions Eqs. (8) and (9) are replaced by the expressions

$$SOH + H_xL = SH_{(x-i)}L^{(1-i)} + H_2O + (i-1)H^+ \quad (129)$$

$$2SOH + H_xL = S_2H_{(x-j)}L^{(2-j)} + 2H_2O + (j-2)H^+ \quad (130)$$

where x is the number of protons present in the undissociated form of the acid, $1 \leq i \leq n$, and $2 \leq j \leq n$, where n is the number of anion surface complexes and is equal to the number of dissociations undergone by the acid. The intrinsic conditional equilibrium constants describing these reactions are

$$K_{\mathrm{L}}^{i}(\mathrm{int}) = \frac{[\mathrm{SH}_{(x-i)}\mathrm{L}^{(1-i)}][\mathrm{H}^{+}]^{(i-1)}}{[\mathrm{SOH}][\mathrm{H}_x\mathrm{L}]} \exp[(1-i)F\Psi/RT] \qquad (131)$$

$$K_{\mathrm{L}}^{j}(\mathrm{int}) = \frac{[\mathrm{S}_2\mathrm{H}_{(x-j)}\mathrm{L}^{(2-j)}][\mathrm{H}^{+}]^{(j-2)}}{[\mathrm{SOH}]^2[\mathrm{H}_x\mathrm{L}]} \exp[(2-j)F\Psi/RT] \qquad (132)$$

Sigg and Stumm (1981) postulated bidentate reactions [Eq. (130)] for phosphate and sulfate adsorption on goethite; Hohl *et al.* (1980) postulated bidentate species for sulfate adsorption on aluminum oxide. However, Goldberg and Sposito (1984a) obtained good fits to the phosphate adsorption data of Sigg (1979) by considering only monodentate species. All other applications of the constant capacitance model have been restricted to monodentate anion adsorption reactions [Eq. (129)]. The fit of the constant capacitance model to sulfate adsorption was not good (Sigg, 1979; Sigg and Stumm, 1981). Sigg (1979) postulated that this poor fit could have been caused by the presence of a $NaSO_4^-$ ion pair that had not been included in model calculations. An alternative explanation is that sulfate adsorbs via an outer-sphere mechanism and that therefore use of the constant capacitance model is not appropriate. Intrinsic conditional equilibrium constants for anions in the constant capacitance model are obtained using the computer program MICROQL (Westall, 1979) or by computer optimization using the program FITEQL (Westall, 1982). Figure 25 presents the ability of the constant capacitance model to describe silicate adsorption on goethite. The ability of the model to describe the adsorption data is very good.

Table XIII provides values for intrinsic inorganic anion surface complexation constants obtained with the constant capacitance model for various materials. In the work of Goldberg and co-workers (Goldberg and Sposito, 1984a; Goldberg, 1985, 1986a,b; Goldberg and Glaubig, 1985, 1988a) values of $\log K_{\pm}(\mathrm{int})$ were averages obtained from a literature compilation of experimental $\log K_{\pm}(\mathrm{int})$ values. Values of the protonation–dissociation constants, the phosphate surface complexation constants (Goldberg and Sposito, 1984a), and the boron surface complexation constants (Goldberg and Glaubig, 1985) obtained in this fashion were not significantly different statistically for aluminum and iron oxide minerals.

Applications of the constant capacitance model to anion adsorption edges on clay minerals have been carried out for boron (Goldberg and

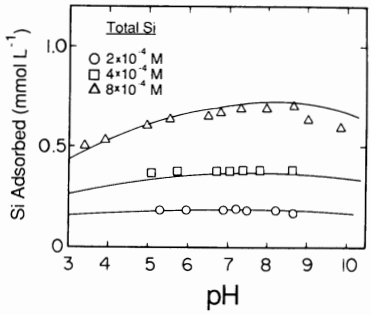

Figure 25. Fit of the constant capacitance model to silicate adsorption on goethite. Model results are represented by solid lines. Model parameters are provided in Table XIII. From Sigg and Stumm (1981).

Glaubig, 1986b), selenium (Goldberg and Glaubig, 1988b), arsenic (Goldberg and Glaubig, 1988c), and molybdenum adsorption (Motta and Miranda, 1989). To describe boron, arsenic, and selenium adsorption on kaolinite and selenium adsorption on montmorillonite, $\log K_{\pm}(\text{int})$ values were based on averages for a literature compilation of aluminum oxides. The assumption was made that adsorption occurs via ligand exchange with aluminol groups on the clay mineral edges (Goldberg and Glaubig, 1986b). To describe boron and arsenic adsorption on montmorillonite and boron adsorption on illite, $\log K_{\pm}(\text{int})$ were optimized with the anion surface complexation constants (Goldberg and Glaubig, 1986b, 1988c). Although the fit to anion adsorption was generally good (see Fig. 26), in some cases the optimized value of $\log K_{+}(\text{int})$ was larger than the optimized absolute value for $\log K_{-}(\text{int})$ or the optimized value for $\log K_{-}(\text{int})$ was insignificantly small. These are chemically unrealistic situations that would potentially reduce the application of the model to a curve-fitting procedure. Additional research is needed. Alternatively, in the application of the constant capacitance model to molybdate adsorption on clays, $\log K_{\pm}(\text{int})$ values were obtained from potentiometric titration data (Motta and Miranda, 1989). Fit of the model to molybdate adsorption data was good, although the zero point of charge values for illite were surprisingly high.

The first application of the constant capacitance model to adsorption on heterogeneous soil systems was the study of Goldberg and Sposito (1984b) of phosphate adsorption on 44 soils. These authors used $\log K_{\pm}(\text{int})$ values that were averages obtained from a literature compilation of $\log K_{\pm}(\text{int})$ values for aluminum and iron oxide minerals. The authors calculated a

Table XIII

Values of Intrinsic Inorganic Anion Surface Complexation Constants Obtained with the Constant Capacitance Model Using Computer Optimization[a]

Solid	Anion	Ionic medium	$\log K_L^1$(int)	$\log K_L^2$(int)	$\log K_L^3$(int)	Reference
γ-Al_2O_3[b]	PO_4^{3-}	0.01 *M* $NaClO_4$	10.34	4.30	−2.81	Goldberg and Sposito (1984a)
γ-Al_2O_3[b]	PO_4^{3-}	0.1 *M* NaCl	8.50	2.21	—	Goldberg and Sposito (1984a)
γ-Al_2O_3[b]	PO_4^{3-}	0.1 *M* NaCl	9.78	—	−3.61	Goldberg and Sposito (1984a)
γ-Al_2O_3	SO_4^{2-}	0.1 *M* $NaClO_4$	−3.6[c]	− 9.4[c]	—	Hohl *et al.* (1980)
δ-Al_2O_3	$Si(OH)_4^-$	0.1 *M* NaCl	4.14	− 3.17	—	Goldberg and Glaubig (1988a)
δ-Al_2O_3	$B(OH)_4$	0.1 *M* NaCl	5.13	—	—	Goldberg and Glaubig (1985)
δ-Al_2O_3	$B(OH)_4$	0.1 *M* NaCl	5.56	—	—	Goldberg and Glaubig (1985)
δ-Al_2O_3	$B(OH)_4^-$	0.1 *M* NaCl	2.87	—	—	Goldberg and Glaubig (1988a)
α-Alumina[b]	PO_4^{3-}	0.01 *M* NaCl	8.69	2.89	−4.78	Goldberg and Sposito (1984a)
Hydrous alumina[b]	PO_4^{3-}	0.01 *M* KCl	7.79	2.19	—	Goldberg and Sposito (1984a)
Activated alumina[b]	$B(OH)_4^-$	$I = 0$	5.09	—	—	Goldberg (1986b)
α-$Al(OH)_3$[b]	PO_4^{3-}	0.1 *M* NaCl	9.46	5.26	0.62	Goldberg and Sposito (1984a)
α-$Al(OH)_3$[b]	PO_4^{3-}	NaCl	11.11	3.98	−3.75	Goldberg and Sposito (1984a)
α-$Al(OH)_3$[b]	PO_4^{3-}	KCl	9.01	2.56	—	Goldberg and Sposito (1984a)
α-$Al(OH)_3$[b]	AsO_4^{3-}	0.1 *M* NaCl	9.72	3.41	−3.58	Goldberg (1986a)
α-$Al(OH)_3$[b]	SeO_3^{2-}	0.1 *M* NaCl	9.74	3.64	—	Goldberg (1986b)
γ-AlOOH	PO_4^{3-}	0.001 *M* KCl	7.28[d]	—	−1.05[d]	Bleam *et al.* (1991)
Pseudoboehmite	$B(OH)_4$	0.1 *M* NaCl	5.09	—	—	Goldberg and Glaubig (1985)
$Al(OH)_3$(am)[b]	AsO_4^{3-}	0.01 *M* $NaClO_4$	9.89	3.32	−4.52	Goldberg (1986a)
$Al(OH)_3$(am)[b]	AsO_4^{3-}	0.01 *M* $NaClO_4$	11.06	3.55	−3.19	Goldberg (1986b)
$Al(OH)_3$(am)	$B(OH)_4^-$	0.1 *M* NaCl	5.92	—	—	Goldberg and Glaubig (1985)

α-FeOOH	PO_4^{3-}	0.1 *M* $NaClO_4$	9.5[e]	5.1[e]	−1.5[e]	Sigg and Stumm (1981)
α-FeOOH[b]	PO_4^{3-}	0.1 *M* $NaClO_4$	10.54	7.25	2.94	Goldberg and Sposito (1984a)
α-FeOOH[b]	PO_4^{3-}	0.1 *M* NaCl	10.43	6.25	0.17	Goldberg (1985)
α-FeOOH[b]	PO_4^{3-}	0.1 *M* NaCl	10.49	6.27	0.17	Goldberg (1985)
α-FeOOH[b]	PO_4^{3-}	0.1 *M* NaCl	11.22	7.06	0.99	Goldberg (1985)
α-FeOOH[b]	AsO_4^{3-}	0.1 *M* NaCl	10.10	5.80	−0.63	Goldberg (1986a)
α-FeOOH[b]	AsO_4^{3-}	0.1 *M* NaCl	10.87	6.52	0.29	Goldberg (1986a)
α-FeOOH[b]	SeO_3^{2-}	0.1 *M* NaCl	10.02	5.36	—	Goldberg (1985)
α-FeOOH[b]	SeO_3^{2-}	0.1 *M* NaCl	11.10	5.80	—	Goldberg (1985)
α-FeOOH	SO_4^{2-}	0.1 *M* $NaClO_4$	−5.8[c]	−13.5[c]	—	Sigg and Stumm (1981)
α-FeOOH	$Si(OH)_4$	0.1 *M* $NaClO_4$	4.1	−3.3	—	Sigg and Stumm (1981)
α-FeOOH[b]	$Si(OH)_4^-$	0.1 *M* $NaClO_4$	3.82	−4.27	—	Goldberg (1985)
α-FeOOH[b]	$Si(OH)_4^-$	0.1 *M* $NaClO_4$	4.48	−3.43	—	Goldberg (1985)
α-FeOOH	F^-	0.1 *M* $NaClO_4$	−4.8[f]	—	—	Sigg and Stumm (1981)
α-FeOOH	$B(OH)_4^-$	0.1 *M* NaCl	5.25	—	—	Goldberg and Glaubig (1985)
α-Fe_2O_3[b]	PO_4^{3-}	$I = 0$	7.43	2.06	−4.23	Goldberg and Sposito (1984a)
α-Fe_2O_3	$B(OH)_4^-$	0.1 *M* NaCl	4.88	—	—	Goldberg and Glaubig (1985)
$Fe(OH)_3$(am)[b]	PO_4^{3-}	0.01 *M* $NaClO_4$	11.84	5.60	−0.65	Goldberg and Sposito (1984a)
$Fe(OH)_3$(am)[b]	PO_4^{3-}	0.125 *M* $NaClO_4$	10.78	3.86	−3.67	Goldberg and Sposito (1984a)
$Fe(OH)_3$(am)[b]	PO_4^{3-}	1 *M* $NaClO_4$	11.75	4.22	−0.27	Goldberg and Sposito (1984a)
$Fe(OH)_3$(am)[b]	PO_4^{3-}	0.1 *M* $NaClO_4$	10.72	4.63	−1.63	Goldberg and Sposito (1984a)
$Fe(OH)_3$(am)[b]	PO_4^{3-}	0.01 *M* $NaClO_4$	—	3.39	−4.57	Goldberg and Sposito (1984a)
$Fe(OH)_3$(am)	$B(OH)_4^-$	0.1 *M* NaCl	5.63	—	—	Goldberg and Glaubig (1985)
Kaolinites[g]	$B(OH)_4^-$	0.1 *M* NaCl	5.28 ± 0.2	—	—	Goldberg and Glaubig (1986b)
Kaolinite	AsO_4^{3-}	0.1 *M* NaCl	11.04	8.24	−3.21	Goldberg and Glaubig (1988c)
Kaolinite	SeO_3^{2-}	0.1 *M* NaCl	11.07	3.34	—	Goldberg and Glaubig (1988b)
Kaolinite	MoO_4^{2-}	0.01 *M* NaCl	4.95	0.95	—	Motta and Miranda (1989)

(*continues*)

Table XIII (*Continued*)

Solid	Anion	Ionic medium	$\log K_L^1$(int)	$\log K_L^2$(int)	$\log K_L^3$(int)	Reference
Montmorillonites[h]	$B(OH)_4^-$	0.1 *M* NaCl	6.37 ± 1.3	—	—	Goldberg and Glaubig (1986b)
Montmorillonite	SeO_3^{2-}	0.1 *M* NaCl	10.92	3.40	—	Goldberg and Glaubig (1988b)
Montmorillonite	MoO_4^{2-}	0.01 *M* NaCl	5.23	—	—	Motta and Miranda (1989)
Illites[i]	$B(OH)_4^-$	0.1 *M* NaCl	5.39 ± 0.8	—	—	Goldberg and Glaubig (1986b)
Illite	MoO_4^{2-}	0.01 *M* NaCl	—	2.75	—	Motta and Miranda (1989)
Soils[j]	PO_4^{3-}		8.71 ± 0.6	2.41 ± 2.3	-5.14 ± 1.7	Goldberg and Sposito (1984b)
Soils[k]	$B(OH)_4^-$	0.01 *M* NaCl	5.48 ± 0.4	—	—	Goldberg and Glaubig (1986a)
Panoche soil	SeO_3^{2-}	0.05 *M* NaCl	7.35[l]	0.85[l]	—	Sposito *et al.* (1988)
Imperial soil	AsO_4^{3-}	0.1 *M* NaCl	9.94	3.71	−4.78	Goldberg and Glaubig (1988c)

[a] The work of Goldberg and co-workers was based on $\log K_+(\text{int}) = 7.38$, $\log K_-(\text{int}) = -9.09$ for aluminum oxides and kaolinites, and $\log K_+(\text{int}) = 7.31$, $\log K_-(\text{int}) = -8.80$ for iron oxides. All soils work was based on $\log K_+(\text{int}) = 7.35$, $\log K_-(\text{int}) = -8.95$ unless indicated otherwise.

[b] Experimental data source provided in the reference.

[c] $\log K_S^1(\text{int})$ and $\log K_S^2(\text{int})$ are defined for reactions Eqs. (8) and (9), respectively.

[d] The aqueous solution species $AlH_2PO_4^{2+}$ and $AlHPO_4^+$ are also included.

[e] The bidentate constants for the formation of S_2HPO_4 and $S_2PO_4^-$, reaction Eq. (9), were also optimized; $\log K_P^1(\text{int}) = 8.5$ and $\log K_P^2(\text{int}) = 4.5$.

[f] $\log K_F^1(\text{int})$ is defined for reaction Eq. (8).

[g] Average for four kaolinites.

[h] $\log K_+(\text{int}) = 10.62 \pm 1.6$ and $\log K_-(\text{int}) = -10.46 \pm 1.3$ were also optimized. Average for three montmorillonites.

[i] $\log K_-(\text{int}) = 9.30 \pm 1.3$ and $\log K_-(\text{int}) = -10.43 \pm 0.5$ were also optimized. Average for three illites.

[j] Average for 44 soils.

[k] $\log K_+(\text{int}) = 9.34 \pm 0.8$ and $\log K_-(\text{int}) = -10.64 \pm 0.9$ were also optimized. Average for 14 soils.

[l] $\log K_{Se}^1(\text{int}) = 20.05$ defined for reaction Eq. (9) was also optimized.

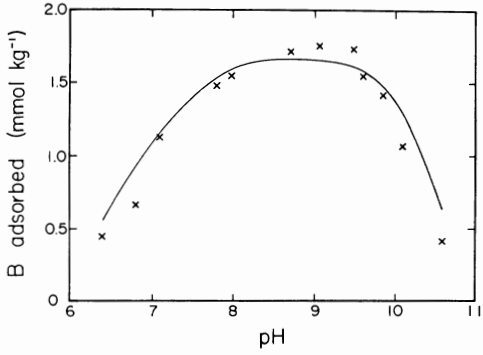

Figure 26. Fit of the constant capacitance model to boron adsorption on Morris illite. Model results are represented by a solid line; log K_+(int) = 8.49, log K_-(int) = −10.16, log K_B(int) = 5.04. From Goldberg and Glaubig (1986b).

phosphate-reactive specific surface area and obtained good fits of the constant capacitance model to phosphate adsorption data. A similar approach was used to describe arsenic adsorption on a soil (Goldberg and Glaubig, 1988b) and selenite adsorption on five alluvial soils (Sposito *et al.*, 1988). Sposito *et al.* (1988) used $\overline{\log K_{\pm}(\text{int})}$ values from Goldberg and Sposito (1984b) and assumed that two types of sites in soil were selenite reactive. Monodentate surface species are formed on one set of sites and bidentate surface species are formed on another set of sites. Using the intrinsic selenium surface complexation constants obtained for one of the soils, Sposito *et al.* (1988) were able to predict qualitatively the selenite adsorption envelopes for four other soils.

To describe boron adsorption on 14 soils (Goldberg and Glaubig, 1986a) and selenium adsorption on a soil (Goldberg and Glaubig, 1988b), log $K_{\pm}$(int) values were optimized with the anion surface complexation constants. As described previously for 2:1 clay minerals, the optimized value of log K_-(int) for some of the soils was insignificantly small. This unrealistic situation reduces the chemical significance of the model application. Using an average set of intrinsic conditional surface complexation constants, the constant capacitance model predicted boron adsorption on most of the soil samples studied (Goldberg and Glaubig, 1986a). The ability of the constant capacitance model to describe boron adsorption on a soil is presented in Fig. 27. Additional research is needed on the application of the constant capacitance model for describing adsorption on natural materials such as clay minerals and soils.

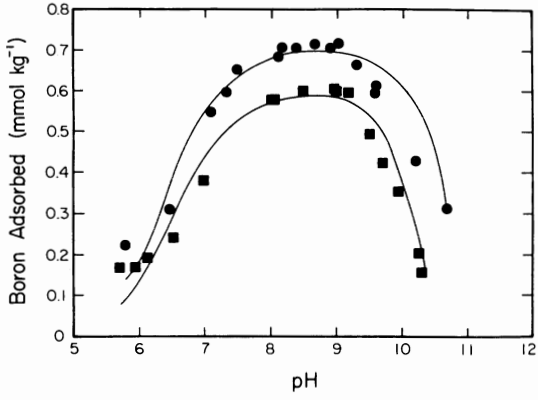

Figure 27. Fit of the constant capacitance model to boron adsorption on Altamont soil. Squares represent 0- to 25-cm samples: $\log K_+(\text{int}) = 8.72$, $\log K_-(\text{int}) = -8.94$, $\log K_B(\text{int}) = 5.57$. Circles represent 25- to 51-cm samples: $\log K_+(\text{int}) = 8.45$, $\log K_-(\text{int}) = -10.07$, $\log K_B(\text{int}) = 5.45$. Model results are represented by solid lines. From Goldberg and Glaubig (1986a).

The constant capacitance model was used to describe ion adsorption in binary oxide mixtures (Anderson and Benjamin, 1990a,b; see Section IV,A for metal adsorption). In the binary Si–Fe oxide system, the presence of dissolved silicate reduced phosphate and selenite adsorption (Anderson and Benjamin, 1990a). The constant capacitance model qualitatively described this effect on phosphate adsorption but not on selenite adsorption.

The surface precipitation model has been incorporated into the constant capacitance model to describe anion retention on oxide minerals (Farley *et al.*, 1985). Reactions of the surface precipitation model for trivalent anion sorption onto a trivalent oxide are as follows:

Adsorption of L^{3-} onto $S(OH)_{3(s)}$:

$$\equiv SOH + L^{3-} + 3H^+ \rightleftarrows \equiv SH_2L + H_2O \tag{133}$$

Precipitation of L^{3-}:

$$\equiv SH_2L + L^{3-} + S^{3+} \rightleftarrows SL_{(s)} + \equiv SH_2L \tag{134}$$

The reaction for the precipitation of S^{3+} has already been defined for metal adsorption by Eq. (112). The equilibrium constants for the reactions

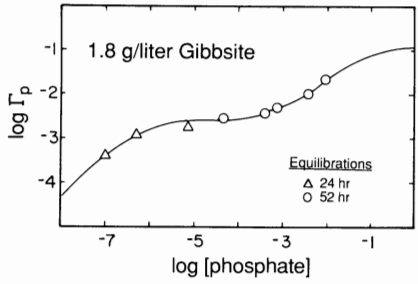

Figure 28. Fit of the constant capacitance model containing the surface precipitation model to a phosphate adsorption isotherm on gibbsite at pH 5.0. Model results are represented by a solid line. $\Gamma_P = ([\equiv AlH_2PO_4] + [AlPO_{4(s)}])/TOT(\equiv AlOH)$; $\log K_{adsP} = 30.8$, $\log K_{spP} = -16.6$, $\log K_{spAl} = 8.5$. From Farley *et al.* (1985), based on experimental data of van Riemsdijk and Lyklema (1980a, triangles; 1980b, circles).

as written are K_{adsL} for Eq. (133), $1/K_{spL}$ for Eq. (134), and $1/K_{spS}$ for Eq. (112). The ability of the surface precipitation model to describe phosphate adsorption on an aluminum oxide is indicated in Fig. 28. The model describes the data very well.

B. Triple-Layer Model

The triple-layer model has been used to describe inorganic anion adsorption envelopes on amorphous iron oxide (Davis and Leckie, 1980; Benjamin and Bloom, 1981; Zachara *et al.*, 1987; Hayes *et al.*, 1988; Balistrieri and Chao, 1990), goethite (α-FeOOH) (Balistrieri and Murray, 1981; Hayes *et al.*, 1988; Hawke *et al.*, 1989; Ainsworth *et al.*, 1989; Zhang and Sparks, 1989, 1990b,c; Goldberg, 1991), magnetite (Fe_3O_4) and zirconium oxide (Blesa *et al.*, 1984b), aluminum oxide (Davis and Leckie, 1980; Mikami *et al.*, 1983a,b), manganese oxide (Balistrieri and Chao, 1990), kaolinite (Zachara *et al.*, 1988), and soils (Charlet, 1986; Charlet and Sposito, 1989; Zachara *et al.*, 1989). Intrinsic conditional equilibrium constants for the triple-layer model have been obtained by using the computer programs MINEQL (Westall *et al.*, 1976), MICROQL (Westall, 1979), and HYDRAQL (Papelis *et al.*, 1988) or by computer optimization using the computer program FITEQL (Westall, 1982). In general, in the application of the triple-layer model to anion adsorption, the reactions Eqs. (24) and (25) with their equilibrium constants Eqs. (30) and (31) are considered.

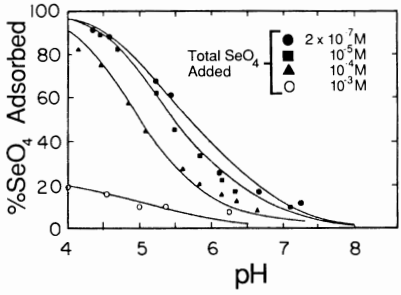

Figure 29. Fit of the triple-layer model to selenate adsorption on amorphous iron oxide. Model results are represented by solid lines; $\log K^1_{SeO_4}(\text{int}) = 9.9$, $\log K^2_{SeO_4}(\text{int}) = 15.9$. From Davis and Leckie (1980).

Figure 29 presents the ability of the triple-layer model to describe selenate adsorption on amorphous iron oxide. The model describes the adsorption data very well. Table XIV provides values for intrinsic inorganic anion surface complexation constants obtained with the triple-layer model for various surfaces. Adsorption of the trivalent anions PO_4^{3-} and AsO_4^{3-} is described by an additional reaction:

$$SOH + 3H^+ + L^{l-} \rightleftarrows SOH_2^+ - LH_2^{(l-2)-} \qquad (135)$$

Table XIV

Values of Intrinsic Inorganic Anion Surface Complexation Constants Obtained with the Triple-Layer Model by Computer Optimization

Solid	Anion	Ionic medium	$\log K^1_L(\text{int})$	$\log K^2_L(\text{int})$	Reference
		Original triple-layer model			
γ-Al_2O_3	PO_4^{3-}	NaCl	25.8[a]	31.6[b]	Mikami *et al.* (1983a)
γ-Al_2O_3	CrO_4^{2-}	$NaNO_3$	10.1	16.8	Mikami *et al.* (1983b)
α-Al_2O_3	CrO_4^{2-}	$NaNO_3$	11.3	18.1	Ainsworth *et al.* (1989)
α-FeOOH	SO_4^{2-}	NaCl	9.10	14.40	Balistrieri and Murray (1981)
α-FeOOH	CrO_4^{2-}	$NaNO_3$	9.8	19.4	Ainsworth *et al.* (1989)
α-FeOOH	F^-	NaCl	11.85	—	Hawke *et al.* (1989)
$Fe(OH)_3$(am)	CrO_4^{2-}	$NaNO_3$	10.6	18.1	Davis and Leckie (1980)
$Fe(OH)_3$(am)	CrO_4^{2-}	$NaNO_3$	10.1	19.3	Zachara *et al.* (1987)
$Fe(OH)_3$(am)	CrO_4^{2-}	$NaNO_3$	11.90	18.00	Benjamin and Bloom (1981)
$Fe(OH)_3$(am)	CrO_4^{2-}	$NaNO_3$	14.40	16.80	Benjamin and Bloom (1981)
$Fe(OH)_3$(am)	SO_4^{2-}	$NaNO_3$	9.9	15.9	Davis and Leckie (1980)

Table XIV (*Continued*)

Solid	Anion	Ionic medium	log K_L^1(int)	log K_L^2(int)	Reference
		Original triple-layer model			
$Fe(OH)_3$(am)	SO_4^{2-}	$NaNO_3$	11.6	17.3	Zachara *et al.* (1987)
$Fe(OH)_3$(am)	SeO_4^{2-}	KCl	9.5	15.15	Balistrieri and Chao (1990)
$Fe(OH)_3$(am)	SeO_4^{2-}	KCl	9.1	16.0	Balistrieri and Chao (1990)
$Fe(OH)_3$(am)	SeO_4^{2-}	$NaNO_3$	9.9	15.9	Davis and Leckie (1980)
$Fe(OH)_3$(am)	SeO_4^{2-}	$NaNO_3$	11.75	15.60	Benjamin and Bloom (1981)
$Fe(OH)_3$(am)	SeO_4^{2-}	$NaNO_3$	15.00	19.00	Benjamin and Bloom (1981)
$Fe(OH)_3$(am)	SeO_3^{2-}	$NaNO_3$	12.80	20.75	Benjamin and Bloom (1981)
$Fe(OH)_3$(am)	SeO_3^{2-}	$NaNO_3$	19.90	22.00	Benjamin and Bloom (1981)
$Fe(OH)_3$(am)	AsO_4^{3-}	$NaNO_3$	27.70[a]	33.50[b]	Benjamin and Bloom (1981)
$Fe(OH)_3$(am)	$Si(OH)_4$	KCl	—	27.3	Balistrieri and Chao (1990)
$Fe(OH)_3$(am)	$S_2O_3^{2-}$	$NaNO_3$	10.0	—	Davis and Leckie (1980)
Kaolinite[d]	CrO_4^{2-}	$NaClO_4$	9.19	17.1	Zachara *et al.* (1988)
Kaolinite[d]	CrO_4^{2-}	$NaClO_4$	9.42	16.9	Zachara *et al.* (1988)
Kaolinite[d]	CrO_4^{2-}	$NaClO_4$	9.42	16.3	Zachara *et al.* (1988)
Kaolinite[d]	CrO_4^{2-}	$NaClO_4$	9.48	16.2	Zachara *et al.* (1988)
Kaolinite	SO_4^{2-}	$NaClO_4$	9.49	15.6	Zachara *et al.* (1988)
Kaolinite	SO_4^{2-}	$NaClO_4$	9.37	15.9	Zachara *et al.* (1988)
		Modified triple-layer model			
ZrO_2	$B(OH)_4^-$	KNO_3	8.7[e]	9.7[f]	Blesa *et al.* (1984a)
Fe_3O_4	$B(OH)_4^-$	KNO_3	6.5[e]	8.3[f]	Blesa *et al.* (1984a)
α-FeOOH	SeO_4^{2-}	$NaNO_3$	8.90	15.70	Hayes *et al.* (1988)
α-FeOOH	SeO_4^{2-}	NaCl	12.94	—	Zhang and Sparks (1990c)
α-FeOOH	SeO_3^{2-}	$NaNO_3$	15.10[g]	14.10[h]	Hayes *et al.* (1988)
α-FeOOH	SeO_3^{2-}	NaCl	15.48[g]	20.42[i]	Zhang and Sparks (1990c)
α-FeOOH	PO_4^{3-}	NaCl	29.70[g]	33.40[j]	Hawke *et al.* (1989)
α-FeOOH	SO_4^{2-}	$NaNO_3$	15.4	—	Zhang and Sparks (1990b)
$Fe(OH)_3$(am)	SeO_4^{2-}	$NaNO_3$	9.60	14.50	Hayes *et al.* (1988)
$Fe(OH)_3$(am)	SeO_3^{2-}	$NaNO_3$	14.45[g]	—	Hayes *et al.* (1988)
$Fe(OH)_3$(am)	SeO_3^{2-}	KCl	25.56 ± 0.5[k]	—	Balistrieri and Chao (1990)
$Fe(OH)_3$(am)	MoO_4^{2-}	KCl	—	18.0[l]	Balistrieri and Chao (1990)
δ-MnO_2	SeO_3^{2-}	KCl	18.28 ± 0.5[l]	—	Balistrieri and Chao (1990)
δ-MnO_2	MoO_4^{2-}	KCl	—	18.7[l]	Balistrieri and Chao (1990)
Oxisol soil	SO_4^{2-}	Li_2SO_4	6.5[g]	—	Charlet (1986)

[a] log K_L^1(int) is defined by Eq. (31).
[b] log K_L^2(int) is defined by Eq. (136).
[c] Based on experimental data of Honeyman (1984).
[d] Also includes a surface complex SiOH—H_2CrO_4 whose equilibrium constant is a fitting parameter.
[e] log K_B(int) is defined for reaction Eq. (137). Inner-sphere surface complex.
[f] log K_{BC^+}(int) is defined for reaction Eq. (138). Inner-sphere surface complex.
[g] Inner-sphere surface complexes as described by Eqs. (129) and (131), where $\Psi = \Psi_o$ and $i = 2$.
[h] Inner-sphere surface complex as described by Eqs. (39) and (40).
[i] Inner-sphere surface complexes as described by Eqs. (129) and (131), where $\Psi = \Psi_o$ and $i = 1$.
[j] Optimization also included an inner-sphere complex as described by Eqs. (129) and (131) where $\Psi = \Psi_o$ and $i = 3$; log K_3^3(int) = 24.00.
[k] Inner-sphere bidentate surface complex as defined for reaction Eq. (139). Average of four suspension densities.
[l] Average of five suspension densities. Inner-sphere surface complex.

The intrinsic conditional equilibrium constant for this reaction is

$$K_{\mathrm{L}}^{3}(\mathrm{int}) = \frac{[\mathrm{SOH}_2^+ - \mathrm{LH}_2^{(l-2)-}]}{[\mathrm{SOH}][\mathrm{H}^+]^3[\mathrm{L}^{l-}]} \exp[F(\Psi_o - (l-2)\Psi_\beta)/RT] \quad (136)$$

The first extension of the triple-layer model to describe anion adsorption using a ligand-exchange mechanism and forming an inner-sphere surface complex was carried out by Blesa *et al.* (1984a) for boron adsorption on magnetite and zirconium dioxide. These researchers defined the following surface reaction for boron:

$$\mathrm{SOH} + \mathrm{B(OH)_3} + \mathrm{OH^-} \rightleftarrows \mathrm{SOB(OH)_3^-} + \mathrm{H_2O} \quad (137)$$

An additional boron surface complex was formed by reaction with the cation from the background electrolyte:

$$\mathrm{SOH} + \mathrm{B(OH)_3} + \mathrm{OH^-} + \mathrm{C^+} \rightleftarrows \mathrm{SOB(OH)_3^-C^+} + \mathrm{H_2O} \quad (138)$$

Blesa *et al.* (1984a) were well able to describe surface charge density data as a function of pH. It is impossible, however, to evaluate the ability of this approach to describe boron adsorption because the experimental adsorption data were not provided.

The modified triple-layer model was applied to describe ionic strength effects on selenate and selenite adsorption on goethite and amorphous iron oxide (Hayes *et al.*, 1988). These authors could only describe the ionic strength dependence of selenite adsorption using an inner-sphere surface complex and that of selenate using an outer-sphere surface complex. In order to improve the fit of the model, reaction Eq. (39) was added to describe selenite adsorption on goethite.

The modified triple–layer model has been successfully used to describe anion adsorption via a ligand-exchange mechanism. Inner-sphere surface complexes were used to describe phosphate (Hawke *et al.*, 1989), molybdate (Zhang and Sparks, 1989), and selenite (Zhang and Sparks, 1990c) adsorption on goethite, and selenite and molybdate adsorption on amorphous iron oxide and manganese oxide (Balistrieri and Chao, 1990). Selenite adsorption on amorphous iron oxide is defined by the reaction

$$2\mathrm{SOH} + \mathrm{SeO_3^{2-}} + 2\mathrm{H} \rightleftarrows \mathrm{S_2SeO_3} + 2\mathrm{H_2O} \quad (139)$$

The pressure-jump relaxation technique has been used to investigate anion adsorption on aluminum (Mikami *et al.*, 1983a,b) and iron oxide surfaces (Zhang and Sparks, 1989, 1990b,c). Mikami *et al.* (1983a) described phosphate adsorption and Mikami *et al.* (1983b) described chromate adsorption on aluminum oxide. These authors used the triple-layer model and its resultant equilibrium constants to describe their kinetic data and concluded that phosphate and chromate ions adsorb as outer-sphere

surface complexes. Various types of experimental evidence support an inner-sphere adsorption mechanism for phosphate on oxides (Goldberg and Sposito, 1985). The modified triple-layer model was used to describe both kinetic and adsorption data for molybdate (Zhang and Sparks, 1989, 1990a), sulfate (Zhang and Sparks, 1990b), and selenium adsorption (Zhang and Sparks, 1990c). Based on the kinetic results, inner-sphere surface complexes were postulated for molybdate and selenite, whereas outer-sphere surface complexes were postulated for sulfate and selenate. The magnitudes of the $\log K_L^i(\text{int})$ values obtained from kinetics were similar to those obtained from equilibrium modeling. This result is not unexpected because an equilibrium surface complexation model is required to analyze the kinetic data.

Application of the triple layer model to anion adsorption envelopes on the clay mineral kaolinite has been carried out (Zachara *et al.*, 1988). Values used for the protonation–dissociation constants for the aluminol group were obtained by Davis (1977) for amorphous aluminum oxide from the data of Anderson *et al.* (1976). Values used for $\log K_{\pm}(\text{int})$ for the silanol group were obtained by Riese (1982) for kaolinite using the double-extrapolation technique. In order to describe chromate adsorption on kaolinite, protonation–dissociation reactions for both aluminol and silanol groups were required. Anion surface complexation reactions for the aluminol group were defined by Eqs. (24) and (25). For the silanol group, an additional complex, $\text{SiOH—H}_2\text{CrO}_4$, is postulated whose surface complexation constant is considered a fitting parameter (Zachara *et al.*, 1988). To describe sulfate adsorption on kaolinite it was not necessary to invoke any reactions for the silanol group. The fit of the model to sulfate adsorption on kaolinite was good (see Fig. 30).

Chromate adsorption on aluminum-substituted goethite, α-(Fe,Al)OOH, was investigated (Ainsworth *et al.*, 1989). The authors considered two sets of reactive sites, partitioned into iron and aluminum sites based on a mole percentage of aluminum substitution. Good description of the adsorption data was obtained with the triple-layer model by considering protonation–dissociation reactions for both aluminum and iron sites and chromate surface complexation reactions only on iron sites (Ainsworth *et al.*, 1989).

The first application of the triple-layer model to anion adsorption on a complex natural system was the study of sulfate adsorption on a Brazilian Oxisol soil (Charlet, 1986; Charlet and Sposito, 1989). Charlet (1986) found good fits of the triple-layer model to sulfate adsorption on the Oxisol using an inner-sphere surface complex. However, Charlet and Sposito (1989) suggested that both inner-sphere and outer-sphere surface complexes for sulfate are likely to form.

Alternatively, the approach used by Ainsworth *et al.* (1989) for aluminum-substituted goethite was used by Zachara *et al.* (1989) to describe

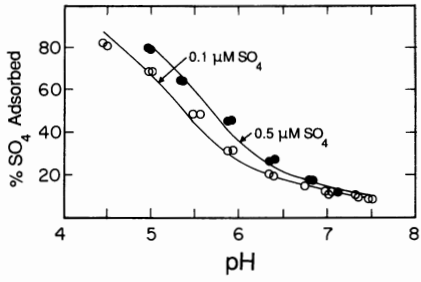

Figure 30. Fit of the triple-layer model to sulfate adsorption on kaolinite. Model results are represented by solid lines; $\log K_s^1 = 9.49$; $\log K_s^2 = 15.6$ for 0.1 μM SO_4; $\log K_s^1 = 9.37$, $\log K_s^2 = 15.9$ for 0.5 μM SO_4. After Zachara *et al.* (1988).

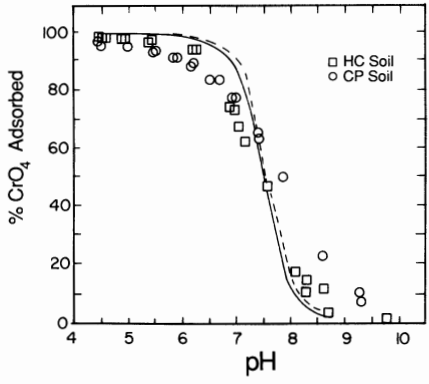

Figure 31. Fit of the triple-layer model to chromate adsorption on two soils. Model results are represented by a solid line (HC soil) and a dashed line (CP soil); $\log K^1_{CrO_4}(\text{int}) = 9.8$, $\log K^2_{CrO_4}(\text{int}) = 19.4$. After Zachara *et al.* (1989).

chromate adsorption on two soils. Aluminum-substituted goethite was assumed to be the chromate-reactive mineral in these soils. As for α-(Fe,Al)OOH, protonation–dissociation reactions were considered for both aluminum and iron sites but chromate adsorption was restricted to iron sites. The surface site density was estimated based on clay content and surface area measurements (Zachara *et al.*, 1989). Figure 31 presents the

ability of the triple-layer model to describe chromate adsorption on two soils. The fit is qualitatively correct.

C. Stern VSC–VSP Model

The Stern VSC–VSP model has been successfully used to describe adsorption of the inorganic anions phosphate, selenite (Bowden *et al.*, 1980; Barrow *et al.*, 1980b), molybdate (McKenzie, 1983), and borate (Bloesch *et al.*, 1987) on the iron oxide, goethite. Application of the model to describe molybdate adsorption on manganese oxide was unsuccessful (McKenzie, 1983). The model failed to describe the lower pH of maximum molybdate adsorption on manganese oxide. McKenzie (1983) attributed this failure to lack of knowledge of adsorbing molybdenum polymers. As for metal adsorption, in the Stern VSC–VSP model, values of surface site density, maximum adsorption, binding constants, and capacitances are optimized to fit charge and/or adsorption data. Table XV presents values of N_S, N_T, $\log K_i$, and C_i obtained by computer optimization for anion adsorption on goethite. For phosphate and selenite, adsorption of the divalent species HPO_4^{2-} and SeO_3^{2-} is postulated (Bowden *et al.*, 1980; Barrow *et al.*, 1980b). For molybdate, adsorption of both $HMoO_4$ and MoO_4^{2-} is considered (McKenzie, 1983). Four adsorbing species are considered for boron: $B(OH)_4^-$, $B_3O_3(OH)_4^-$, $B_4O_5(OH)_4^{2-}$, and $B_5O_6(OH)_4^-$ (Bloesch *et al.*, 1987). The ability of the Stern VSC–VSP model to describe boron adsorption on goethite is indicated in Fig. 32. The model describes the data well, as would be expected given the large number of adjustable parameters. The Stern VSC–VSP model was also able to describe ionic strength effects on phosphate adsorption by goethite (Barrow *et al.*, 1980b).

As discussed in Section IV,C, the Stern VSC–VSP model was extended to describe phosphate adsorption by soil (Barrow, 1983). This model was used to describe the effect of pH on phosphate sorption by various soils (Barrow, 1984) and was further extended to describe the rate of sorption (Barrow, 1986a). The equations and assumptions of this extended mechanistic Stern VSC–VSP model are provided in Section IV,C. As discussed in detail in Section IV,C, use of the mechanistic Stern VSC–VSP model should be regarded as a curve-fitting procedure.

The mechanistic Stern VSC–VSP model has been used to describe the effects of time and temperature on fluoride, molybdate (Barrow, 1986b), selenite, and selenate adsorption on an Australian soil (Barrow and Whelan, 1989b), the effect of pH on fluoride (Barrow and Ellis, 1986a), phosphate (Barrow, 1986c), selenite, selenate (Barrow and Whelan, 1989a),

Table XV

Values of Maximum Surface Charge Density, Maximum Adsorption Density, Binding Constants, and Capacitances Obtained with the Stern VSC–VSP Model by Computer Optimization for Anion Adsorption on Goethite

Parameter	Phosphate[a]	Selenite[a]	Molybdate[b]	Borate[c]	Citrate[a]
Maximum surface charge density (μmol m^{-2})	10.0	10.0	10.0	10.0	10.0
Maximum anion adsorption density (μmol m^{-2})	2.43	2.71	6.0	4.34	1.74
Capacitances					
$C_{o\alpha}$ (F m^{-2})	3.03	4.06	3.03	2.92	3.36
$C_{o\beta}$ (F m^{-2})	1.93	1.93	1.93	0.914	1.12
$C_{\beta d}$ (F m^{-2})	—[d]	—[d]	—[d]	0.965	—[d]
Binding constants					
log K_H	7.0	8.3	6.0	7.94	7.0
log K_{OH}	4.0	5.0	4.6	3.98	4.0
log K_{cat}	0	0.08	0	−0.0862	0
log K_{an}	−1.2	−1.7	−1.2	−0.183	−1.2
log K_{L^-}	0	0	5.5	2.74	0
log $K_{L^{2-}}$	6.86	6.95	4.8	—	0
log $K_{L^{3-}}$	0	—	—	—	4.79
log $K_{B_3O_3(OH)_4^-}$	—	—	—	1.21	—
log $K_{B_4O_5(OH)_4^{2-}}$	—	—	—	4.69	—
log $K_{B_5O_6(OH)_4^-}$	—			1.12	—

[a] From Bowden *et al.* (1980).
[b] From McKenzie (1983).
[c] From Bloesch *et al.* (1987).
[d] This value was made very large so that the β and d planes virtually coincide.

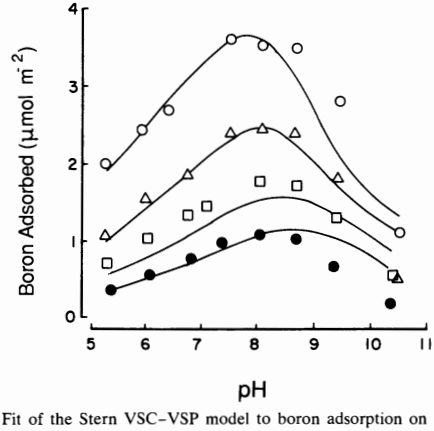

Figure 32. Fit of the Stern VSC–VSP model to boron adsorption on goethite. Model result are represented by solid lines. Model parameters are provided in Table XV. From Bloesch *et al.* (1987).

and borate sorption on soils (Barrow, 1989b), the effect of ionic strength on phosphate, sulfate (Bolan *et al.*, 1986), selenite, selenate (Barrow and Whelan, 1989a), and borate sorption on soils (Barrow, 1989b), and the point of zero salt effect for phosphate sorption on an Australian soil (Barrow and Ellis, 1986b). The model was able to describe the data well in all cases using one or two anion binding constants. As discussed previously in Section IV,C, difficulties in the use of the mechanistic Stern VSC–VSP model may arise from specific calcium adsorption because calcium carbonate was added to raise the pH. The mechanistic Stern VSC–VSP model has also been used to describe the effect of time on phosphate adsorption by iron and aluminum oxides (Bolan *et al.*, 1985).

D. Generalized Two-Layer Model

Application of the generalized two-layer model to anion adsorption has been restricted to inorganic anions on the hydrous ferric oxide surface (Dzombak and Morel, 1990). As for metal adsorption, intrinsic conditional equilibrium constants for the generalized two-layer model for anion adsorption were obtained using the computer program FITEQL (Westall, 1982). Individual values of $\log K_L^i(\text{int})$ and best estimates of $\overline{\log K_L^i(\text{int})}$ were obtained as described in Section III,D for $\log K_{\pm}(\text{int})$. Anion adsorption is defined by the reactions given in Eqs. (53) and (54). For some anions the following anion surface complexation reactions are also considered:

$$\text{SOH} + \text{L}^{l-} + 3\text{H}^+ \rightleftarrows \text{SH}_2\text{L}^{(l-3)-} + \text{H}_2\text{O} \tag{140}$$

$$\text{SOH} + \text{L}^{l-} \rightleftarrows \text{SOHL}^{l-} \tag{141}$$

The intrinsic conditional equilibrium constants for these reactions are

$$K_L^3(\text{int}) = \frac{[\text{SH}_2\text{L}^{(l-3)-}]}{[\text{SOH}][\text{L}^{l-}][\text{H}^+]^3} \exp[-(l-3)F\Psi/RT] \tag{142}$$

$$K_L^4(\text{int}) = \frac{[\text{SOHL}^{l-}]}{[\text{SOH}][\text{L}^{l-}]} \exp[-lF\Psi/RT] \tag{143}$$

For arsenite (H_3AsO_3) and borate (H_3BO_3) adsorption, surface complexation is defined by the reaction, Eq. (129), where $i = 1$. Table XVI presents values of best estimates of $\overline{\log K_L^i(\text{int})}$ obtained by computer optimization with FITEQL. Figure 33 depicts the ability of the generalized two-layer

Table XVI

Values of Intrinsic Anion Surface Complexation Constants Obtained with the Generalized Two-Layer Model Using FITEQL Computer Optimization for Hydrous Ferric Oxide[a]

Anion	$\log K^1_L$(int)	$\log K^2_L$(int)	$\log K^3_L$(int)	$\log K^4_L$(int)	Number of data sets[b]
PO_4^{3-}	17.72 ± 0.51	25.39 ± 0.17	31.29 ± 2.88	—	9
AsO_4^{3-}	—	23.51 ± 0.18	29.31 ± 1.02	10.58 ± 0.57	6
VO_4^{3-}	—	—	—	13.57 ± 0.06	12
SO_4^{2-}	7.78	—	—	0.79	1
SeO_4^{2-}	7.73 ± 0.08	—	—	0.80 ± 0.10	7
SeO_3^{2-}	12.69	—	—	5.17	1
CrO_4^{2-}	10.85 ± 0.07	—	—	—	14
$S_2O_3^{2-}$	—	—	—	0.49 ± 0.09	2
$H_3AsO_3^0$	5.41 ± 0.15[c]	—	—	—	6
$H_3BO_3^0$	0.62 ± 0.66[c]	—	—	—	2

[a] From Dzombak and Morel (1990). 95% confidence intervals.
[b] Experimental data sources provided in Chapter 7 of Dzombak and Morel (1990).
[c] Log K^1_L(int) is defined for reaction Eq. (131), where $i = 1$.

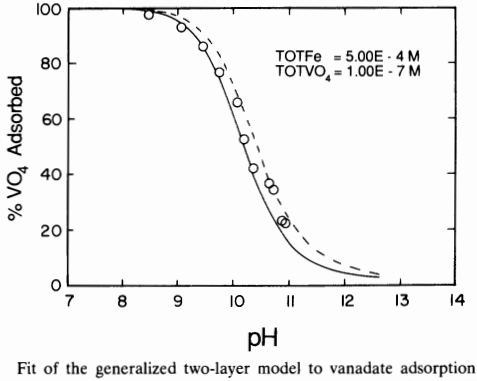

Figure 33. Fit of the generalized two-layer model to vanadate adsorption on hydrous ferric oxide. Model results are represented by a solid line for individual $\log K^4_V$(int) and a dashed line for $\overline{\log K^4_V(\text{int})}$; $\log K^4_V(\text{int}) = 13.34$; $\overline{\log K^4_V(\text{int})}$ is provided in Table XVI. From Dzombak and Morel (1990), based on experimental data of Leckie *et al.* (1984), reproduced with permission from John Wiley and Sons.

model to describe vanadate adsorption on hydrous ferric oxide. The model describes the data well using both the individual data set value and the best estimate of log K_V^4(int).

The incorporation of the surface precipitation model into the generalized two-layer model to describe anion sorption has been carried out and is described by Dzombak and Morel (1990). However, no applications to actual anion sorption data are available.

E. One-p*K* Model

Application of the one-p*K* model to anion adsorption has so far been restricted to phosphate adsorption on the iron oxide, goethite (van Riemsdijk and van der Zee, 1991). Adsorption of phosphate is modeled as occurring at the *d*-plane and described by reaction Eq. (67) and equilibrium constant Eq. (73). The adsorption of potassium in the *d*-plane is also considered: reaction Eq. (68) and equilibrium constant Eq. (74). The equilibrium constant for potassium adsorption is optimized both with the phosphate adsorption equilibrium constant and for the charging data in the absence of phosphate. The ability of the one-p*K* model to describe phosphate adsorption on goethite is indicated in Fig. 34. The fit of the model is excellent over the entire, wide pH range investigated.

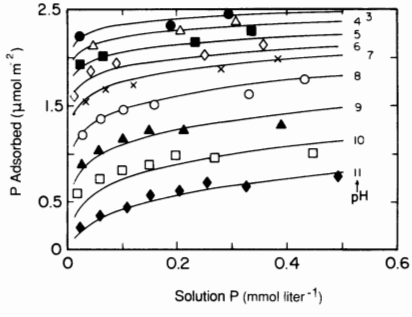

Figure 34. Fit of the one-p*K* model to phosphate adsorption on goethite. Model results are represented by solid lines; $\log K_{HPO_4} = 6.65$, $\log K_K = -0.5$. From van Riemsdijk and van der Zee (1991), based on experimental data of Bowden *et al.* (1980), reproduced with permission from Kluwer Academic Publishers.

VI. APPLICATION OF MODELS TO ORGANIC LIGAND ADSORPTION REACTIONS ON OXIDES

A. Constant Capacitance Model

The constant capacitance model has been used to describe organic ligand adsorption envelopes on aluminum oxide (Kummert and Stumm, 1980), silicon oxide, titanium oxide (Gisler, 1980), iron oxide (goethite) (Sigg and Stumm, 1981), and natural organic matter (Baccini *et al.*, 1982). In the application of the constant capacitance model to organic anion adsorption, the surface complexation reactions are written in terms of undissociated acids as for inorganic anions (Kummert and Stumm, 1980; Sigg and Stumm, 1981). However, only monodentate surface complexes are considered as described by reaction Eq. (129) and intrinsic conditional equilibrium constant Eq. (131), where $i = 1$ or 2. In the application of the model to adsorption of amino acids on oxides, the following reactions leading to bidentate surface complexes are defined (Gisler, 1980):

$$\mathrm{SOH} + \mathrm{SOH_2^+} + \mathrm{HL^{\pm}} \rightleftarrows (\mathrm{SOH})\mathrm{HL}(\mathrm{SOH_2^+}) \tag{144}$$

$$\mathrm{SO^-} + \mathrm{SOH_2^+} + \mathrm{HL^{\pm}} \rightleftarrows (\mathrm{SO^-})\mathrm{HL}(\mathrm{SOH_2^+}) \tag{145}$$

$$\mathrm{SO^-} + \mathrm{SOH} + \mathrm{HL^{\pm}} \rightleftarrows (\mathrm{SO^-})\mathrm{HL}(\mathrm{SOH}) \tag{146}$$

where $\mathrm{HL^{\pm}}$ represents an amino acid, $\mathrm{H_3N^+—CHR—COO^-}$. The intrinsic conditional equilibrium constants are equal to the conditional equilibrium constants because the surface charge remains unchanged and are as follows:

$$K_{\mathrm{L}}^{1} = \frac{[(\mathrm{SOH})\mathrm{HL}(\mathrm{SOH_2^+})]}{[\mathrm{SOH}][\mathrm{SOH_2^+}][\mathrm{HL^{\pm}}]} \tag{147}$$

$$K_{\mathrm{L}}^{2} = \frac{[(\mathrm{SO^-})\mathrm{HL}(\mathrm{SOH_2^+})]}{[\mathrm{SO^-}][\mathrm{SOH_2^+}][\mathrm{HL^{\pm}}]} \tag{148}$$

$$K_{\mathrm{L}}^{3} = \frac{[(\mathrm{SO^-})\mathrm{HL}(\mathrm{SOH})]}{[\mathrm{SO^-}][\mathrm{SOH}][\mathrm{HL^{\pm}}]} \tag{149}$$

For adsorption on titanium oxide, all three of the above reactions are considered. For adsorption on silicon oxide, only reaction Eq. (146) is considered because no positive $\mathrm{SiOH_2^+}$ surface groups are found in the experimental pH range (Gisler, 1980). Figure 35 presents the ability of the constant capacitance model to describe phthalate adsorption on aluminum oxide. The model describes the data well at various total organic acid

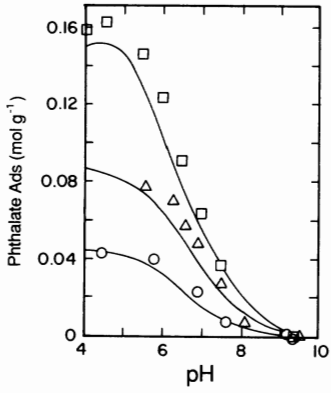

Figure 35. Fit of the constant capacitance model to phthalate adsorption on aluminum oxide. Model results are represented by solid lines. Model parameters are provided in Table XVII. After Kummert and Stumm (1980).

concentrations. Table XVII provides values for intrinsic organic ligand surface complexation constants obtained with the constant capacitance model for oxide minerals.

B. Triple-Layer Model

The triple-layer model has been used to describe organic ligand adsorption envelopes on the iron oxide, goethite (Balistrieri and Murray, 1987) and on amorphous iron oxide (Davis and Leckie, 1979). In the application of the triple-layer model to organic anion adsorption on goethite, the reactions Eqs. (24) and (25) and the equilibrium constants Eqs. (30) and (31) are considered. For adsorption of glutamate on amorphous iron oxide, reaction Eq. (24) is replaced by the formation of a neutral surface complex, SOH—H_2L (Davis and Leckie, 1979). Figure 36 presents the ability of the triple-layer model to describe glutamate adsorption on amorphous iron oxide. The model describes the data well for three different total organic ligand concentrations. Unfortunately, values for the intrinsic surface complexation constants were not provided by the authors. Table XVIII provides values for intrinsic organic ligand surface complexation constants obtained with the triple-layer model for iron oxides.

Table XVII

Values of Intrinsic Organic Ligand Surface Complexation Constants Obtained with the Constant Capacitance Model

Solid	Ligand	Ionic medium	$\log K_L^1$(int)	$\log K_L^2$(int)	$\log K_L^3$(int)	Reference
γ-Al_2O_3	Benzoate	0.1 *M* $NaClO_4$	3.7	—	—	Kummert and Stumm (1980)
γ-Al_2O_3	Catechol	0.1 *M* $NaClO_4$	3.7	<-5	—	Kummert and Stumm (1980)
γ-Al_2O_3	Phthalate	0.1 *M* $NaClO_4$	7.3	2.4	—	Kummert and Stumm (1980)
γ-Al_2O_3	Salicylate	0.1 *M* $NaClO_4$	6.0	−0.6	—	Kummert and Stumm (1980)
α-FeOOH	Acetate	0.1 *M* $NaClO_4$	2.9	—	—	Sigg and Stumm (1981)
Amino acids						
SiO_2(am)	Glycine	1.0 *M* $NaClO_4$	—	—	0.04	Gisler (1980)
SiO_2(am)	α-Alanine	1.0 *M* $NaClO_4$	—	—	−0.14	Gisler (1980)
SiO_2(am)	β-Alanine	1.0 *M* $NaClO_4$	—	—	−0.26	Gisler (1980)
SiO_2(am)	γ-Aminobutyric acid	1.0 *M* $NaClO_4$	—	—	−0.68	Gisler (1980)
TiO_2, rutile	Glycine	1.0 *M* $NaClO_4$	3.0	4.9	2.9	Gisler (1980)
TiO_2, rutile	Glycine	1.0 *M* $NaClO_4$	3.3	5.5	3.3	Gisler (1980)

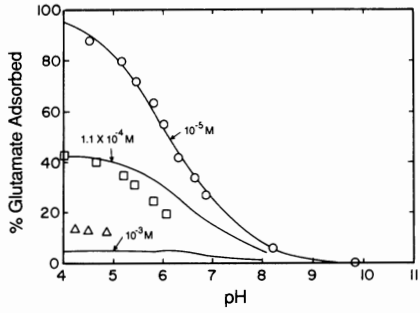

Figure 36. Fit of the triple-layer model to glutamate adsorption on amorphous iron oxide. Model results are represented by solid lines. Model parameters were not provided by the authors. From Davis and Leckie (1979), reproduced with permission from the American Chemical Society.

Table XVIII

Values of Intrinsic Organic Ligand Surface Complexation Constants Obtained with the Triple-Layer Model

Solid	Ligand	Ionic medium	$\log K_L^1$(int)	$\log K_L^2$(int)	Reference
α-FeOOH	Oxalate	NaCl	10.8	15.5	Balistrieri and Murray (1987)
α-FeOOH	Phthalate	NaCl	9.7	15.7	Balistrieri and Murray (1987)
α-FeOOH	Salicylate	NaCl	—	22.9	Balistrieri and Murray (1987)
α-FeOOH	Lactate	NaCl	9.2	—	Balistrieri and Murray (1987)

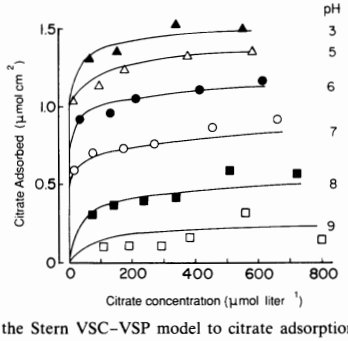

Figure 37. Fit of the Stern VSC–VSP model to citrate adsorption on goethite. Model results are represented by solid lines. Model parameters are provided in Table XV. From Bowden *et al.* (1980).

C. Stern VSC-VSP Model

Application of the Stern VSC–VSP model to organic anion adsorption has been restricted to citrate adsorption on goethite (Bowden *et al.*, 1980). As for inorganic anion adsorption, values of surface site density, maximum adsorption, binding constants, and capacitances are optimized to fit charge and adsorption data. Table XV presents parameter values obtained by computer optimization for citrate adsorption on goethite. The adsorption of the trivalent ion L^{3-} is postulated. The ability of the Stern VSC–VSP model to describe citrate adsorption is good and is presented in Fig. 37.

VII. APPLICATION OF MODELS TO COMPETITIVE ADSORPTION REACTIONS ON OXIDES

A. Metal–Metal Competition

1. Constant Capacitance Model

The effects of metal–metal competition on the description of adsorption with the constant capacitance model have been investigated only preliminarily. The constant capacitance model containing the surface precipitation model was used to describe the effect of copper on cadmium adsorption by amorphous iron hydroxide (Farley *et al.*, 1985). These authors overpredicted the competitive effect for the data of Benjamin (1978) obtained after 4 hr of reaction time. Using one competitive data point after 30 hr of reaction time, the authors concluded that the surface precipitation model is capable of predicting competitive adsorption of metal ions if slow kinetics are considered. Additional research is needed to substantiate the conclusion of Farley *et al.* (1985).

2. Triple-Layer Model

The competitive adsorption of alkaline earth cations (Balistrieri and Murray, 1981) and trace metal cations has been investigated on goethite (Balistrieri and Murray, 1982b), manganese oxide (Catts and Langmuir, 1986), and amorphous iron oxide (Cowan *et al.*, 1991) using the triple-layer model. Using intrinsic surface complexation constants from single-cation systems, Balistrieri and Murray (1981) were able to quantitatively predict calcium and magnesium adsorption on goethite in a synthetic major-ion seawater solution. Using this same approach, Balistrieri and Murray (1982b) were able to predict decreases in lead, zinc, and cadmium adsorp-

tion on goethite in the presence of magnesium in major-ion seawater. The competitive effect of magnesium was quantitatively described for zinc adsorption over the entire pH range and for lead adsorption above pH 5. Deviations from the experimental data occurred for lead adsorption below pH 5 and for cadmium adsorption over the entire pH range (Balistrieri and Murray, 1982b). Competitive adsorption of the trace metal ions copper, lead, and zinc on manganese oxide from a solution containing all three ions was predicted from single-ion systems (Catts and Langmuir, 1986). The adsorption of lead was predicted quantitatively, whereas the description of copper and zinc adsorption was qualitatively correct (see Fig. 38).

In order to describe cadmium and calcium adsorption on amorphous iron oxides in single-ion systems, as well as to predict competitive adsorption, Cowan *et al.* (1991) hypothesized inner-sphere surface complexes for cadmium and a combination of inner- and outer-sphere surface complexes for calcium. This study represents the first time that both inner- and outer-sphere complexes have been postulated for a single adsorbing ion. Cowan *et al.* (1991) were able to describe competitive adsorption of cadmium in the presence of calcium, qualitatively. However, because a better fit was obtained using a nonelectrostatic model with fewer adjustable parameters, these authors suggested that competitive adsorption of cadmium and calcium on amorphous iron oxide is due to a mass-action effect.

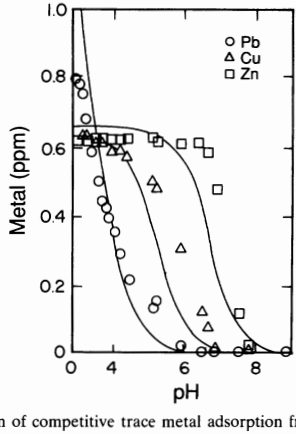

Figure 38. Prediction of competitive trace metal adsorption from single-ion systems on manganese oxide using the triple-layer model. Model results are represented by solid lines. Model parameters are provided in Table X. From Catts and Langmuir (1986).

B. Anion–Anion Competition

1. Constant Capacitance Model

The ability of the constant capacitance model to predict competitive anion adsorption on goethite from solutions containing phosphate and selenite or phosphate and silicate using the intrinsic surface complexation constants obtained from single-anion systems has been tested (Goldberg, 1985). The model predicted anion competition qualitatively, reproducing the shapes of the adsorption curves; however, phosphate adsorption was overestimated and adsorption of the competing anion was underestimated. Competitive anion adsorption of phosphate and arsenate on gibbsite (Goldberg, 1986a) and goethite (Goldberg, 1986b), phosphate and selenite on goethite, and phosphate and silicate on gibbsite and goethite (Goldberg and Traina, 1987) could be described by direct optimization of the mixed-ligand data. The fit of the constant capacitance model to the adsorption data using the mixed-ligand approach was much better than that obtained by prediction from single-anion systems (see Fig. 39). In the mixed-ligand approach, the intrinsic surface complexation constants are conditional constants, dependent upon the surface composition of the oxide surface. Goldberg and Traina (1987) suggested that the composition dependence is due to heterogeneity of oxide surface sites. Goldberg (1986a) found that arsenate and phosphate surface complexation constants obtained using the

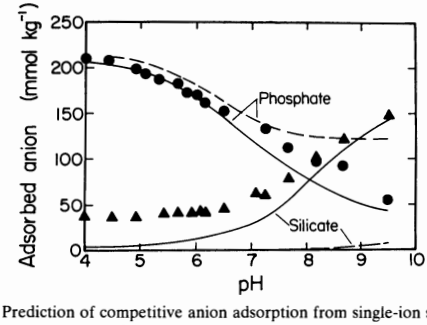

Figure 39. Prediction of competitive anion adsorption from single-ion systems and fit of the mixed-ligand approach on gibbsite using the constant capacitance model. Model results are represented by dashed lines for single-ion fits and solid lines for mixed-ligand fits. Single-ion model parameters are provided in Table XIII. Mixed-ligand parameters: $\log K_P^1 = 9.43$, $\log K_P^2 = 3.01$, $\log K_P^3 = -2.26$, $\log K_{Si}^1 = 3.53$, $\log K_{Si}^2 = -4.62$. From Goldberg and Traina (1987).

mixed-ligand approach for one ternary gibbsite system could be used to predict competitive adsorption for other ternary gibbsite systems containing different amounts of arsenate and phosphate in solution.

2. Triple-Layer Model

The application of the triple-layer model to describe competitive adsorption of anions has been investigated on goethite (Balistrieri and Murray, 1987; Hawke *et al.*, 1989), amorphous iron oxide (Zachara *et al.*, 1987; Balistrieri and Chao, 1990), manganese oxide (Balistrieri and Chao, 1990), and soils (Zachara *et al.*, 1989). Using intrinsic surface complexation constants from single-anion systems, Balistrieri and Murray (1987) were able to predict oxalate adsorption but grossly underestimated salicylate adsorption in the presence of sulfate anions on goethite. Using this same approach, Hawke *et al.* (1989) were able to predict phosphate adsorption on goethite in the presence of sulfate; phosphate adsorption in the presence of fluoride was not well predicted. Chromate adsorption on amorphous iron oxide in the presence of the competing anions carbonate and sulfate was qualitatively predicted using anion surface complexation constants from single-anion systems (Zachara *et al.*, 1987). Balistrieri and Chao (1990) were unable to predict selenite adsorption on amorphous iron oxide or manganese oxide in the presence of phosphate, silicate, or molybdate from single-anion systems. These researchers were able to describe selenite adsorption in the presence of molybdate by decreasing the magnitude of the selenite equilibrium constants with increasing molybdate concentration.

The first application of a surface complexation model to describe competitive adsorption on soil was carried out by Zachara *et al.* (1989). These researchers used the triple-layer model to describe competitive adsorption of chromate in the presence of sulfate and dissolved inorganic carbon. As described in more detail in Section V,B, aluminum-substituted goethite was assumed to be the reactive mineral surface in the soil. Using the surface complexation constants obtained for amorphous iron oxide by Zachara *et al.* (1987), Zachara *et al.* (1989) were able to predict qualitatively chromate and sulfate adsorption on a soil from a solution containing both anions.

3. Stern VSC–VSP Model

The mechanistic Stern VSC–VSP model, discussed in detail in Section IV,C, has been applied to competitive anion adsorption on soils (Barrow, 1989a). The author described phosphate–arsenate, phosphate–molybdate,

and arsenate–molybdate competition using the same parameters as for single-anion systems for two of the three soils studied. The mechanistic Stern VSC–VSP model described the competitive adsorption data very well. However, as discussed in Section IV,C, use of the mechanistic Stern VSC–VSP model should be regarded as a curve-fitting procedure.

C. Metal–Ligand Interactions

1. Constant Capacitance Model

Ternary surface complexes are formed when metal–ligand complexes, ML, react with the mineral surface. A type A ternary surface complex, S—O—M—L, is formed when attachment of the solution complex to the surface occurs through the metal ion (Schindler, 1990). The constant capacitance model has been used to describe adsorption of metal ligand complexes to form type A ternary surface complexes on silicon oxide (Bourg and Schindler, 1978; Gisler, 1980; Schindler, 1990) and on titanium oxide (Gisler, 1980). In the application of the constant capacitance model to metal–ligand complex adsorption, the following reactions are defined (Gisler, 1980):

$$\mathrm{SOH} + \mathrm{ML}^{(m-1)+} \rightleftarrows \mathrm{SOML}^{(m-2)} + \mathrm{H}^{+} \tag{150}$$

$$2\mathrm{SOH} + \mathrm{ML}^{(m-1)+} \rightleftarrows (\mathrm{SO})_2\mathrm{ML}^{(m-3)} + 2\mathrm{H}^{+} \tag{151}$$

The conditional equilibrium constants for these reactions are

$$K^{1}_{\mathrm{ML}} = \frac{[\mathrm{SOML}^{(m-2)}][\mathrm{H}^{+}]}{[\mathrm{SOH}][\mathrm{ML}^{(m-1)+}]} \tag{152}$$

$$K^{2}_{\mathrm{ML}} = \frac{[(\mathrm{SO})_2\mathrm{ML}^{(m-3)}][\mathrm{H}^{+}]^2}{[\mathrm{SOH}]^2[\mathrm{ML}^{(m-1)+}]} \tag{153}$$

Table XIX provides values for type A ternary surface complexation constants obtained with the constant capacitance model. The fit of the model to the data was good over most of the pH range.

2. Triple-Layer Model

A type B ternary complex, S—L—M, is formed when the solution complex, ML, attaches to the mineral surface through the ligand (Schindler,

Table XIX

Values of Type A Ternary Surface Complexation Constants Obtained with the Constant Capacitance Model

Solid	Metal	Ligand	Ionic medium	$\log K^1_{ML}$	$\log K^2_{ML}$	Reference
SiO_2	Cu^{2+}	Ethylenediamine	1 *M* $NaClO_4$	−5.22	−12.57	Bourg and Schindler (1978)
SiO_2	Mg^{2+}	Glycine	1 *M* $NaClO_4$	−8.24	−17.21	Gisler (1980)
SiO_2	Mg^{2+}	α-Alanine	1 *M* $NaClO_4$	−8.23	−17.21	Gisler (1980)
SiO_2	Mg^{2-}	β-Alanine	1 *M* $NaClO_4$	−8.23	−17.21	Gisler (1980)
SiO_2	Mg^{2+}	γ-Aminobutyric acid	1 *M* $NaClO_4$	−8.23	−17.21	Gisler (1980)
SiO_2	Cu^{2+}	Glycine	1 *M* KNO_3	−5.64	−12.29	Schindler (1990)
TiO_2, rutile	Mg^{2+}	Glycine	1 *M* $NaClO_4$	−5.94	−13.62	Gisler (1980)
TiO_2, rutile	Co^{2+}	Glycine	1 *M* $NaClO_4$	−4.40	−10.94	Gisler (1980)

1990). The triple-layer model has been used to describe adsorption of a silver–thiosulfate complex on amorphous iron oxide (Davis and Leckie, 1979). In the application of the triple-layer model to ligand–metal complex adsorption, the following reaction is defined:

$$SOH + H^+ + M^{m+} + L^{l-} \rightleftarrows SOH_2^+ - LM^{(l-m)-} \tag{154}$$

The intrinsic conditional equilibrium constant for this reaction is

$$K_{ML}(\text{int}) = \frac{[SOH_2^+ - LM^{(l-m)-}]}{[SOH][H^+][M^{m+}][L^{l-}]} \exp[F(\Psi_o - (l-m)\Psi_\beta)/RT] \tag{155}$$

Figure 40 presents the ability of the triple-layer model to describe silver adsorption on amorphous iron oxide by postulating the formation of a type B ternary complex. The fit of the model to the data is qualitatively correct.

Adsorption reactions of actinide elements on oxides have been described in the presence of carbonate and bicarbonate ion using the triple-layer model (Hsi and Langmuir, 1985; Sanchez *et al.*, 1985). These authors postulated the existence and adsorption of actinide–carbonate ion pairs to describe their adsorption data for uranyl (Hsi and Langmuir, 1985) and plutonium adsorption on iron oxides (Sanchez *et al.*, 1985). Carbonate adsorption was not verified in these experiments.

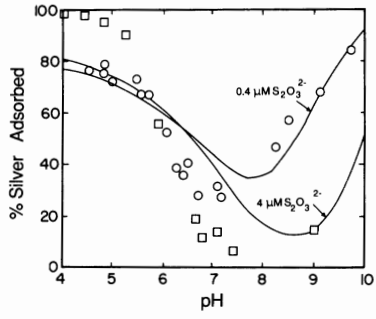

Figure 40. Fit of the triple-layer model to silver adsorption on amorphous iron oxide using a type B ternary silver–thiosulfate surface complex. Model results are represented by solid lines; $\log K_{AgS_2O_3}$ −(int) = −19.5. From Davis and Leckie (1979), reproduced with permission from the American Chemical Society.

Metal–ligand interactions can occur without the formation of ternary surface complexes. The ability of the triple-layer model to predict competitive adsorption of cations and anions has been investigated on goethite (Balistrieri and Murray, 1981, 1982b) and amorphous iron oxide (Benjamin and Bloom, 1981; Zachara *et al.*, 1987). Using intrinsic surface complexation constants from single-ion systems, Balistrieri and Murray (1981) were able to quantitatively predict calcium, magnesium, and sulfate adsorption on goethite from a synthetic seawater solution containing these ions. Using this same approach, Balistrieri and Murray (1982b) were able to predict the changes in lead, zinc, and cadmium adsorption on goethite from the presence of sulfate in major-ion seawater. Benjamin and Bloom (1981) were unable to predict competitive adsorption of the metals cadmium, cobalt, and zinc in the presence of the anions selenate, selenite, arsenate, arsenite, chromate, and phosphate on amorphous iron oxide from single-ion systems. The enhanced metal adsorption in the presence of anions was grossly overpredicted by the triple-layer model. Benjamin and Bloom (1981) suggested that either a new surface phase forms or that cations and anions bind to separate sets of sites. An alternative explanation may be that the outer-sphere adsorption mechanism is inappropriate to describe the adsorption behavior of some or all of these ions. Competitive adsorption of chromate on amorphous iron oxide in the presence of calcium and magnesium could be predicted using intrinsic surface complexation constants from single-ion systems (Zachara *et al.*, 1987).

VIII. INCORPORATION OF SURFACE COMPLEXATION MODELS INTO COMPUTER CODES

A. Incorporation into Chemical Speciation Models

The surface complexation models have been incorporated into various chemical speciation models. The first addition of a surface complexation model to a chemical speciation model was when Davis *et al.* (1978) added the triple-layer model to the computer program MINEQL (Westall *et al.*, 1976). The computer program MINTEQ (Felmy *et al.*, 1984) combines the mathematical framework of MINEQL (Westall *et al.*, 1976) with the thermodynamic database of WATEQ3 (Ball *et al.*, 1981). This program contains the surface complexation modeling approach. The constant capacitance model has been added to the computer speciation program GEOCHEM (Sposito and Mattigod, 1980) in the development of its successor, the chemical speciation program SOILCHEM (Sposito and Coves, 1988). The computer program HYDRAQL (Papelis *et al.*, 1988) was developed from the computer program MINEQL (Westall *et al.*, 1976) and contains the constant capacitance model, the diffuse layer model, the Stern model, the triple-layer model, and the Stern VSC–VSP model. The computer programs MICROQL (Westall, 1979) and FITEQL (Westall, 1982) do not contain thermodynamic data files. Instead, the equilibrium constants are entered by the user and specified for the problem under investigation.

B. Incorporation into Transport Models

Surface complexation models have not yet been widely incorporated into transport models (Mangold and Tsang, 1991). Jennings *et al.* (1982) incorporated the constant capacitance model into a transport model and simulated competitive metal sorption at constant pH. Cederberg *et al.* (1985) have linked the program MICROQL (Westall, 1979) containing the constant capacitance model with the transport program ISOQUAD (G. F. Pinder, unpublished manuscript 1976) to produce the computer program TRANQL. This program was used to simulate cadmium transport in a one-dimensional laboratory column. The STEADYQL computer program (Furrer *et al.*, 1989, 1990) is based on the MICROQL program (Westall, 1979) and calculates chemical speciation of a flow-through system

at steady state considering both fast, reversible processes described in terms of chemical equilibrium and slow processes described by kinetic equations. Although this program considers inflow and outflow for one box, the approach can form the basis for a transport model (J. C. Westall, personal communication 1991). The computer program FASTCHEM linking MINTEQ and transport modeling has been developed (Krupka *et al.*, 1988). However, the adsorption model in the FASTCHEM program is nonelectrostatic. The computer program HYDROGEOCHEM links a MINEQL version containing surface complexation models with transport modeling (Yeh and Tripathi, 1990).

IX. SUMMARY

Surface complexation models provide a molecular description of adsorption phenomena using an equilibrium approach. Five such models, the constant capacitance model (Stumm *et al.*, 1980), the triple-layer model (Davis *et al.*, 1978), the Stern VSC–VSP model (Bowden *et al.*, 1980), the generalized two-layer model (Dzombak and Morel, 1990), and the one-pK model (van Riemsdijk *et al.*, 1986) were discussed. Unlike empirical models, surface complexation models define surface species, chemical reactions, equilibrium constant expressions, surface activity coefficients, mass and charge balance, and consider the charge of both the adsorbate and the adsorbent. Common model characteristics are surface charge balance, electrostatic potential terms, equilibrium constants, capacitances, and surface charge density. Each surface complexation model was discussed in detail and its application to protonation–dissociation reactions, metal ion, inorganic anion, and organic ligand adsorption reactions on soil minerals and soils was described. Extensive tables of surface equilibrium constants have been provided. It must be emphasized that because all five surface complexation models contain different basic assumptions for the mineral–solution interface, the chemical species defined and the equilibrium constants obtained with one model must never be used in any other model. Surface complexation models have been incorporated into chemical speciation programs and into transport programs. Application of these models to describe surface reactions on heterogeneous surfaces such as clay minerals and soils requires various simplifying approximations. Additional research is needed to develop consistent protocols for the use of surface complexation models in describing reactions of natural chemical systems such as soils.

Acknowledgments

Gratitude is expressed to Dr. G. Sposito and Dr. R. van Genuchten for peer reviews, Mr. H. Forster for library assistance, Ms. P. Speckman for typing, Ms. G. O'Donnell for drafting, and Ms. P. Howard for photography.

References

Ainsworth, C. C., Girvin, D. C., Zachara, J. M., and Smith, S. C. (1989). Chromate adsorption on goethite: Effects of aluminum substitution. *Soil Sci. Soc. Am. J.* **53,** 411–418.

Anderson, M. A., Ferguson, J. F., and Gavis, J. (1976). Arsenate adsorption on amorphous aluminum hydroxide. *J. Colloid Interface Sci.* **54,** 391–399.

Anderson, P. R., and Benjamin, M. M. (1990a). Constant-capacitance surface complexation model. Adsorption in silica–iron binary oxide suspension. *ACS Symp. Ser.* **416,** 272–281.

Anderson, P. R., and Benjamin, M. M. (1990b). Modeling adsorption in aluminium–iron binary oxide suspensions. *Environ. Sci. Technol.* **24,** 1586–1592.

Baccini, P., Grieder, E., Stierli, R., and Goldberg, S. (1982). The influence of natural organic matter on the adsorption properties of mineral particles in lake water. *Schweiz. Z. Hydrol.* **44,** 99–116.

Balistrieri, L. S., and Chao, T. T. (1990). Adsorption of selenium by amorphous iron oxyhydroxide and manganese dioxide. *Geochim. Cosmochim. Acta* **54,** 739–751.

Balistrieri, L. S., and Murray, J. W. (1979). Surface of goethite (αFeOOH) in seawater. *ACS Symp. Ser.* **93,** 275–298.

Balistrieri, L. S., and Murray, J. W. (1981). The surface chemistry of goethite (αFeOOH) in major ion seawater. *Am. J. Sci.* **281,** 788–806.

Balistrieri, L. S., and Murray, J. W. (1982a). The surface chemistry of δMnO_2 in major ion seawater. *Geochim. Cosmochim. Acta* **46,** 1041–1052.

Balistrieri, L. S., and Murray, J. W. (1982b). The adsorption of Cu, Pb, Zn, and Cd on goethite from major ion seawater. *Geochim. Cosmochim. Acta* **46,** 1253–1265.

Balistrieri, L. S., and Murray, J. W. (1987). The influence of the major ions of seawater on the adsorption of simple organic acids by goethite. *Geochim. Cosmochim. Acta* **51,** 1151–1160.

Ball, J. W., Jenne, E. A., and Cantrell, M. W. (1981). WATEQ3: A geochemical model with uranium added. *Geol. Surv. Open-File Rep. (U.S.)* **81–1183.**

Barrow, N. J. (1979). "Computer Programmes for Calculating Charge and Adsorption of Ions in Variable Charge Surfaces," Tech. Memo. 79/3. CSIRO, Div. Land Resour. Manage. Perth, Australia.

Barrow, N. J. (1983). A mechanistic model for describing the sorption and desorption of phosphate by soil. *J. Soil Sci.* **34,** 733–750.

Barrow, N. J. (1984). Modelling the effects of pH on phosphate sorption by soils. *J. Soil Sci.* **35,** 283–297.

Barrow, N. J. (1986a). Testing a mechanistic model. I. The effects of time and temperature on the reaction of fluoride and molybdate with a soil. *J. Soil Sci.* **37,** 267–275.

Barrow, N. J. (1986b). Testing a mechanistic model. II. The effects of time and temperature on the reaction of zinc with a soil. *J. Soil Sci.* **37,** 277–286.

Barrow, N. J. (1986c). Testing a mechanistic model. IV. Describing the effects of pH on zinc retention by soils. *J. Soil Sci.* **37,** 295–302.

Barrow, N. J. (1987). "Reactions with Variable-Charge Soils." Martinus Nijhoff, Dordrecht, The Netherlands.

Barrow, N. J. (1989a). Testing a mechanistic model. IX. Competition between anions for sorption by soil. *J. Soil Sci.* **40,** 415–425.

Barrow, N. J. (1989b). Testing a mechanistic model. X. The effect of pH and electrolyte concentration on borate sorption by a soil. *J. Soil Sci.* **40,** 427–435.

Barrow, N. J., and Bowden, J. W. (1987). A comparison of models for describing the adsorption of anions on a variable charge mineral surface. *J. Colloid Interface Sci.* **119,** 236–250.

Barrow, N. J., and Ellis, A. S. (1986a). Testing a mechanistic model. III. The effects of pH on fluoride retention by a soil. *J. Soil Sci.* **37,** 287–293.

Barrow, N. J., and Ellis, A. S. (1986b). Testing a mechanistic model. V. The points of zero salt effect for phosphate retention, for zinc retention and for acid/alkali titration of a soil. *J. Soil Sci.* **37,** 303–310.

Barrow, N. J., and Whelan, B. R. (1989a). Testing a mechanistic model. VII. The effects of pH and of electrolyte on the reaction of selenite and selenate with a soil. *J. Soil Sci.* **40,** 17–28.

Barrow, N. J., and Whelan, B. R. (1989b). Testing a mechanistic model. VIII. The effects of time and temperature of incubation on the sorption and subsequent desorption of selenite and selenate by a soil. *J. Soil Sci.* **40,** 29–37.

Barrow, N. J., Bowden, J. W., Posner, A. M., and Quirk, J. P., (1980a). An objective method for fitting models of ion adsorption on variable charge surfaces. *Aust. J. Soil Res.* **18,** 37–47.

Barrow, N. J., Bowden, J. W., Posner, A. M., and Quirk, J. P. (1980b). Describing the effects of electrolyte on adsorption of phosphate by a variable charge surface. *Aust. J. Soil Res.* **18,** 395–404.

Barrow, N. J., Bowden, J. W., Posner, A. M., and Quirk, J. P. (1981). Describing the adsorption of copper, zinc and lead on a variable charge mineral surface. *Aust. J. Soil Res.* **19,** 309–321.

Barrow, N. J., Gerth, J., and Brümmer, G. W. (1989). Reaction kinetics of the adsorption and desorption of nickel, zinc and cadmium by goethite. II. Modelling the extent and rate of reaction. *J. Soil Sci.* **40,** 437–450.

Benjamin, M. M. (1978). Effects of competing metals and complexing ligands on trace metal adsorption at the oxide/solution interface. Ph.D. Thesis, Stanford University, Stanford, California.

Benjamin, M. M., and Bloom, N. S. (1981). Effects of strong binding of anionic adsorbates on adsorption of trace metals on amorphous iron oxyhydroxide. *In* "Adsorption from Aqueous Solutions" (P. H. Tewari, ed.), pp. 41–60. Plenum, New York.

Benjamin, M. M., and Leckie, J. O. (1980). Adsorption of metals at oxide interfaces: Effects of the concentration of adsorbate and competing minerals. *In* "Contaminants and Sediments" (R. A. Baker, ed.), Vol. 2, pp. 305–322. Ann Arbor Sci. Ann Arbor, Michigan.

Benjamin, M. M., and Leckie, J. O. (1981). Multiple-site adsorption of Cd, Cu, Zn, and Pb on amorphous iron oxyhydroxide. *J. Colloid Interface Sci.* **79,** 209–221.

Bérubé, Y. G., and deBruyn, P. L. (1968a). Adsorption at the rutile-solution interface. I. thermodynamic and experimental study. *J. Colloid Interface Sci.* **27,** 305–318.

Bérubé, Y. G., and deBruyn, P. L. (1968b). Adsorption at the rutile-solution interface. II. model of the electrochemical study. *J. Colloid Interface Sci.* **28,** 92–105.

Bleam, W. F., Pfeffer, P. E., Goldberg, S., Taylor, R. W., and Dudley, R. (1991). A ^{31}P solid-state nuclear magnetic resonance study of phosphate adsorption at the boehmite/aqueous-solution interface. *Langmuir* **7,** 1702–1712.

Blesa, M. A., Maroto, A. J. G., and Regazzoni, A. E. (1984a). Boric acid adsorption on magnetite and zirconium dioxide. *J. Colloid Interface Sci.* **99,** 32–40.

Blesa, M. A., Figliolia, N. M., Maroto, A. J.G., and Regazzoni, A. E. (1984b). The influence of temperature on the interface magnetite-aqueous electrolyte solution. *J. Colloid Interface Sci.* **101,** 410–418.

Bloesch, P. M., Bell, L. C., and Hughes, J. D. (1987). Adsorption and desorption of boron by goethite. *Aust. J. Soil Res.* **25,** 377–390.

Bolan, N. S., Barrow, N. J., and Posner, A. M. (1985). Describing the effect of time on sorption of phosphate by iron and aluminum hydroxides. *J. Soil Sci.* **36,** 187–197.

Bolan, N. S., Syers, J. K., and Tillman, R. W. (1986). Ionic strength effects on surface charge and adsorption of phosphate and sulphate by soils. *J. Soil Sci.* **37,** 379–388.

Bolland, M. D., Posner, A. M., and Quirk, J. P. (1977). Zinc adsorption by goethite in the absence and presence of phosphate. *Aust. J. Soil Res.* **15,** 279–286.

Bolt, G. H., and van Riemsdijk, W. H. (1982). Ion adsorption on inorganic variable charge constituents. *In* "Soil Chemistry. Part B. Physico-Chemical Methods" (G. H. Bolt, ed.), pp. 459–503. Elsevier, Amsterdam.

Bourg, A. C. M., and Schindler, P. W. (1978). Ternary surface complexes. 1. Complex formation in the system silica-Cu(II)-ethylenediamine. *Chimia* **32,** 166–168.

Bowden, J. W., Posner, A. M., and Quirk, J. P. (1977). Ionic adsorption on variable charge mineral surfaces. Theoretical-charge development and titration curves. *Aust. J. Soil Res.* **15,** 121–136.

Bowden, J. W., Nagarajah, S., Barrow, N. J., Posner, A. M., and Quirk, J. P. (1980). Describing the adsorption of phosphate, citrate and selenite on a variable charge mineral surface. *Aust. J. Soil Res.* **18,** 49–60.

Breeuwsma, A., and Lyklema, J. (1971). Interfacial electrochemistry of haematite (α-Fe_2O_3). *Discuss. Faraday Soc.* **52,** 324–333.

Catts, J. G., and Langmuir, D. (1986). Adsorption of Cu, Pb and Zu by δMnO_2: Applicability of the site binding-surface complexation model. *Appl. Geochem.* **1,** 255–264.

Cederberg, G. A., Street, R. L., and Leckie, J. O. (1985). A groundwater mass transport and equilibrium chemistry model for multicomponent systems. *Water Resour. Res.* **21,** 1095–1104.

Charlet, L. (1986). Adsorption of some macronutrient ions on an oxisol. An application of the triple layer model. Ph.D. Thesis, University of California, Riverside.

Charlet, L., and Sposito, G. (1987). Monovalent ion adsorption by an oxisol. *Soil Sci. Soc. Am. J.* **51,** 1155–1160.

Charlet, L., and Sposito, G. (1989). Bivalent ion adsorption by an oxisol. *Soil Sci. Soc. Am. J.* **53,** 691–695.

Comans, R. N. J., and Middelburg, J. J. (1987). Sorption of trace metals on calcite: Applicability of the surface precipitation model. *Geochim. Cosmochim. Acta.* **51,** 2587–2591.

Cowan, C. E., Zachara, J. M., and Resch, C. T. (1991). Cadmium adsorption on iron oxides in the presence of alkaline-earth elements. *Environ. Sci. Technol.* **25,** 437–446.

Davis, J. A. (1977). Adsorption of trace metals and complexing ligands at the oxide/water interface. Ph.D. Thesis, Stanford University, Stanford, California.

Davis, J. A., and Leckie, J. O. (1978). Surface ionization and complexation at the oxide/water interface. II. Surface properties of amorphous iron oxyhydroxide and adsorption of metal ions. *J. Colloid Interface Sci.* **67,** 90–107.

Davis, J. A., and Leckie, J. O. (1979). Speciation of adsorbed ions at the oxide/water interface. *ACS Symp. Ser.* **93,** 299–317.

Davis, J. A., and Leckie, J. O. (1980). Surface ionization and complexation at the oxide/water interface. 3. Adsorption of anions. *J. Colloid Interface Sci.* **74,** 32–43.

Davis, J. A., James, R. O., and Leckie, J. O. (1978). Surface ionization and complexation at the oxide/water interface. I. Computation of electrical double layer properties in simple electrolytes. *J. Colloid Interface Sci.* **63,** 480–499.

Dzombak, D. A., and Morel, F. M. M. (1990). "Surface Complexation Modeling. Hydrous Ferric Oxide." Wiley, New York.

Farley, K. J., Dzombak, D. A., and Morel, F. M. M. (1985). A surface precipitation model for the sorption of cations on metal oxides. *J. Colloid Interface Sci.* **106,** 226–242.

Felmy, A. R., Girvin, D. C., and Jenne, E. A. (1984). "MINTEQ: A Computer Program for Calculating Aqueous Geochemical Equilibria," EPA-600/3-84-032. Office of Research and Development, U.S. Environ. Prot. Agency, Athens, Georgia.

Forbes, E. A., Posner, A. M., and Quirk, J. P. (1976). The specific adsorption of divalent Cd, Co, Cu, Pb and Zn on goethite. *J. Soil Sci.* **27,** 154–166.

Furrer, G., Westall, J., and Sollins, P. (1989). The study of soil chemistry through quasi-steady-state models. I. Mathematical definition of model. *Geochim. Cosmochim. Acta* **53,** 595–601.

Furrer, G., Sollins, P., and Westall, J. C. (1990). The study of soil chemistry through quasi-steady-state models. II. Acidity of soil solution. *Geochim. Cosmochim. Acta* **54,** 2363–2374.

Fürst, B. (1976). Das Koordinationschemische Adsorptionsmodel: Oberflächenkomplexbildung von Cu(II), Cd(II) und Pb(II) an SiO_2 (Aerosil) und TiO_2 (Rutil). Ph.D. Thesis, University of Bern, Bern, Switzerland.

Gallez, A., Juo, A. S. R., and Herbillon, A. J. (1976). Surface and charge characteristics of selected soils in the tropics. *Soil Sci. Soc. Am. J.* **40,** 601–608.

Girvin, D. C., Ames, L. L., Schwab, A. P., and McGarran, J. E. (1991). Neptunium adsorption on synthetic amorphous iron oxyhydroxide. *J. Colloid Interface Sci.* **141,** 67–78.

Gisler, A. (1980). Die Adsorption von Aminosäuren an Grenzflächen Oxid-Wasser. Ph.D. Thesis, University of Bern, Bern, Switzerland.

Goldberg, S. (1985). Chemical modeling of anion competition on goethite using the constant capacitance model. *Soil Sci. Soc. Am. J.* **49,** 851–856.

Goldberg, S. (1986a). Chemical modeling of arsenate adsorption on aluminum and iron oxide minerals. *Soil Sci. Soc. Am. J.* **50,** 1154–1157.

Goldberg, S. (1986b). Chemical Modeling of Specific Anion Adsorption on Oxides, Clay Minerals, and Soils, ENVIROSOFT 86, pp. 671–688. CML Publications, Ashurst, Southampton, U.K.

Goldberg, S. (1991). Sensitivity of surface complexation modeling to the surface site density parameter. *J. Colloid Interface Sci.* **145,** 1–9.

Goldberg, S., and Glaubig, R. A. (1985). Boron adsorption on aluminum and iron oxide minerals. *Soil Sci. Soc. Am. J.* **49,** 1374–1369.

Goldberg, S., and Glaubig, R. A. (1986a). Boron adsorption on California soils. *Soil Sci. Soc. Am. J.* **50,** 1173–1176.

Goldberg, S., and Glaubig, R. A. (1986b). Boron adsorption and silicon release by the clay minerals kaolinite, montmorillonite, and illite. *Soil Sci. Soc. Am. J.* **50,** 1442–1448.

Goldberg, S., and Glaubig, R. A. (1988a). Boron and silicon adsorption on an aluminum oxide. *Soil Sci. Soc. Am. J.* **52,** 87–91.

Goldberg, S., and Glaubig, R. A. (1988b). Anion sorption on a calcareous, montmorillonitic soil—selenium. *Soil Sci. Soc. Am. J.* **52,** 954–958.

Goldberg, S., and Glaubig, R. A. (1988c). Anion sorption on a calcareous, montmorillonitic soil—Arsenic. *Soil Sci. Soc. Am. J.* **52,** 1297–1300.

Goldberg, S., and Sposito, G. (1984a). A chemical model of phosphate adsorption by soils. I. Reference oxide minerals. *Soil Sci. Soc. Am. J.* **48,** 772–778.

Goldberg, S., and Sposito, G. (1984b). A chemical model of phosphate adsorption by soils. II. Noncalcareous soils. *Soil Sci. Soc. Am. J.* **48,** 779–783.

Goldberg, S., and Sposito, G. (1985). On the mechanism of specific phosphate adsorption by hydroxylated mineral surfaces: A review. *Commun. Soil Sci. Plant Anal.* **16,** 801–821.

Goldberg, S., and Traina, S. J. (1987). Chemical modeling of anion competition on oxides using the constant capacitance model—mixed-ligand approach. *Soil Sci. Soc. Am. J.* **51,** 929–932.

Hawke, D., Carpenter, P. D., and Hunter, K. A. (1989). Competitive adsorption of phosphate on goethite in marine electrolytes. *Environ. Sci. Technol.* **23,** 187–191.

Hayes, K. F. (1987). Equilibrium, spectroscopic and kinetic studies of ion adsorption at the oxide/aqueous interface. Ph.D. Thesis, Stanford University, Stanford, California.

Hayes, K. F., and Leckie, J. O. (1986). Mechanism of lead ion adsorption at the goethite–water interface. *ACS Symp. Ser.* **323,** 114–141.

Hayes, K. F., and Leckie, J. O. (1987). Modeling ionic strength effects on cation adsorption at hydrous oxide/solution interfaces. *J. Colloid Interface Sci.* **115,** 564–572.

Hayes, K. F., Papelis, C., and Leckie, J. O. (1988). Modeling ionic strength effects on anion adsorption at hydrous oxide/solution interfaces. *J. Colloid Interface Sci.* **125,** 717–726.

Hayes, K. F., Redden, G., Ela, W., and Leckie, J. O. (1991). Surface complexation models: An evaluation of model parameter estimation using FITEQL and oxide mineral titration data. *J. Colloid Interface Sci.* **142,** 448–469.

Hiemstra, T., van Riemsdijk, W. H., and Bruggenwert, M. G. M. (1987). Proton adsorption mechanism at the gibbsite and aluminium oxide solid/solution interface. *Neth. J. Agric. Sci.* **35,** 281–293.

Hiemstra, T., van Riemsdijk, W. H., and Bolt, G. H. (1989a). Multisite proton adsorption modeling at the solid/solution interface of (hydr)oxides: A new approach. I. Model description and evaluation of intrinsic reaction constants. *J. Colloid Interface Sci.* **133,** 91–104.

Hiemstra, T., de Wit, J. C. M., and van Riemsdijk, W. H. (1989b). Multisite proton adsorption modeling at the solid/solution interface of (hydr)oxides: A new approach. II. Application to various important (hydr)oxides. *J. Colloid Interface Sci.* **133,** 105–117.

Hingston, F. J. (1970). Specific adsorption of anions on goethite and gibbsite. Ph.D. Thesis, University of Western Australia, Nedlands.

Hohl, H., and Stumm, W. (1976). Interaction of Pb^{2+} with hydrous γ-Al_2O_3. *J. Colloid Interface Sci.* **55,** 281–288.

Hohl, H., Sigg, L., and Stumm, W. (1980). Characterization of surface chemical properties of oxides in natural waters. *Adv. Chem. Ser.* **189,** 1–31.

Honeyman, B. D. (1984). Cation and anion adsorption at the oxide/solution interface in systems containing binary mixtures of adsorbents: An investigation of the concept of adsorptive additivity. Ph.D. Thesis, Stanford University, Stanford, California.

Hsi, C.-K.D., and Langmuir, D. (1985). Adsorption of uranyl onto ferric oxyhydroxides: Application of the surface complexation site-binding model. *Geochim. Cosmochim. Acta* **49,** 1931–1941.

Huang, C.-P., and Stumm, W. (1973). Specific adsorption of cations on hydrous γ-Al_2O_3. *J. Colloid Interface Sci.* **43,** 409–420.

Hunter, K. A., Hawke, D. J., and Choo, L. K. (1988). Equilibrium adsorption of thorium by metal oxides in marine electrolytes. *Geochim. Cosmochim. Acta* **52,** 627–636.

James, R. O., and Parks, G. A. (1982). Characterization of aqueous colloids by their electrical double-layer and intrinsic surface chemical properties. *Surf. Colloid Sci.* **12,** 119–216.

James, R. O., Davis, J. A., and Leckie, J. O. (1978). Computer simulation of the conductometric and potentiometric titrations of the surface groups on ionizable latexes. *J. Colloid Interface Sci.* **65,** 331–343.

Jennings, A. A., Kirkner, D. J., and Theis, T. L. (1982). Multicomponent equilibrium chemistry in groundwater quality models. *Water Resour. Res.* **18,** 1089–1096.

Koopal, L. K., van Riemsdijk, W. H., and Roffey, M. G. (1987). Surface ionization and complexation models: A comparison of methods for determining model parameters. *J. Colloid Interface Sci.* **118,** 117–136.

Krupka, K. M., Erikson, R. L., Mattigod, S. V., Schramke, J. A., and Cowan, C. E. (1988). "Thermochemical Data Used by the FASTCHEM™ Package," EPRI EA-5872. Electr. Power Res. Inst., Palo Alto, California.

Kummert, R., and Stumm, W. (1980). The surface complexation of organic acids on hydrous γ-Al_2O_3. *J. Colloid Interface Sci.* **75,** 373–385.

LaFlamme, B. D., and Murray, J. W. (1987). Solid/solution interaction: The effect of carbonate alkalinity on adsorbed thorium. *Geochim. Cosmochim. Acta* **51,** 243–250.

Leckie, J. O., Benjamin, M. M. Hayes, K. F., Kaufmann, G., and Altmann, S. (1980). "Adsorption/Coprecipitation of Trace Elements from Water with Iron Oxyhydroxide," EPRI RP-910-1. Electr. Power Res. Inst. Palo Alto, California.

Leckie, J. O., Appleton, A. R., Ball, N. B., Hayes, K. F., and Honeyman, B. D. (1984). "Adsorptive Removal of Trace Elements from Fly-Ash Pond Effluents onto Iron Oxyhydroxide," EPRI RP-910-1. Electr. Power Res. Inst. Palo Alto, California.

Lövgren, L., Sjöberg, S., and Schindler, P. W. (1990). Acid/base reactions and Al(III) complexation at the surface of goethite. *Geochim. Cosmochim. Acta* **54,** 1301–1306.

Madrid, L., and Diaz-Barrientos, E. (1988). Description of titration curves of mixed materials with variable and permanent surface charge by a mathematical model. 1. Theory. 2. Application to mixtures of lepidocrocite and montmorillonite. *J. Soil Sci.* **39,** 215–225.

Madrid, L., Diaz, E., Cabrera, F., and de Arambarri, P. (1983). Use of a three-plane model to describe charge properties of some iron oxides and soil clays. *J. Soil Sci.* **34,** 57–67.

Madrid, L., Diaz-Barrientos, E., and Sanchez-Soto, P. J. (1989). Description of titration curves of mixed materials with variable and permanent charge by a mathematical model. 3. Influence of the nature of the permanent charge mineral. *J. Soil Sci.* **40,** 799–806.

Mangold, D. C., and Tsang, C.-F. (1991). A summary of subsurface hydrological and hydrochemical models. *Rev. Geophys.* **29,** 51–79.

McKenzie, R. M. (1981). The surface charge on manganese dioxides. *Aust. J. Soil Res.* **19,** 41–50.

McKenzie, R. M. (1983). The adsorption of molybdenum on oxide surfaces. *Aust. J. Soil Res.* **21,** 505–513.

Mikami, N., Sasaki, M., Hachiya, K., Astumian, R. D., Ikeda, T., and Yasunaga, T. (1983a). Kinetics of the adsorption–desorption of phosphate on the γ-Al_2O_3 surface using the pressure-jump technique. *J. Phys. Chem.* **87,** 1454–1458.

Mikami, N., Sasaki, M., Kikuchi, T., and Yasunaga, T. (1983b). Kinetics of adsorption–desorption of chromate on γ-Al_2O_3 surfaces using the pressure-jump technique. *J. Phys. Chem.* **87,** 5245–5248.

Milonjić, S. K. (1987). Determination of surface ionization and complexation constants at colloidal silica/electrolyte interface. *Colloids Surf.* **23,** 301–312.

Motta, M. M., and Miranda, C. F. (1989). Molybdate adsorption on kaolinite, montmorillonite, and illite: Constant capacitance modeling. *Soil Sci. Soc. Am. J.* **53,** 380–385.

Osaki, S., Kuroki, Y., Sugihara, S., and Takashima, Y. (1990a). Effects of metal ions and organic ligands on the adsorption of Co(II) onto silicagel. *Sci. Total Environ.* **99,** 93–103.

Osaki, S., Miyoshi, T., Sugihara, S., and Takashima, Y. (1990b). Adsorption of Fe(III),

Co(II) and Zn(II) onto particulates in fresh waters on the basis of the surface complexation model. I. Stabilities of metal species adsorbed on particulates. *Sci. Total Environ.* **99,** 105–114.

Papelis, C., Hayes, K. F., and Leckie, J. O. (1988). "HYDRAQL: A Program for the Computation of Chemical Equilibrium Composition of Aqueous Batch Systems Including Surface-Complexation Modeling of Ion Adsorption at the Oxide/Solution Interface," Tech. Rep. No. 306. Department of Civil Engineering, Stanford University, Stanford, California.

Pulfer, K., Schindler, P. W., Westall, J. C., and Grauer, R. (1984). Kinetics and mechanism of dissolution of bayerite (γ-$Al(OH)_3$) in HNO_3-HF solutions at 298.2 K. *J. Colloid Interface Sci.* **101,** 554–564.

Regazzoni, A. E., Blesa, M. A., and Maroto, A. J.G. (1983). Interfacial properties of zirconium dioxide and magnetite in water. *J. Colloid Interface Sci.* **91,** 560–570.

Riese, A. C. (1982). Adsorption of radium and thorium onto quartz and kaolinite: A comparison of solution/surface equilibria models. Ph.D. Thesis, Colorado School of Mines, Golden.

Rochester, C. H., and Topham, S. A. (1979a). Infrared study of surface hydroxyl groups on goethite. *J. Chem. Soc., Faraday Trans. 1* **75,** 591–602.

Rochester, C. H., and Topham, S. A. (1979b). Infrared study of surface hydroxyl groups on haematite. *J. Chem. Soc., Faraday Trans. 1.* **75,** 1073–1088.

Sanchez, A. R., Murray, J. W., and Sibley, T. H. (1985). The adsorption of plutonium IV and V on goethite. *Geochim. Cosmochim. Acta* **49,** 2297–2307.

Sasaki, M., Moriya, A. M., Yasunaga, T., and Astumian, R. D. (1983). A kinetic study of ion-pair formation on the surface of α-FeOOH in aqueous suspensions using the electric field pulse technique. *J. Phys. Chem.* **87,** 1449–1453.

Schindler, P. W. (1990). Co-adsorption of metal ions and organic ligands: Formation of ternary surface complexes. *Rev. Mineral.* **23,** 281–307.

Schindler, P. W., and Gamsjäger, H. (1972). Acid-base reactions of the TiO_2 (anatase)–water interface and the point of zero charge of TiO_2 suspensions. *Kolloid-Z. Z. Polym.* **250,** 759–763.

Schindler, P. W., and Kamber, H. R. (1968). Die Acidität von Silanolgruppen. *Helv. Chim. Acta* **51,** 1781–1786.

Schindler, P. W., and Stumm, W. (1987). The surface chemistry of oxides, hydroxides, and oxide minerals. *In* "Aquatic Surface Chemistry" (W. Stumm, ed.), pp. 83–110. Wiley (Interscience), New York.

Schindler, P. W., Fürst, B., Dick, R., and Wolf, P. U. (1976). Ligand properties of surface silano groups. I. Surface complex formation with Fe^{3+}, Cu^{2+}, Cd^{2+}, and Pb^{2+}. *J. Colloid Interface Sci.* **55,** 469–475.

Schindler, P. W., Liechti, P., and Westall, J. C. (1987). Adsorption of copper, cadmium and lead from aqueous solution to the kaolinite/water interface. *Neth. J. Agric. Sci.* **35,** 219–230.

Sigg, L. (1973). Untersuchungen über Protolyse und Komplexbildung mit zweiwertigen Kationen von Silikageloberflächen, M.Sc. Thesis, University of Bern, Bern, Switzerland.

Sigg, L. M. (1979). Die Wechselwirkung von Anionen und schwachen Säuren mit αFeOOH (Goethit) in wässriger Lösung. Ph.D. Thesis, Swiss Federal Institute of Technology, Zürich.

Sigg, L., and Stumm, W. (1981). The interaction of anions and weak acids with the hydrous goethite (α-FeOOH) surface. *Colloids Surf.* **2,** 101–117.

Smit, W., and Holten, C. L. M. (1980). Zeta-potential and radiotracer adsorption measurement on EFG α-Al_2O_3 single crystals in NaBr solutions. *J. Colloid Interface Sci.* **78,** 1–14.

Sposito, G. (1981). Cation exchange in soils: An historical and theoretical perspective. *ASA Spec. Publ.* **40,** 13–28.

Sposito, G. (1983). Foundations of surface complexation models of the oxide-aqueous solution interface. *J. Colloid Interface Sci.* **91,** 329–340.

Sposito, G. (1984a). "The Surface Chemistry of Soils." Oxford Univ. Press, Oxford, U.K.

Sposito, G. (1984b). Chemical models of inorganic pollutants in soils. *CRC Crit. Rev. Environ. Control* **15,** 1–24.

Sposito, G., and Coves, J. (1988). "SOILCHEM: A Computer Program for the Calculation of Chemical Speciation in Soils." Kearney Foundation of Soil Science, University of California, Riverside.

Sposito, G., and Mattigod, S. V. (1980). "GEOCHEM: A Computer Program for the Calculation of Chemical Equilibria in Soil Solutions and Other Natural Water Systems." Kearney Foundation of Soil Science, University of California, Riverside.

Sposito, G., deWit, J. C. M., and Neal, R. H. (1988). Selenite adsorption on alluvial soils. III. Chemical modeling. *Soil Sci. Soc. Am. J.* **52,** 947–950.

Sprycha, R. (1983). Attempt to estimate σ_β charge components on oxides from anion and cation adsorption measurements. *J. Colloid Interface Sci.* **96,** 551–554.

Sprycha, R. (1984). Surface charge and adsorption of background electrolyte ions at anatase/electrolyte interface. *J. Colloid Interface Sci.* **102,** 173–185.

Sprycha, R. (1989a). Electrical double layer at alumina/electrolyte interface. I. Surface charge and zeta potential. *J. Colloid Interface Sci.* **127,** 1–11.

Sprycha, R. (1989b). Electrical double layer at alumina/electrolyte interface. II. Adsorption of supporting electrolyte ions. *J. Colloid Interface Sci.* **127,** 12–25.

Sprycha, R., and Szczypa, J. (1984). Estimation of surface ionization constants from electrokinetic data. *J. Colloid Interface Sci.* **102,** 288–291.

Stiglich, P. J. (1976). Adsorption of cadmium(II) complexes at the oxide/water interface. M. S. Thesis, University of Melbourne, Melbourne, Australia.

Stumm, W., Huang, C. P., and Jenkins, S. R. (1970). Specific chemical interaction affecting the stability of dispersed systems. *Croat. Chem. Acta* **42,** 223–245.

Stumm, W., Hohl, H., and Dalang, F. (1976). Interaction of metal ions with hydrous oxide surfaces. *Croat. Chem. Acta* **48,** 491–504.

Stumm, W., Kummert, R., and Sigg, L. (1980). A ligand exchange model for the adsorption of inorganic and organic ligands at hydrous oxide interfaces. *Croat. Chem. Acta* **53,** 291–312.

Swallow, K. C. (1978). Adsorption of trace metals by hydrous ferric oxide. Ph.D. Thesis, Massachusetts Institute of Technology, Cambridge, Massachusetts.

Tamura, H., Matijevic, E., and Meites, L. (1983). Adsorption of Co^{2+} ions on spherical magnetite particles. *J. Colloid Interface Sci.* **92,** 303–314.

van Raij, B., and Peech, M. (1972). Electrochemical properties of some oxisols and alfisols of the tropics. *Soil Sci. Soc. Am. Proc.* **36,** 587–593.

van Riemsdijk, W. H., and Lyklema, J. (1980a). The reaction of phosphate with aluminum hydroxide in relation with phosphate bonding in soils. *Colloids Surf.* **1,** 33–44.

van Riemsdijk, W. H., and Lyklema, J. (1980b). Reaction of phosphate with gibbsite [$Al(OH)_3$] beyond the adsorption maximum. *J. Colloid Interface Sci.* **76,** 55–66.

van Riemsdijk, W. H., and van der Zee, S. E. A. T. M. (1991). Comparison of models for adsorption, solid solution and surface precipitation. *In* "Interactions at the Soil Colloid-Soil Solution Interface" (G. H. Bolt, ed.), pp. 241–256. Kluwer Academic Publishers, The Netherlands.

van Riemsdijk, W. H., Bolt, G. H., Koopal, L. K., and Blaakmeer, J. (1986). Electrolyte adsorption on heterogeneous surfaces: Adsorption models. *J. Colloid Interface Sci.* **109,** 219–228.

van Riemsdijk, W. H., deWit, J. C. M., Koopal, L. K., and Bolt, G. H. (1987). Metal ion adsorption on heterogeneous surfaces: Adsorption models. *J. Colloid Interface Sci.* **116,** 511–522.

Wersin, P., Charlet, L., Karthein, R., and Stumm, W. (1989). From adsorption to precipitation: Sorption of Mn^{2+} on $FeCO_3$(s). *Geochim. Cosmochim. Acta* **53,** 2787–2796.

Westall, J. C. (1979). "MICROQL. I. A Chemical Equilibrium Program in BASIC. II. Computation of Adsorption Equilibria in BASIC," Tech. Rep. Swiss Federal Institute of Technology, EAWAG, Dübendorf.

Westall, J. (1980). Chemical equilibrium including adsorption on charged surfaces. *Adv. Chem. Ser.* **189,** 33–44.

Westall, J. C. (1982). "FITEQL: A Computer Program for Determination of Equilibrium Constants from Experimental Data," Rep. 82-01. Department of Chemistry, Oregon State University, Corvallis.

Westall, J. C. (1986). Reactions at the oxide-solution interface: Chemical and electrostatic models. *ACS Symp. Ser.* **323,** 54–78.

Westall, J., and Hohl, H. (1980). A comparison of electrostatic models for the oxide/solution interface. *Adv. Colloid Interface Sci.* **12,** 265–294.

Westall, J. C., Zachary, J. L., and Morel, F. M. M. (1976). "MINEQL: A Computer Program for the Calculation of Chemical Equilibrium Composition of Aqueous Systems," Tech. Note 18. Ralph M. Parsons Laboratory, Department of Civil Engineering, Massachusetts Institute of Technology, Cambridge, Massachusetts.

Wood, R., Fornasiero, D., and Ralston, J. (1990). Electrochemistry of the boehmite-water interface. *Colloids Surf.* **51,** 389–403.

Yates, D. E. (1975). The structure of the oxide-aqueous electrolyte interface. Ph.D. Thesis, University of Melbourne, Melbourne, Australia.

Yates, D. E., Levine, S., and Healy, T. W. (1974). Site-binding model of the electrical double layer at the oxide/water interface. *J. Chem. Soc., Faraday Trans. 1* **70,** 1807–1818.

Yeh, G. T., and Tripathi, V. S. (1990). "HYDROGEOCHEM: A Coupled Model of HYDROlogic Transport and GEOCHEMical Equilibria in Reactive Multicomponent Systems," Rep. ORNL-6371. Oak Ridge Natl. Lab., Oak Ridge, Tennessee.

Zachara, J. M., Girvin, D. C., Schmidt, R. L., and Resch, C. T. (1987). Chromate adsorption on amorphous iron oxyhydroxide in the presence of major groundwater ions. *Environ. Sci. Technol.* **21,** 589–594.

Zachara, J. M., Cowan, C. E., Schmidt, R. L., and Ainsworth, C. C. (1988). Chromate adsorption by kaolinite. *Clays Clay Miner.* **36,** 317–326.

Zachara, J. M., Ainsworth, C. C., Cowan, C. E., and Resch, C. T. (1989). Adsorption of chromate by subsurface soil horizons. *Soil Sci. Soc. Am. J.* **53,** 418–428.

Zhang, P. C., and Sparks, D. L. (1989). Kinetics and mechanisms of molybdate adsorption/desorption at the goethite/water interface using pressure-jump relaxation. *Soil Sci. Soc. Am. J.* **53,** 1028–1034.

Zhang, P. C., and Sparks, D. L. (1990a). Erratum—Kinetics and mechanisms of molybdate adsorption/desorption on the goethite/water interface using pressure-jump relaxation. *Soil Sci. Soc. Am. J.* **54,** 624.

Zhang, P. C., and Sparks, D. L. (1990b). Kinetics and mechanisms of sulfate adsorption/desorption on goethite using pressure-jump relaxation. *Soil Sci. Soc. Am. J* **54,** 1266–1273.

Zhang, P., and Sparks, D. L. (1990c). Kinetics of selenate and selenite adsorption/desorption at the goethite/water interface. *Environ. Sci. Technol.* **24,** 1848–1856.